The PHILOSOPHICAL MAGAZINE

FIRST PUBLISHED IN 1798

L. 43 SEVENTH SERIES No. 336 January, 1952

A Journal of Theoretical Experimental and Applied Physics

PRICE 15s. 0d.
Annual Subscription £8 0s. 0d. payable in advance

D AND PUBLISHED BY TAYLOR & FRANCIS LTD., RED LION COURT, FLEET ST., LONDON, E.C.4

ADVANCES IN PHYSICS

A QUARTERLY SUPPLEMENT OF THE PHILOSOPHICAL MAGAZINE

On 1st Jan., 1952, the Philosophical Magazine will publish the first number of a new quarterly supplement. The aim of this supplement will be to give those interested in physics comprehensive and authoritative accounts of recent important developments. It is felt by the Editor that in view of the rapid advances in many branches of physics, scientists will welcome a journal devoted to articles of this type.

VOLUME 1 JANUARY 1952 NUMBER 1

PRICE *per part* 15/- *plus postage* **PRICE** *per annum* £2 15s. 0d. *post free*

Printed and Published by
TAYLOR & FRANCIS, LTD., RED LION COURT, FLEET ST., LONDON, E.C.4

THE

PHILOSOPHICAL MAGAZINE

A JOURNAL OF THEORETICAL EXPERIMENTAL AND APPLIED PHYSICS

First published in 1798

[SEVENTH SERIES—VOL. 43]

I. *Theory of Radio Reflections from Meteor Trails: I*

By T. R. KAISER* and R. L. CLOSS
Jodrell Bank Experimental Station, University of Manchester†

[Received October 22, 1951]

ABSTRACT

This paper deals with the evaluation of the reflection coefficient for backward scattering of an electromagnetic wave from a column of ionization having cylindrical symmetry. The application of the theory to meteors thus depends on the assumption that a meteor instantaneously forms a narrow column of ionization which subsequently diffuses radially.

The theory predicts two qualitatively different categories of meteor echoes, depending on whether the electron line density, α, is greater or less than about 10^{12} per cm, the properties of which may be summarized as follows:

(1) $\alpha < 10^{12}$

If the incident electric vector is parallel to the axis of the trail (parallel scattering) it is sufficient to assume that the electrons scatter coherently and independently, each contributing an amount $4\pi(e^2/mc^2)^2$ to the backward scattering cross section. As the column expands radially, the echo amplitude decreases, the form of decay being exponential if the electron density is a Gaussian function of radius.

When the incident electric vector is normal to the column (transverse scattering) the echo amplitude differs from the above in that the reflection coefficient may pass through a resonance, followed by the exponential decay. The magnitude of the resonance (measured as the ratio of the

---

* I.C.I. Research Fellow.
† Communicated by Professor A. C. B. Lovell.

resonant reflection coefficient to that for parallel scattering) depends mainly on the diffuseness of the column (i.e. on the gradient of electron density at the radius of critical density). It has been evaluated for an electron density varying with radius as $n=n_0 \exp[-(r/r_0)^s]$ and is found to range from 2·0 when $s=2$ (Gaussian distribution) to 10 when $s=20$. The echo amplitude in both cases is proportional to α, while the echo duration is independent of α.

The short duration echoes which form the bulk of the experimental observations appear to have the above forms.

(2) $\alpha \gg 10^{12}$

In this case the column is expected to reflect similarly to a metallic cylinder. Except initially, when the parallel reflection coefficient exceeds the transverse, the reflection coefficients are equal and substantially constant. The duration is approximately proportional to α, and the peak echo amplitude is a slowly increasing function of α ($\sim\alpha^{1/4}$).

These predictions are in agreement with the experimental data on long duration echoes.

Some particular electron distributions, including a small diffuse sphere, which exhibit multipole resonant scattering are discussed in Appendix II, and laboratory experiments which may be of some interest are suggested.

---

§1. Introduction

The passage of a meteor through the atmosphere is accompanied by the emission of visible radiation, and by the creation of an ionized column of air, both of which processes reach a maximum at heights between 80 and 120 km. The latter effect has been made the basis of an intensive study of the properties of meteors and of meteor streams, notably by Lovell and co-workers in Great Britain, and by Millman and McKinley in Canada (see Lovell (1948) for a review article).

It is believed that the major part of the ionization arises from collisions between evaporated neutral molecules of the meteor material and air molecules leading to a narrow column of electrons and positive ions which rapidly diffuses outwards.

Lovell and Clegg (1948) derived the radar equation for such an ionized column, assuming it to be narrow compared with the wavelength and to have a small enough electron density to enable the incident wave to penetrate the column without significant modification. In spite of these limitations, the theory gives an adequate explanation of many of the observed phenomena. Herlofson (1951) has shown that when the column is somewhat more than critically dense, this formula is applicable only when the electric vector of the incident wave is parallel to the axis of the trail (parallel scattering) and that in general the reflection coefficient

may exhibit a critical dependence on the orientation of the electric vector with respect to the column. Theoretical studies by Herlofson (1951) and by Feinstein (1951) predict that if the incident electric vector is normal to the axis (transverse scattering) the reflection coefficient will exhibit a resonance when the electron density is somewhat above the critical value, provided that the transverse dimensions of the column are small compared with the wavelength.

The magnitude of the resonance (measured as the ratio of the resonant reflection coefficient to that for parallel scattering) will depend on the radius of the trail and more critically on its diffuseness, i.e. on the gradient of electron density near the region where the column is critically dense. Herlofson has considered a model in which the electron density is constant from the axis to a given radius and then decreases linearly to zero over a small radius interval, while Feinstein has derived the reflection coefficient for a column in which the electron density decreases linearly to zero from the axis.

The purpose of this paper is to obtain the scattering parameters of a meteor trail without restriction on the electron line density or on its radius. Part is devoted to the derivation of an approximate method of solution of the wave equation for transverse scattering when the electron line density is less than 10^{12} cm^{-1} and the radius of the column is small compared with the wavelength (which are the conditions for the existence of a resonance). The method is applied to an electron distribution given by

$$n=n_0 \exp\left[-(r/r_0)^s\right], \quad . \quad . \quad . \quad . \quad . \quad . \quad (1)$$

where n=electron density and r=radius.

The important physical case of $s=2$ (Gaussian electron distribution) is studied in detail while other values of s are considered in the neighbourhood of the resonance.

The method is shown to be applicable to ionized clouds of geometrical configurations other than the circular cylinder. An example is the spherical cloud considered in Appendix II, where resonance effects are again to be expected. A later paper will deal with the problem of scattering from a diffuse elliptic cylinder which can be treated on similar lines and which may have a physical significance owing to the possibility of anisotropic diffusion in the earth's magnetic field.

Both the Lovell–Clegg result for parallel scattering and the above mentioned theory break down when the electron line density, α, reaches the order of 10^{12} cm^{-1}. It is shown that for larger line densities than this the expanding meteor column reflects in a similar manner to a metallic cylinder of appropriate radius. On this basis, the reflection coefficients have been evaluated for these high densities and for both parallel and transverse scattering. By joining smoothly the two solutions in the vicinity of $\alpha=10^{12}$ a complete solution for columns having a Gaussian electron distribution has been obtained, which is not limited as regards the electron line density or the radius of the column.

§2. General Theory for a Circular Cylinder

Transverse Scattering

The existence of a resonant process for the scattering from a column of radius small compared with the wavelength may be demonstrated by considering the cylinder as one of dielectric constant,

$$\kappa(r)=1-\frac{4\pi \boldsymbol{e}^2 n(r)}{k^2 \boldsymbol{m}\boldsymbol{c}^2}, \quad \ldots\ldots\ldots \quad (2)$$

immersed in a uniform transverse electrostatic field. The units in (2) are Gaussian (as throughout the paper), $n(r)$=electron density as a function of radius, $k=2\pi/\lambda$, λ=free space wavelength, $\boldsymbol{e}$, $\boldsymbol{m}$ and $\boldsymbol{c}$ are the charge and mass of the electron and the velocity of light respectively. This is a purely formal treatment and is not in itself, of course, physically realizable.

For the simple case of a homogeneous cylinder, along the z-axis of cylindrical polar coordinates, having $\kappa(r)=\kappa$, $r<a$; $\kappa(r)=1$, $r>a$, and in a uniform field E_0 parallel to the y coordinate axis, standard text books give the following expressions for the electrostatic potentials, V_i and V_e, interior and exterior to the cylinder respectively,

$$V_e=-E_0\left(r+\frac{1-\kappa}{1+\kappa}\frac{a^2}{r}\right)\sin\phi, \quad \ldots\ldots \quad (3)$$

$$V_i=-E_0\frac{2r\sin\phi}{1+\kappa}. \quad \ldots\ldots\ldots \quad (4)$$

The first term in (3) corresponds to the applied field and the second to the distortion introduced by the cylinder. This latter tends to infinity when $\kappa=-1$ which, in the electrodynamic case, we might thus expect to be the condition for resonant scattering.

Herlofson (1951) shows that the existence of resonances may be demonstrated using a similar model to the above. He evaluates the restoring forces between the surface charges of a polarized ionized cylinder and finds that the system is a resonant oscillator when $\kappa=-1$.

We may likewise treat parallel scattering. The internal field will now be equal to the applied electrostatic field, E_0, compared with $2E_0/(1+\kappa)$ in the above case. Denoting the dynamic reflection coefficients by $g_\perp$ and $g_\parallel$ we would expect that on this simple model

$$g_\perp/g_\parallel=2/(1+\kappa). \quad \ldots\ldots\ldots \quad (5)$$

The infinity at $\kappa=-1$ will be removed physically by the small but finite column radius, collision damping etc.

The generalization of the above treatment, including its extension to a non-homogeneous column involves the solution of the equation

$$\text{div}\,(\kappa\,\text{grad}\,V)=0, \quad \ldots\ldots\ldots \quad (6)$$

which, in cylindrical coordinates and on separation of variables, leads to

$$\frac{d}{dr}\left(\kappa r \frac{dV_m}{dr}\right) = \frac{m^2 \kappa V_m}{r}, \quad \ldots \ldots \quad (7)$$

where

$$V(r, \phi) = \sum_0^\infty V_m(r) \sin m\phi ; \quad \ldots \ldots \quad (8)$$

κ is a function only of radius, and m is a positive integer or zero whose values specify the various modes of excitation of the column.

An exact study of transverse scattering gives the equations

$$H_m'' + \left(\frac{1}{r} - \frac{\kappa'}{\kappa}\right) H_m' + \left(k^2\kappa - \frac{m^2}{r^2}\right) H_m = 0, \quad \ldots \quad (9)$$

$$H(r, \phi) = \sum_0^\infty H_m(r) \cos m\phi, \quad \ldots \ldots \quad (10)$$

where the magnetic vector has only a z-component, H (primes indicate differentiation with respect to r). The term $k^2\kappa H_m$ takes account of phase variation in the field and (7) and (9) can be shown to be equivalent if it is negligible, i.e. if we place upon r and κ the restriction $|\kappa(kr)^2| \ll m^2$ or, for the dipole mode,

$$|\kappa(kr)^2| \ll 1. \quad \ldots \ldots \quad (11)$$

With this restriction, using $\mathbf{E} = -\text{grad } V$, curl $\mathbf{H} = jk\kappa\mathbf{E}$, where $\mathbf{E}$ is the electric vector, we obtain

$$\left.\begin{aligned} H_m &= jk\kappa r V_m'/m, \\ V_m &= r H_m'/(jk\kappa m). \end{aligned}\right\} \quad \ldots \ldots \quad (12)$$

The solution of (7) in the region outside a column (i.e. where $\kappa = 1$) whose parameters satisfy (11) is

$$V_m(r) = A_m r^m + B_m r^{-m}, \quad \ldots \ldots \quad (13)$$

i.e.

$$H_m(r) = jk\kappa(A_m r^m - B_m r^{-m}), \quad \ldots \ldots \quad (14)$$

where A_m and B_m are constants and $m = 1, 2, 3, \ldots$. Except in special cases, A_m and B_m must be determined by numerical integration of (7).

The exact solution of (9) for the region outside the column involves the Bessel functions of the first and second kinds, $J_m(kr)$ and $N_m(kr)$, which reduce to the independent solutions r^m and r^{-m} respectively when $(kr)^2 \ll 1$.

Let us now consider a plane electromagnetic wave of unit amplitude, incident in the negative x direction and polarized in the direction of the y-axis. Omitting the time varying factor, $\exp(j\omega t)$, the expansion of the incident wave as a series of cylindrical waves is

$$H_{\text{inc}} = \exp(jkx) = J_0(kr) + 2\sum_1^\infty j^m J_m(kr) \cos m\phi, \quad \ldots \quad (15)$$

remembering that the magnetic vector has only a z-component.

The reflected wave may be written

$$H_{\text{refl}} = \sum_0^\infty t_m [J_m(kr) - jN_m(kr)] \cos m\phi, \quad \ldots \quad (16)$$

which, at large distances from the column, $(kr)^2 \gg 1$, describes an outward travelling cylindrical wave whose value on the positive x-axis, $(\phi=0)$, is

$$(H_{\text{refl}})_{(\varphi=0)}=\left[\sum_0^\infty j^m t_m\right][2/(\pi kr)]^{1/2}\exp[-j(kr-\pi/4)]. \quad . \quad (17)$$

The total external magnetic component is

$$H_{\text{ext}}=\sum_0^\infty H_m \cos m\phi, \quad . \quad . \quad . \quad . \quad . \quad . \quad . \quad . \quad (18)$$

where

$$\left.\begin{aligned} H_m&=(2j^m+t_m)J_m(kr)-jt_m N_m(kr), \qquad m=1, 2, 3, \ldots, \\ H_0&=(1+t_0)J_0(kr)-jt_0 N_0(kr). \end{aligned}\right\} \quad . \quad (19)$$

When $(kr)^2 \ll 1$, $J_m(kr) \simeq (kr)^m/(2^m m\,!)$, $N_m(kr) \simeq -2^m(m-1)\,!/[\pi(kr)^m]$, $m=1, 2, 3, \ldots$. Using these approximations and comparing (19) with (14) we obtain, for the transverse scattering reflection coefficients, t_m,

$$-\frac{2j^m}{t_m} \simeq 1+j\frac{m\,!\;(m-1)\,!\;4^m}{\pi k^{2m}}\frac{A_m}{B_m}. \quad . \quad . \quad . \quad . \quad . \quad (20)$$

We have not considered $m=0$, however it is not difficult to show that to the degree of approximation of (20), $t_0=0$.

With (20), the reflection coefficients, t_m, may be evaluated for any electron distribution, $n(r)$, by integrating (7) using the appropriate function $\kappa(r)$. Note that (20) is subject to the two conditions $|\kappa(kr)^2| \ll 1$ within the column, and $(kr_0)^2 \ll 1$ where r_0 is the radius of the column.

The total reflection coefficient for transverse backward scattering, denoted by $g_\perp$, is, from (17),

$$g_\perp=\left|\sum_0^\infty j^m t_m\right|. \quad . \quad . \quad . \quad . \quad . \quad . \quad . \quad . \quad . \quad (21)$$

When A_m is real (which occurs only for a non-diffuse trail), the mth mode exhibits a resonance (i.e. $|t_m|$ is a maximum) when $A_m=0$. In general the condition for resonance is $Re\,(A_m)=0$.

The scattering diameter of the column is defined as the width of the equivalent strip of material which reradiates, as an azimuthally isotropic cylindrical wave, all of the energy incident upon its surface, and which produces a backward scattered energy flux equal to that produced by the actual column. Denoting it by d, and using (17), it is given by

$$kd=4\left|\sum_0^\infty j^m t_m\right|^2=4g_\perp{}^2. \quad . \quad . \quad . \quad . \quad . \quad . \quad (22)$$

The total cross-section for backward scattering, denoted by σ, is

$$\sigma=8g_\perp{}^2 r/k=2dr. \quad . \quad . \quad . \quad . \quad . \quad . \quad . \quad (23)$$

If we have α electrons per cm, then the reflected amplitude at a large distance, r, from the column is equivalent to that produced by $\alpha\sqrt{(r\lambda)}$ electrons radiating coherently. The contribution of each electron to the scattering cross-section is thus

$$\sigma_e=4g_\perp{}^2/(\pi\alpha^2). \quad . \quad . \quad . \quad . \quad . \quad . \quad . \quad . \quad (24)$$

Parallel Scattering

We now consider a plane wave of unit amplitude incident in the direction of the negative x-axis and polarized parallel to the z-axis.

The appropriate wave equation is now

$$\nabla^2 E + k^2 \kappa E = 0,$$

and hence

$$r\frac{d}{dr}\left(r\frac{dE_m}{dr}\right) + [\kappa(kr)^2 - m^2]E_m = 0,$$

where

$$E = \sum_0^\infty E_m \cos m\phi.$$

The expansion of the incident wave into a set of cylindrical waves is identical with (15) replacing H by E. The reflected wave, the total external field, and the scattering parameters, will likewise be represented by (16), (17), (18), (19), (21), (22), (23), and (24), substituting l_m for t_m and $g_{\parallel}$ for $g_{\perp}$ to avoid confusion.

When $|\kappa(kr)^2| \ll 1$ throughout the column, there will be negligible attenuation of the wave as we pass from the exterior to the axis, the only significant mode will be $m=0$, and the Lovell–Clegg scattering formula will be valid. The reflection coefficient, in this case, becomes

$$\left.\begin{aligned} g_{\parallel} = |l_0| &= \frac{\pi k^2}{2}\int_0^\infty r(1-\kappa)dr \\ &= \pi\alpha \boldsymbol{e}^2/(\boldsymbol{mc}^2), \end{aligned}\right\} \quad \ldots\ldots \quad (25)$$

and

$$kd = [2\pi\alpha \boldsymbol{e}^2/(\boldsymbol{mc}^2)]^2,$$

$$\sigma_e = 4\pi(\boldsymbol{e}^2/\boldsymbol{mc}^2)^2.$$

The latter is just the cross-section of a free electron for backward scattering, completing the identity with the Lovell–Clegg formula.

Relation between the Reflection Coefficient and the Signal received from a Meteor Column

In the above discussion we have, for simplicity, considered a plane wave incident normally to the axis of the cylindrical column, leading to the reflected amplitude given by (17).

In meteor experiments we normally have a transmitter and receiver, matched through a common T–R network to an aerial, distant R from the meteor column, hence the incident wave is spherical. The curvature of the incident wave front results in a central Fresnel zone, seen from radius R, of effective length $\sqrt{(\lambda R/2)}$ instead of $\sqrt{(\lambda R)}$. In this case the ratio of the power flux in the reflected wave at the aerial to the incident flux is

$$\Phi_R/\Phi_I = g^2(\pi kR)^{-1}, \quad \ldots\ldots \quad (26)$$

and the power delivered to the receiver terminals is

$$P_R = \frac{P_T G^2 \lambda^3}{32\pi^4 R^3} g^2 \text{ watts}, \quad \ldots\ldots \quad (27)$$

where P_T=transmitted power and G=aerial power gain referred to an isotropic source.

§3. Homogeneous Cylinder

The case of a cylinder of constant electron density represents a considerable idealization as far as a physical meteor trail is concerned, however, it illustrates certain important features of the scattering process. The more general electron distribution of eqn. (1) is studied in §§ 5 and 6.

We will consider a dielectric cylinder of radius a and of constant dielectric constant κ.

The solution of (7) external to the cylinder is now

$$V_m = A_m \left[r^m + \left(\frac{1-\kappa}{1+\kappa} \right) a^{2m} r^{-m} \right], \quad \ldots \quad (28)$$

which reduces to (3) when we put $m=1$ and introduce the angular factor. Thus $A_m/B_m = [(1+\kappa)/(1-\kappa)]a^{-2m}$, and

$$-\frac{2j^m}{t_m} \simeq 1 + j \frac{m\,!\,(m-1)\,!\,4^m}{\pi (ka)^{2m}} \left(\frac{1+\kappa}{1-\kappa} \right). \quad \ldots \quad (29)$$

We see that $|t_m|$ is a maximum when $\kappa = -1$ and thus, at resonance, $|t_m|_{\text{res}} = 2$ for all modes.

Except near resonance only the dipole mode is significant, and even then, as we shall see, all physical damping processes tend to reduce the resonant reflection coefficient for higher modes below that for $m=1$. In this case $g_\perp \simeq |t_1|$ where

$$-\frac{2j}{t_1} \simeq 1 + \frac{4j}{\pi (ka)^2} \left(\frac{1+\kappa}{1-\kappa} \right), \quad \ldots \quad (30)$$

and $g_{\perp \text{res}} = 2$ independent of the radius of the column. The resonant scattering parameters are thus

$$d_{\text{res}} = 8\lambda/\pi, \qquad \sigma_{\text{res}} = 16 r\lambda/\pi. \quad \ldots \quad (31)$$

For parallel scattering, from (25),

$$g_{\parallel} = \pi (ka^2)(1-\kappa)/4. \quad \ldots \quad (32)$$

Ignoring higher modes than $m=1$, the ratio of reflected amplitudes for the two polarizations is

$$\frac{g_\perp}{g_{\parallel}} \simeq 2 \left| j \frac{\pi (ka)^2 (1-\kappa)}{4} - (1+\kappa) \right|^{-1}, \quad \ldots \quad (33)$$

which, except in the neighbourhood of the resonance, remembering the condition $(ka)^2 \ll 1$, reduces to the simple result (5).

At resonance,

$$g_\perp / g_{\parallel} = 4[\pi (ka)^2]^{-1}. \quad \ldots \quad (34)$$

Fig. 1 shows $g_\perp/g_{\parallel}$ as a function of $(1-\kappa)$ for various values of ka, and in fig. 2 the resonant ratio is plotted against ka. The broken part of this latter curve indicates the behaviour over the region in which the assumptions break down. This ratio, unlike the resonant reflection coefficient itself, is a function of ka. It is a measure of the magnitude of the resonance, which decreases with increasing column dimensions, becoming unity when $ka \gtrsim 1$.

The condition for resonance to be possible, namely that $\kappa=-1$ and $(ka)^2<1$ becomes $2\alpha e^2/(mc^2)<1$ or, substituting numerical values, $\alpha<2\times10^{12}$.

Fig. 1

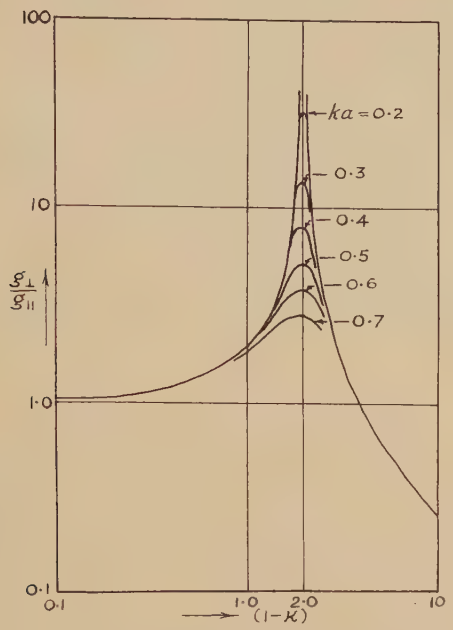

Resonance curves for a homogeneous cylinder of radius a and dielectric constant κ.

Fig. 2

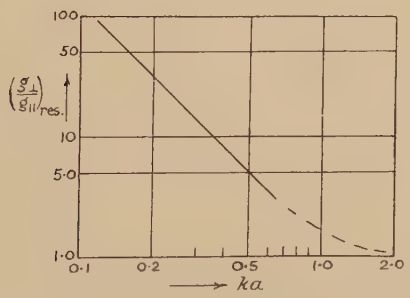

Resonant polarization ratio vs ka for a homogeneous cylinder of radius a.

When $\kappa<0$ and $|\kappa(ka)^2|\gg1$, the above formulae break down and the column tends to behave as a metallic cylinder of radius a. In this case, when $(ka)^2<1$, the condition is $\kappa\ll-1$ and the reflection coefficients become

$$g_\perp\simeq|t_1|\simeq\pi(ka)^2/2, \quad . \quad . \quad . \quad . \quad . \quad . \quad . \quad (35)$$

and

$$g_\parallel\simeq|l_0|\simeq|1-j(2/\pi)\ln(\gamma ka/2)|^{-1}, \quad . \quad . \quad . \quad . \quad . \quad (36)$$

where $\gamma=1{\cdot}781$. When $(ka)^2 \gg 1$, the scattering diameter is obtained from geometrical optics to be $d=\pi a$, and thus, from (22),

$$g_\perp = g_\parallel = (\pi ka/4)^{1/2}. \quad \ldots\ldots\ldots \quad (37)$$

If we let $(ka)^2$ tend to infinity, the cylinder tends to a plane and the condition for metallic reflection is $\kappa<0$ as we should expect. Using (35), (36) and (37) the curve of fig. 3 has been plotted by smoothly joining the three branches in the vicinity of $ka=1$.

Factors, other than the radiation damping of the cylinder oscillations connected with the finite trail dimensions, which tend to reduce the magnitude of the resonance are radiation damping of individual electron oscillations, collision damping, and the diffuseness of the column, so that (34) gives only an upper limit. We will consider only the first two in relation to the above model, leaving the third, and most important (at least for meteor echoes) to § 5. The effect of both is to introduce a complex term into the expression for the dielectric constant.

Fig. 3

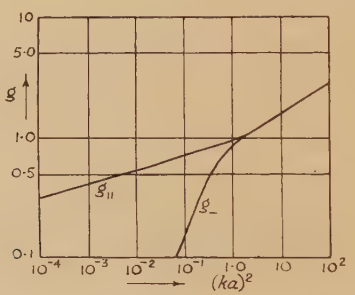

Reflection coefficients for transverse ($g_\perp$) and parallel ($g_\parallel$) scattering from a metallic cylinder of radius a.

If radiation damping of individual electrons was the sole mechanism limiting the resonance, then each electron would contribute an amount $9\lambda^2/(4\pi)$ to the scattering cross-section. Comparison with (34) shows that radiation damping could only be significant if $\lambda \lesssim 8/(3\alpha)$, which is, in fact, an impossible condition. Thus this effect will never compete with that of finite radius.

Collisions between electrons and neutral molecules leads to the following expression for the complex dielectric constant (when $\nu \ll \omega$) :

$$\left.\begin{aligned} \kappa &= 1 - \frac{4\pi e^2 n}{k^2 mc^2}\left(1 + j\frac{\nu}{\omega}\right) \\ &= \kappa_1 - j\kappa_2 \end{aligned}\right\}, \quad \ldots\ldots \quad (38)$$

where ν=collision frequency, ω=angular radio frequency. Resonance occurs when $\kappa_1 = -1$ and the resonant reflection coefficient for the dipole mode is

$$-\frac{2j}{t_1} \simeq 1 + \frac{2}{\pi(ka)^2}\frac{\nu}{\omega}. \quad \ldots\ldots\ldots \quad (39)$$

Collisions are thus significant for this mode if the radius at resonance satisfies

$$a^2 \lesssim \nu\lambda^3/(4\pi^4 \mathbf{c}). \quad \ldots\ldots\ldots \quad (40)$$

For $\lambda=4$ metres and using plausible figures for ν in the meteor ionization region, we find the radius satisfying (40) to be of the order of only a few times the molecular mean free path. Since our assumption that the column may be regarded as a continuous dielectric will restrict the radius to something greater than this, collisions will in general not be important.

We will not pursue further the discussion on collisions (except to say that the effect will be much larger for the higher modes), since the discussion in §5 reveals that in an actual meteor column the effect of its necessarily diffuse boundary will be predominant. Collision damping considerations may, of course, be important in laboratory experiments with discharge tubes of the type made by Denno, Prime, and Craggs (1950) and by Romell (1951).

§4. Fine Structure of the Plasma Resonance Spectrum

Although modes other than $m=1$ are unlikely to be of importance in connection with meteor echoes, there is a matter of some theoretical interest concerning the splitting of the resonances. As we have seen, for a homogeneous cylinder, the resonant modes are degenerate, all occurring when $\kappa=-1$ (a higher degree of approximation would in fact have shown a slight splitting, tending to disappear when $ka \to 0$). The reason for the degeneracy can be seen by writing $r^m=x$ when (7) becomes

$$\frac{d}{dx}\left[x\kappa \frac{dV_m}{dx}\right] = \frac{\kappa V_m}{x}, \quad \ldots\ldots\ldots \quad (41)$$

with the solution $V_m=A_m x+B_m x^{-1}$ outside the ionized region. In general κ will be a different function of x for each mode, hence the condition that the real part of A_m be zero will be different and the resonant modes will not be degenerate. Only for a homogeneous cylinder is κ the same function of x for all m, namely,

$$\kappa(x)=\begin{cases}\kappa=\text{const.}, & x<x_0=a^m,\\ 1, & x>x_0,\end{cases}$$

and we have $A_m/B_m=x_0^{-2}(1+\kappa)/(1-\kappa)$, irrespective of m.

Examples which show non-degenerate resonant modes are given in Appendix II.

§5. Diffuse Column of Ionization

We expect the passage of a meteor through the atmosphere to form an ionized column with initial radius of the order of the molecular mean free path. The column will then expand according to the laws of diffusion, however, since its initial temperature may greatly exceed that of the atmosphere, the diffusion coefficient, D, may be a function (decreasing)

of radius and time. For simplicity we will assume that D is constant, in which case the solution of the diffusion equation leads to the electron distribution

$$\left.\begin{aligned} n(r) &= \frac{\alpha}{4\pi Dt}\exp\left[-r^2/(4Dt)\right] \\ &= \frac{\alpha}{\pi r_0^2}\exp\left[-(r/r_0)^2\right] \end{aligned}\right\}, \quad \ldots\ldots \quad (42)$$

where $r_0^2 = 4Dt$ and we have made the simplifying assumption that at time $t=0$ there is a line distribution of ions and electrons. The effect of a radial temperature gradient may be to cause the column to have a somewhat less diffuse boundary than Gaussian, but without more information of the process involved it is difficult to estimate the extent to which this will occur.

For the electron distribution (42), we obtain

$$\left.\begin{aligned} \kappa(r) &= 1 - f\exp\left[-(r/r_0)^2\right] \\ f &= 4\alpha(e^2/mc^2)/(kr_0)^2 \end{aligned}\right\}, \quad \ldots\ldots \quad (43)$$

which is sketched in fig. 4.

Fig. 4

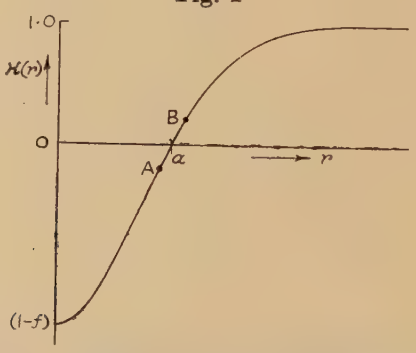

Dielectric constant of a cylindrical column with electron density a Gaussian function of radius.

The differential eqn. (7) now has singularities at $r=0$ and $r=a$, where a is the radius at which $\kappa=0$. The first is dealt with by requiring V_m to be well behaved at the origin, but the second requires a more careful study.

Consider a thin region around $r=a$. Putting $x=r^m$ in (7) we can obtain

$$\frac{d}{dx}\left(\kappa\frac{dV_m}{dx}\right) = -\kappa\frac{d}{dx}\left(\frac{V_m}{x}\right),$$

which, in this region is approximately

$$\frac{d}{dx}\left(\kappa\frac{dV_m}{dx}\right) = -\frac{\kappa}{a^m}\frac{dV_m}{dx},$$

i.e. $$\kappa\frac{dV_m}{dx} \simeq (\text{const.})\exp\left[-x/a^m\right] \simeq \text{const. when } |r-a| \ll a,$$

or

$$\kappa\frac{dV_m}{dr} \simeq h, \quad \ldots\ldots \quad (44)$$

where h is a constant.

Thus, referring to fig. 4,

$$V_{m\mathrm{B}}-V_{m\mathrm{A}}=h\int_{\mathrm{A}}^{\mathrm{B}}\kappa^{-1}\,dr. \quad . \quad . \quad . \quad . \quad . \quad . \quad (45)$$

If we express κ by (38), i.e. we consider collisions, then in the region near $r=a$ we have $\kappa_1\simeq(r-a)\kappa_1'(a)$ and κ_2 remains substantially constant. Putting $\kappa=(r-a)\kappa_1'(a)-j\kappa_2$ into (45) we have

$$\begin{aligned} V_{m\mathrm{B}}-V_{m\mathrm{A}} &= \frac{h}{\kappa_1'(a)}\,\mathrm{Ln}\left(\frac{\kappa_{\mathrm{B}}}{\kappa_{\mathrm{A}}}\right) \\ &= \frac{h}{\kappa_1'(a)}\left[\ln\left|\frac{\kappa_{\mathrm{B}}}{\kappa_{\mathrm{A}}}\right|+j(\pi-\theta)\right], \quad . \quad . \quad . \quad . \quad (46) \end{aligned}$$

where Ln denotes the complex logarithmic function and

$$0<\theta=\tan^{-1}\left[\frac{\kappa_2(\kappa_{1\mathrm{A}}-\kappa_{1\mathrm{B}})}{\kappa_{1\mathrm{A}}\kappa_{1\mathrm{B}}+\kappa_2{}^2}\right]<\pi.$$

When $\kappa_2\to 0$,

$$V_{m\mathrm{B}}-V_{m\mathrm{A}}=\frac{h}{\kappa'(a)}\left[\ln\left|\frac{\kappa_{\mathrm{B}}}{\kappa_{\mathrm{A}}}\right|+j\pi\right], \quad . \quad . \quad . \quad . \quad (47)$$

Fig. 5

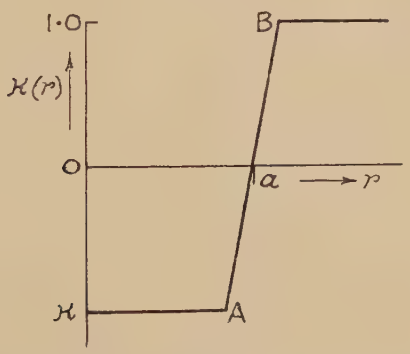

Herlofson's model of a diffuse electron distribution.

i.e. even when the collision frequency vanishes, we are left with a finite imaginary part of V_m. The physical explanation of this is that the term $\ln|\kappa_{\mathrm{B}}/\kappa_{\mathrm{A}}|$ has a maximum at $r=a$ which becomes infinite when $\kappa_2=0$, i.e. the electric field intensity becomes infinite and a negligible collision frequency can have a finite effect. The electric displacement, $\kappa\mathbf{E}$, remains finite and continuous over the region, in fact (44) is just the condition that it be so. The integral of the energy density over the region is also finite and represents a negligible proportion of the total electromagnetic energy in the column.

By a procedure of numerical integration outlined in Appendix I, and using (47) in the vicinity of the singularity, the ratio A_m/B_m may be evaluated for a given electron distribution.

Herlofson's Model of a Diffuse Column

Herlofson considers a column which is homogeneous except in a thin region near $r=a$ (fig. 5).

Within the homogeneous region we may put $V_m=r^m$ thus, from (44) $h=m\kappa a^{m-1}$ and from (47)

$$\left.\begin{aligned} V_{m\mathrm{B}}&=a^m+\frac{m\kappa a^m}{a\kappa'(a)}(j\pi-\ln|\kappa|)\\ aV_{m\mathrm{B}}{}'&=m\kappa a^m \end{aligned}\right\}. \quad . \quad . \quad . \quad . \quad . \quad (48)$$

Now, outside the column, $V_m=A_m r^m+B_m r^{-m}$,

i. e.

$$\left.\begin{aligned} V_{m\mathrm{B}}&=A_m a^m+B_m a^{-m}\\ aV_{m\mathrm{B}}{}'&=m(A_m a^m-B_m a^{-m}) \end{aligned}\right\}. \quad . \quad . \quad . \quad . \quad . \quad (49)$$

Equating the eqns. (48) with (49) we obtain

$$\frac{A_m}{B_m}\simeq a^{-2m}\frac{(1+\kappa)+[m\kappa/(a\kappa')](j\pi-\ln|\kappa|)}{(1-\kappa)+[m\kappa/(a\kappa')](j\pi-\ln|\kappa|)}, \quad . \quad . \quad . \quad (50)$$

which reduces to (51) when $a\kappa'(a)\gg 1$ and $\kappa\sim -1$.

$$\frac{A_m}{B_m}\simeq a^{-2m}\frac{(1+\kappa)+jm\pi\kappa/(a\kappa')}{1-\kappa}. \quad . \quad . \quad . \quad . \quad . \quad (51)$$

The value of $[a\kappa'(a)]^{-1}$ at resonance measures the degree of diffuseness of the column.

Substituting (51) into (20) gives

$$-\frac{2j^m}{t_m}\simeq 1+j\frac{m\,!\,(m-1)\,!\,4^m}{\pi(ka)^{2m}}\frac{(1+\kappa)+jm\pi\kappa/(a\kappa')}{(1-\kappa)}, \quad . \quad . \quad (52)$$

which is the result obtained by Herlofson (1951).

The effect of the diffuseness on the dipole resonance is significant when

$$(ka)^2 a\kappa'(a)\lesssim 2,$$

or

$$a\kappa'(a)(\boldsymbol{e}^2/\boldsymbol{mc}^2)\alpha\lesssim 1, \quad . \quad . \quad . \quad . \quad . \quad . \quad (53)$$

i.e.

$$a\kappa'(a)\lesssim\begin{cases} 3{\cdot}5, & \alpha\sim 10^{12}\\ 350, & \alpha\sim 10^{10}\end{cases}.$$

The electron distribution of fig. 6 corresponds to

$$\kappa(r)=1-f\exp[-(r/r_0)^s], \quad . \quad . \quad . \quad . \quad . \quad . \quad (54)$$

which is similar to the Herlofson model when $s\gg 1$ and is Gaussian when $s=2$. We have $(a/r_0)^s=\ln f$, $a\kappa'(a)=s\ln f$.

At resonance, when $s\gg 1$, $f=2$ and

$$a\kappa'(a)=0{\cdot}69s. \quad . \quad . \quad . \quad . \quad . \quad . \quad . \quad . \quad (55)$$

Thus, unless the distribution has a significantly sharper boundary than Gaussian, the diffuseness will in general be the major limiting factor. The diffuseness limited reflection coefficients using (20), (50), and (55), are

$$|t_m|_{\mathrm{res}}\simeq\frac{2(ka)^{2m}}{(m\,!)^2 4^m}|2s\ln 2-jm\pi|, \quad . \quad . \quad . \quad . \quad (56)$$

$$|t_1|_{\mathrm{res}}\simeq\frac{(ka)^2}{2}|2s\ln 2-j\pi|$$

$$\simeq\alpha(\boldsymbol{e}^2/\boldsymbol{mc}^2)|2s\ln 2-j\pi|. \quad . \quad . \quad . \quad . \quad . \quad (57)$$

It is clear from (56) that the diffuseness tends to eliminate the higher modes.

Using (25) and (57), ignoring modes other than $m=1$ the ratio of the resonant reflection coefficients for the two polarizations is

$$(g_\perp/g_\parallel)_{\text{res}} \simeq |\, 0{\cdot}44s-j\,|, \qquad \ldots\ldots\ldots \quad (58)$$

which is plotted in fig. 9, curve (*b*).

The resonance phenomenon will result in the column acting as a frequency selective reflector and hence a bandwidth can be assigned to it. We can show that the reflection coefficient is reduced to $1/\sqrt{2}$ times its resonant value when the angular frequency differs from the resonant frequency by $\delta\omega$ given by

$$\omega_{\text{res}}/\delta\omega = 2(g_\perp/g_\parallel)_{\text{res}}. \qquad \ldots\ldots\ldots \quad (59)$$

Fig. 6

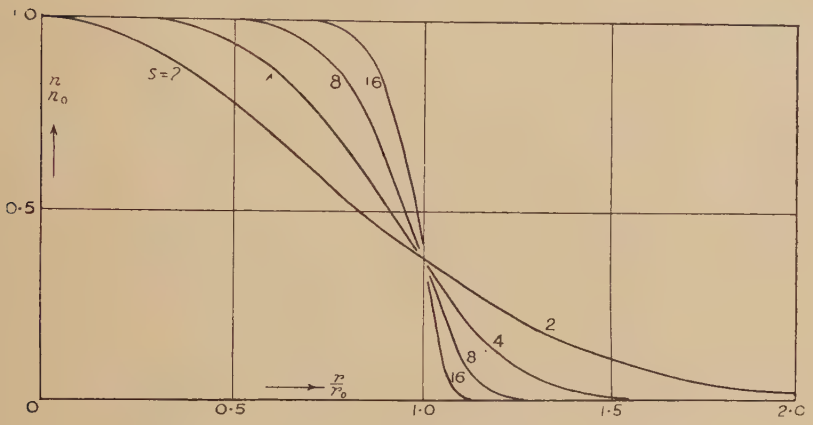

Electron density $n=n_0 \exp[-(r/r_0)^s]$ for various s.

§6. Gaussian Electron Distribution

Because of the physical importance of this distribution we have considered the reflection problem in detail, and over a wide range of α and r_0.

(*a*) *Dilute Column*

The column is termed dilute when $(1-\kappa) \ll 1$ throughout, in which case the incident wave penetrates the column without modification. Substituting for κ from (43), the condition for diluteness is

$$(kr_0)^2 \gg 11{\cdot}24 \times 10^{-13}\alpha. \qquad \ldots\ldots\ldots \quad (60)$$

The reflection coefficient is independent of polarization, being given by (25) when $(kr_0)^2 \ll 1$, and in general by

$$g_\parallel = g_\perp = \pi\alpha(\boldsymbol{e}^2/\boldsymbol{mc}^2) \exp[-(kr_0)^2], \qquad \ldots\ldots \quad (61)$$

where the exponential decay results from phase differences within the column (Herlofson 1951).

(*b*) *Line Density* $\alpha < 2{\cdot}4 \times 10^{12}$ cm^{-1}

Eqns. (7) and (25) are valid only when $(kr_0)^2 \ll 1$ and if $|\kappa(kr)^2| \ll 1$ throughout the column, which latter condition requires $\alpha \ll 2{\cdot}4 \times 10^{12}$.

Subject to these restrictions, from (25)

$$g_{\parallel} = \pi(kr_0)^2 f/4. \quad . \quad . \quad . \quad . \quad . \quad . \quad . \quad . \quad (62)$$

Transverse scattering requires the solution of (7) for the dipole mode, $m=1$, which we have evaluated numerically for a range of values of f. Because of the diffuse character of the column both A_1 and B_1 are complex quantities and within the limits imposed by $(kr_0)^2 \ll 1$ the diffuseness is the main limiting factor, while for $(kr_0)^2 > 1$ the resonance disappears.

Thus

$$g_{\perp} \simeq |t_1| \simeq 2\left|1 + \frac{4j}{\pi(kr_0)^2}\frac{A'}{B'}\right|^{-1}, \quad . \quad . \quad . \quad . \quad . \quad . \quad (63)$$

where $A_1 = A' r_0^{-1}$, $B_1 = B' r_0$.

Fig. 7

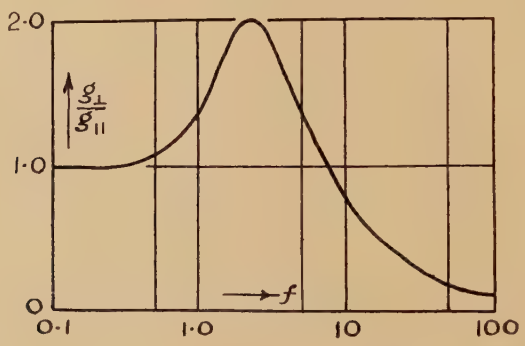

Polarization ratio vs f for a Gaussian cylinder, when the resonance is diffuseness limited.

From (62) and (63) the polarization ratio when the resonance is diffuseness limited is

$$g_{\perp}/g_{\parallel} \simeq \frac{2}{f}\left|\frac{B'}{A'}\right|. \quad . \quad . \quad . \quad . \quad . \quad . \quad . \quad . \quad (64)$$

The values of A' and B' are given in Appendix I together with a description of the method by which they were obtained. The resonance condition is $Re\,(A')=0$, which occurs when $f=2{\cdot}4$, i.e. when the dielectric constant on the axis is $-1{\cdot}4$. Using the computed values of A' and B' with (64), we have plotted $g_{\perp}/g_{\parallel}$ as a function of f in fig. 7 which shows that the resonant ratio is reduced to 2·0 by the diffuse boundary.

From (43), (62), and (63) we can determine $g_{\perp}/g_{\parallel}$ as a function of $(kr_0)^2/\alpha$, which is given in fig. 8 for various values of α. Since $r_0^2 = 4Dt$, fig. 8 represents the form of the time envelope of the echo obtained with transverse polarization from a column of α electrons per cm.

We have also evaluated the solution of (7) in the vicinity of the resonance for the more general distribution, (54). The diffuseness limited resonant

Fig. 8

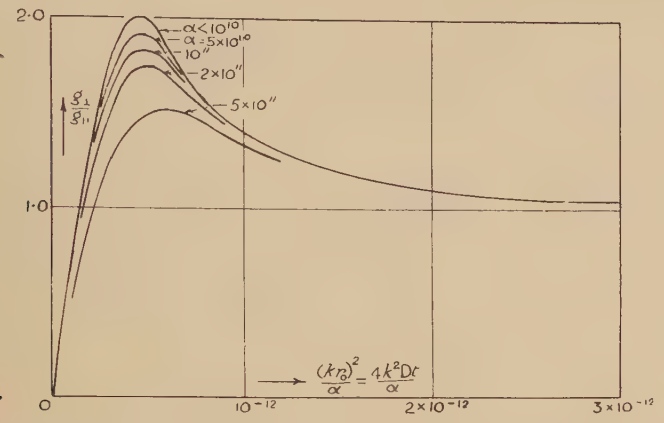

Polarization ratio vs $(kr_0)^2/\alpha = 4k^2Dt/\alpha$ for various values of the electron line density, α.

Fig. 9

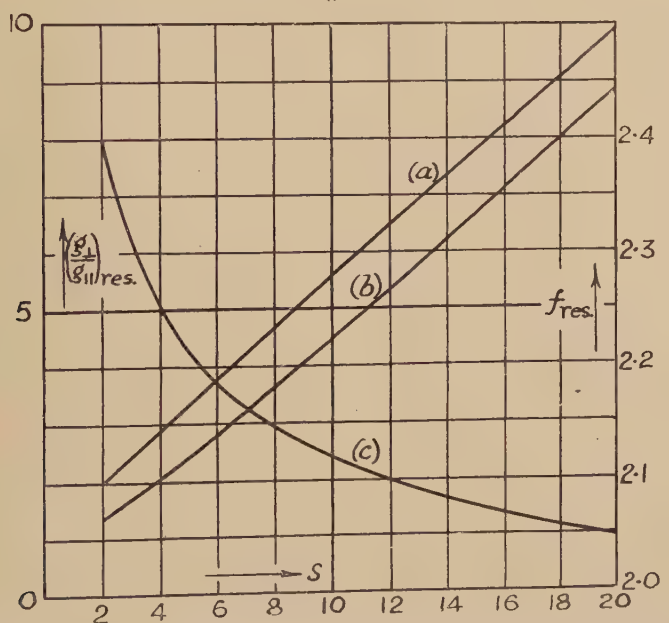

Cylindrical column with electron distribution $n = n_0 \exp[-(r/r_0)^8]$

(*a*) Diffuseness limited resonant polarization ratio, computed as described in Appendix I.

(*b*) Diffuseness limited resonant polarization ratio derived from Herlofson's model.

(*c*) Resonance condition, f_{res} vs s, ($1-f$ = axial dielectric constant),

ratio is plotted in fig. 9 (curve (*a*)) as a function of s, together with the values obtained from the Herlofson model (curve (*b*)). The value of f at resonance, as a function of s, is also plotted in fig. 9 (curve (*c*)), which indicates that $f_{res} \to 2$ when $s \to \infty$.

When $\alpha \ll 2{\cdot}4 \times 10^{12}$ and $(kr_0)^2 > 1$, we see that (60) is automatically satisfied and the reflection coefficients follow (61), completing the description of echo amplitude as a function of $(kr_0)^2$.

(*c*) *Line Density* $\alpha > 2{\cdot}4 \times 10^{12}$

We may now have the conditions $\kappa < 0$ and $|\kappa(kr)^2| \gg 1$ over a region within the column. For a homogeneous cylinder, as we have seen, this is just the condition for metallic reflection. We will assume here that the Gaussian column behaves as a metallic cylinder of radius r_c given by the larger of the two values satisfying

$$\kappa(r_c)(kr_c)^2 = -1, \quad . \quad . \quad . \quad . \quad . \quad . \quad . \quad . \quad (65)$$

which expresses r_c as a function of r_0 for given α.

The justification for this assumption may be seen as follows. When $(kr_c)^2 \gg 1$ it is obvious, since r_c becomes the radius at which $\kappa = 0$ and the problem can be treated by geometrical optics with reflection taking place at the surface of critical density. When $(kr_c)^2 \lesssim 1$ we still expect the column to behave as a metallic cylinder and (65) must at least give the order of magnitude of the equivalent radius. In fact the reflection coefficients derived using this radius join smoothly in the region of $\alpha = 2 \times 10^{12}$ to those obtained in (*b*) above.

Solving (65) for r_c and using fig. 3 with $r_c = a$ we find the reflection coefficients as a function of $(kr_0)^2$.

When the column has expanded to a radius satisfying (61), exponential decay will set in, and we can join the solution as obtained above with that of (*a*). This is not important when $\alpha > 10^{13}$, since the coefficient as determined above remains large compared with (60) out to some radius and then drops sharply.

Approximate expressions for the maximum reflection coefficient and duration, τ, are

$$g_{max} \simeq 7{\cdot}1 \times 10^{-4} \alpha^{1{\cdot}4}, \quad . \quad . \quad . \quad . \quad . \quad . \quad . \quad (66)$$

$$4k^2 D\tau \simeq 11{\cdot}24 \times 10^{-13} \alpha. \quad . \quad . \quad . \quad . \quad . \quad . \quad . \quad (67)$$

(*d*) *No Restriction on Line Density and Radius*

By joining smoothly the solutions for the two ranges of line density to each other and to the dilute column solution we obtain the complete result given in fig. 10, which gives both transverse and parallel reflection coefficients for a Gaussian electron distribution, without restriction on line density or column radius. In fig. 11 we have sketched some of the curves of fig. 10 with linear scales. These curves give the predicted form of the time envelope of the echoes.

Fig. 10

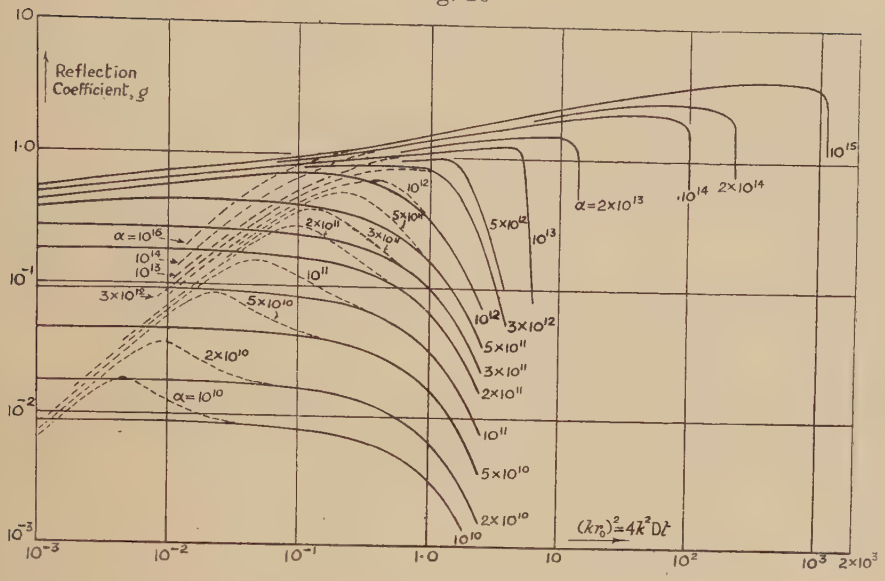

——— Parallel scattering.
– – – – – Transverse scattering.

Reflection coefficients vs $(kr_0)^2 = 4k^2Dt$ for a Gaussian cylinder having electron density α, plotted with logarithmic scales.

Fig. 11

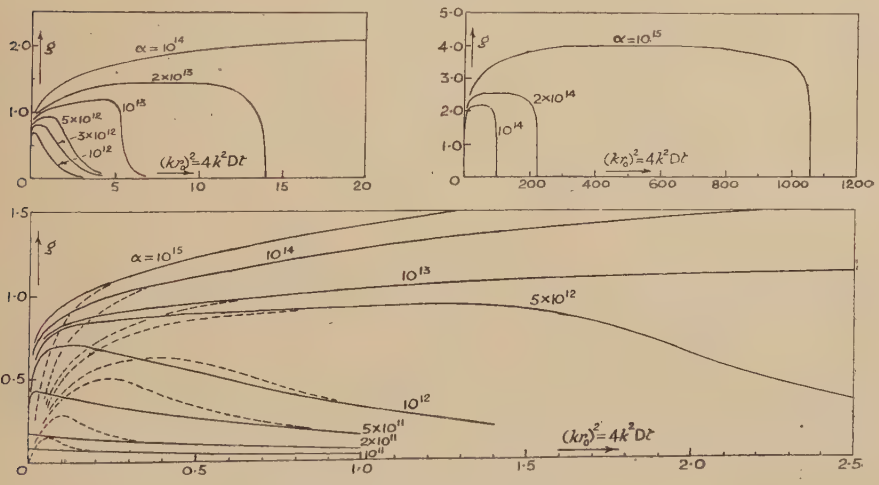

——— Parallel scattering.
– – – – – Transverse scattering.

As for fig. 10, but with linear scales. These curves give the expected amplitude-time envelope of the received echo, assuming the meteor instantaneously to form a narrow column of electrons which expands radially at a rate determined by the diffusion coefficient, D.

§ 7. Discussion

The complete scheme outlined in fig. 10 has obvious application to the analysis of experimental results, particularly to the derivation of diffusion coefficients, electron line densities, etc. from observed echo amplitudes and durations.

Certain important features are immediately apparent.

As predicted by Herlofson we may expect a resonance phenomenon for transverse scattering to be exhibited by columns having line densities of less than 10^{12} cm^{-1}. The resonant amplitude will depend on the diffuseness of the column, being about twice the parallel scattering amplitude for a Gaussian electron distribution and increasing for trails with sharper boundaries. Such resonances have been detected by Clegg and Closs (1951) who find resonant ratios of the expected order of magnitude. Larger ratios than 2 may also be associated with an anisotropy in the diffusion coefficient caused by the earth's magnetic field. A solution of the scattering problem for a thin diffuse elliptic cylinder will be given in a second paper, when it will be shown that quite a small anisotropy may lead, under certain conditions, to a significant increase in the resonant ratio.

We mentioned, in connection with collision damping, that we expect the column to be formed with a certain minimum radius and it was sufficient for the previous argument to consider this as set by the finite molecular mean free path. Another limit is set by the finite meteor velocity, since if we consider its formation we find that the column deviates from the ideal picture of an infinite cylinder. We cannot, in fact, consider the column as an infinite cylinder until it at least fills the first Fresnel zone of length $\sqrt{(\lambda R/2)}$, situated symmetrically about the normal from the observer to its axis. In the time taken by the meteor to traverse this distance, diffusion will have taken place and the trail will be in the form of a paraboloid of revolution, of average square radius (over the Fresnel zone)

$$r_{0\,\mathrm{min}}^{2} = D\sqrt{(2\lambda R)}/v, \quad . \quad . \quad . \quad . \quad . \quad . \quad . \quad (68)$$

where v is the meteor velocity. We may regard $r_{0\mathrm{min}}$ as an effective lower limit to the column radius set by the finite velocity and for a typical case, with $\lambda = 4$m, $R = 150$ km, $v = 40$ km/s, $D = 3 \times 10^4$ c.g.s. units (as determined from echo durations at a height of 85 km) we get $r_0 \sim 28$ cm, which considerably exceeds the mean free path at this height. For the above parameters $(kr_0)^2_{\mathrm{min}} \sim 0{\cdot}2$, thus, referring to fig. 10, the smallest meteor exhibiting a polarization effect will be one producing a few times 10^{11} electrons per cm. The apparatus of Clegg and Closs (1951) was sufficiently sensitive to detect a reflection coefficient of about 0·1, i.e. a line density of 10^{11} with parallel scattering. It is not therefore surprising that a substantial number of the short duration echoes appeared to exhibit ratios, $g_\perp/g_{\parallel}$, greater than unity. Fig. 10 indicates that we would expect initial ratios of less than unity for some echoes and a few such examples have been observed.

It is of interest to compare the durations of echoes having different line densities. In fig. 12 we have plotted $4k^2D\tau$ (where τ is the duration to exp (-1) times maximum amplitude) against α. For a given diffusion coefficient, the duration is almost independent of line density up to $\alpha=10^{12}$ and then increases approximately proportionately to α. This agrees well with the experimental observation that at a given height most echoes have about the same duration except for a few which persist for a longer time (up to several hundred times as long). With the previous parameters we find $\tau=0{\cdot}03$ sec for $\alpha<10^{12}$ and $\tau=30$ sec for $\alpha=10^{15}$.

In fig. 12 we have also plotted the maximum reflection coefficient against α. It increases approximately linearly up to $\alpha=10^{12}$ and then much more slowly ($\sim\alpha^{1/4}$). This again is in agreement with observation.

The ideal picture of a uniform cylindrical column of ionization fails to take account of any distortion of the trail which may occur through atmospheric turbulence. Such effects have been considered by Greenhow

Fig. 12

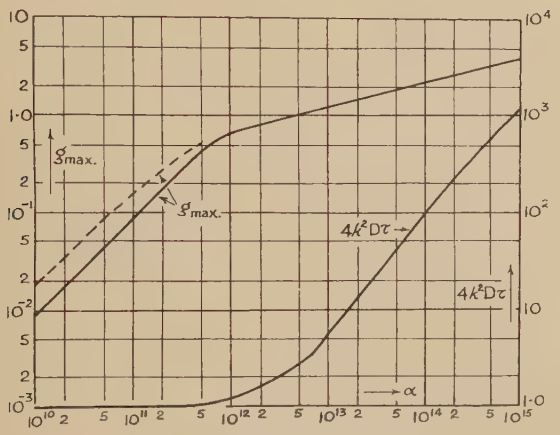

——— Parallel scattering.
– – – – – Transverse scattering.

Echo amplitude reflection coefficient g, and duration τ, vs electron line density.

(1950) as an explanation of the amplitude fluctuations which occur with almost all long duration echoes. The theory given here supports the view of Greenhow against that of other authors (notably Feinstein 1951) who suggest that fluctuations may derive from interference between waves reflected at different levels in an expanding column. For this purpose it is necessary to postulate a fairly sharp boundary to the cylinder, since it is clear from (61) that no such effect exists for a Gaussian electron distribution. Now the long duration echoes, on the above theory (and irrespective of the radial electron distribution), correspond to columns which are so dense that they behave like an expanding metallic cylinder and it is clear from fig. 3 that they will not exhibit fluctuations (at least during the main body of the echo), unless disturbed in some manner. Only short

duration echoes ($\tau \sim 0{\cdot}03$ sec with the previous parameters) could exhibit fluctuations of the type suggested by Feinstein and the fact that they are not observed favours a Gaussian, or near Gaussian, distribution. Both atmospheric turbulence and loss of electrons by attachment (which may be important at the lower heights) may reduce the amplitudes and durations of very dense columns, particularly on long wavelengths.

Summarizing the above, we may say that a qualitative change occurs in the character of the echoes at line densities in the vicinity of a few times 10^{12} per cm, which result, surprisingly enough, is independent of both wavelength and diffusion coefficient. When α is less than 10^{12}, the echo amplitude for parallel scattering obeys the Lovell–Clegg law with an exponential decay, while that for transverse scattering exhibits a resonance phenomenon when the axial electron density corresponds to a dielectric constant of $-1{\cdot}4$ (for a Gaussian distribution). In addition, the echo duration is independent of α, being a function only of λ and D, while the maximum echo amplitude is proportional to α. These are the typical short duration echoes which form the bulk of the experimental observations. When $\alpha \gg 10^{12}$, the meteor trail reflects as a metallic cylinder and, while $(kr_0)^2 \ll 1$, the echo amplitude for parallel scattering exceeds that for transverse. The duration is approximately proportional to α, while the maximum amplitude is only a slowly increasing function of α. These are the columns which give rise to the long duration echoes (up to several minutes) studied by Greenhow (1950). An important result of this is that it enables us to determine α (when $\alpha > 10^{13}$) independently of the equipment parameters, provided that D is known.

The method developed for the solution of the wave equation, namely the reduction of the problem to a formal electrostatic one, while restricted as to the dimensions of the scatterer, nevertheless has a certain generality. The solution may be obtained for any given dielectric constant as a function of radius and may be extended to geometrical shapes other than the circular cylinder, for instance the diffuse sphere of Appendix II. In a later paper the same general technique will be applied to the problem of scattering from a thin diffuse column of elliptical cross-section.

The theory is also of importance in connection with laboratory experiments with discharge tubes such as have been made by Romell (1951) and by Denno, Prime and Craggs (1950), both in the analysis of results and in suggesting new experiments. For instance Appendix II enables account to be taken of the walls of the discharge tube, and also suggests that it may be of interest to study a discharge confined between concentric tubes. In this latter case we can arrange for the dielectric constant at resonance to range between 0 and $-\infty$ and in principle have a method of verifying the relation (2) over this range. This may make possible, in particular, an experimental test of the existence or otherwise of the Lorentz term for a neutral plasma (Darwin 1934, 1944). Providing that collision damping is not prohibitive, the removal of the mode degeneracy should enable the higher order resonant modes to be detected.

Acknowledgments

We are indebted to Dr. R. E. B. Makinson and to Dr. N. Herlofson for helpful discussions and suggestions concerning the plasma resonance phenomenon, in particular to the former for his suggestion of a formal electrostatic approach to the problem of transverse scattering from a thin ionized column.

We would emphasize the great value of our intimate association with the experimental meteor research programme at the Jodrell Bank Experimental Station under the direction of Professor A. C. B. Lovell, which besides providing the stimulus for a theoretical study of meteor echoes, enabled us to benefit from the continued interest and advice of many colleagues, amongst whom we must especially mention Dr. J. A. Clegg.

References

Clegg, J. A., and Closs, R. L., 1951, *Proc. Phys. Soc.* B, **64,** 718.
Darwin, C. A., 1934, *Proc. Roy. Soc.* A, **146,** 17 ; 1943, *Proc. Roy. Soc.* A, **182,** 152.
Denno, S. N., Prime, H. A., and Craggs, J. D., 1950, *Proc. Phys. Soc.* B, **63,** 726.
Feinstein, J., 1951, *Jour. Geophys. Res.*, **56,** 37.
Greenhow, J. S., 1950, *Phil. Mag.*, **41,** 682.
Herlofson, N., 1951, *Arkiv För Fysik*, **3,** 247.
Lovell, A. C. B., 1948, *Phys. Soc. Rep. Prog. Phys.*, **11,** 415.
Lovell, A. C. B., and Clegg, J. A., 1948, *Proc. Phys. Soc.*, **60,** 491.
Romell, D., 1951, *Nature*, **167,** 243.
Stratton, J. A., 1941, *Electromagnetic Theory*, 564 (New York and London : McGraw-Hill).

APPENDIX I

Evaluation of the Reflection Coefficients for an Electron Density Proportional to $\exp[-(r/r_0)^s]$

This defines a cylindrical column of electrons, the diffuseness of which depends on s, and leads to the relation (54) for $\kappa(r)$. Writing $\rho=r/r_0$, (54) becomes

$$\kappa(\rho)=1-f\exp(-\rho^s). \quad . \quad . \quad . \quad . \quad . \quad . \quad . \quad (69)$$

We are concerned only with the dipole mode, hence the differential equation to be solved is, from (7)

$$\frac{d}{d\rho}\left(\rho\kappa\frac{dV}{d\rho}\right)=\frac{\kappa V}{\rho}, \quad . \quad . \quad . \quad . \quad . \quad . \quad . \quad (70)$$

where the mode subscript has been dropped.

External to the column, $\kappa=1$, and we may write $V=A'\rho+B'\rho^{-1}$, where A' and B' are the parameters in the equation (63) for the transverse

reflection coefficient ((63), although derived for a Gaussian electron distribution, is valid for all s).

From (25), the parallel scattering reflection coefficient is

$$g_{\parallel}=\frac{\pi}{4}f(kr_0)^2\int_0^{\infty}\exp\left(-x^{s/2}\right)dx=\frac{\pi(2/s)\,!}{4}\,f(kr_0)^2, \quad . \quad . \quad (71)$$

where $x=\rho^2$. Using (63) and (71), the ratio of reflection coefficients when the resonance is diffuseness limited is

$$\frac{g_{\perp}}{g_{\parallel}}=\frac{2}{(2/s)\,!\,f}\left|\frac{B'}{A'}\right|, \quad . \quad . \quad . \quad . \quad . \quad . \quad . \quad (72)$$

reducing to (64) when $s=2$.

To determine A' and B', V must be expressed as a function of ρ. When $\rho\ll 1$, $\kappa\simeq$ const. and the solution of (70) in the vicinity of the origin may be taken as $V\simeq\rho$. Hence, when $\rho=0$ we have $V=0$, $V'=1$, $\kappa V/\rho=\kappa(0)$. Integration of (70) thus gives

$$\left.\begin{aligned}\rho\kappa V'&=\int_0^{\varrho}\frac{\kappa V}{\rho}\,d\rho,\\ V&=\int_0^{\varrho}V'd\rho,\end{aligned}\right\} \quad . \quad . \quad . \quad . \quad . \quad . \quad . \quad (73)$$

where the prime here refers to differentiation with respect to ρ.

By commencing at the origin and taking successive small increments in ρ we can, with the help of (73), evaluate V, point by point, using a method of successive approximations. Suppose V and V' are known for $\rho=\rho_1$, then they may be evaluated when $\rho=\rho_2=\rho_1+\delta\rho$ as follows. We assume a value for $(\kappa V/\rho)_2$ whence

$$\begin{aligned}(\rho\kappa V')_2&\simeq(\rho\kappa V')_1+\frac{\delta\rho}{2}\left[(\kappa V/\rho)_1+(\kappa V/\rho)_2\right]\\ &=(\rho\kappa V')_1+\delta(\rho\kappa V'), \quad . \quad . \quad . \quad . \quad . \quad . \quad . \quad . \quad (74)\end{aligned}$$

(where subscripts 1 and 2 refer to values at ρ_1 and ρ_2 respectively).

From (74) we find $V'(\rho_2)$ and hence

$$\begin{aligned}V(\rho_2)&\simeq V(\rho_1)+\frac{\delta\rho}{2}\left[V'(\rho_1)+V'(\rho_2)\right]\\ &=V(\rho_1)+\delta V. \quad . \quad . \quad . \quad . \quad . \quad . \quad . \quad . \quad . \quad (75)\end{aligned}$$

From (75) we obtain a second approximation to $(\kappa V/\rho)_2$ and we repeat the sequence until sufficient accuracy is achieved. By carefully choosing the first approximation we never need, in practice, go beyond the second. The only error remaining is that involved in the approximate integrations (74) and (75), which may be made as small as we please by taking a sufficiently small increment, $\delta\rho$.

The procedure is illustrated in table 1 for the example $s=4$, $f=2$. Table 1 (a) is restricted to the range $\rho<0{\cdot}9124$; i.e. $\kappa<0$, since when $\kappa=0$ both V and V' go to infinity, while $\rho\kappa V'$ passes through a broad minimum.

Table 1. Evaluation of V as a Function of ρ for $\kappa(\rho)=1-2\exp(-\rho^4)$

1 (*a*)

ρ	$\kappa(\rho)$	$\kappa V/\rho$	$\delta(\rho\kappa V')$	$\rho\kappa V'$	V'	δV	V	$\kappa V/\rho$
0	−1	−1	—	0	1	—	0	—
0·2	−1	−1	—	−0·2	1	—	0·2	—
0·4	−0·950	−0·95	−0·195	−0·395	1·040	0·204	0·404	−0·959
—	—	−0·959	−0·196	−0·396	1·041	0·204	0·404	−0·959
0·5	−0·879	−0·90	−0·093	−0·489	1·113	0·1077	0·5117	−0·900
0·86	−0·1574	−0·21	−0·0049	−0·7149	5·28	0·0920	1·2007	−0·220
—	—	−0·220	−0·0050	−0·7150	5·28	0·0920	1·2007	−0·220
0·88	−0·0980	−0·14	−0·0036	−0·7186	8·33	0·1361	1·3368	−0·1487
—	—	−0·1487	−0·0037	−0·7187	8·33	0·1361	1·3368	−0·1487

Table 1 (*b*)

ρ	$\kappa(\rho)$	$\kappa V_R/\rho$	$\delta(\rho\kappa V_R')$	$\rho\kappa V_R'$	V_R'	δV_R	V_R	$\kappa V_R/\rho$
0·94	0·0834	0·1222	—	—0·715	—9·13	—	1·379	—
0·96	0·1442	0·186	0·00308	—0·7119	—5·14	—0·1427	1·2363	0·1859
1·50	0·9874	0·452	0·0473	—0·4665	—0·3145	—0·0349	0·6873	0·4525
1·60	0·9972	0·408	0·0430	—0·4235	—0·2652	—0·0290	0·6583	0·410
—	—	0·410	0·0431	—0·4234	—0·2652	—0·0290	0·6583	0·410
1·70	0·9996	0·374	0·0392	—0·3842	0·226	—0·0246	0·6337	0·3725
—	—	0·3725	0·0391	—0·3843	—0·226	—0·0246	0·6337	0·3725

Table 1 (*c*)

ρ	$\kappa(\rho)$	$\kappa V_I/\rho$	$\delta(\rho\kappa V_I')$	$\rho\kappa V_I'$	V_I'	δV_I	V_I	$\kappa V/\rho$
0·9124	0	0	—	0	0	—	—0·815	0
0·94	0·0834	—0·0723	—0·00100	—0·00100	—0·01273	—0·0002	—0·8152	—0·0723
0·96	0·1442	—0·1227	—0·00195	—0·00295	—0·02130	—0·0003	—0·8155	—0·1227
1·50	0·9874	—0·574	—0·0580	—0·2571	—0·1737	—0·0161	—0·8710	0·574
1·60	0·9972	—0·555	—0·0564	—0·3135	—0·1962	—0·0185	—0·8895	—0·555
1·70	0·9996	—0·535	—0·0545	—0·3680	—0·2164	—0·0206	—0·9101	—0·535

In order to bypass the singularity we use (47) which becomes

$$V_B = V_A + \left(\frac{\rho\kappa V'}{s\rho^s}\right)_{\kappa=0}\left(\ln\left|\frac{\kappa_B}{\kappa_A}\right| + j\pi\right)$$
$$= V_{BR} + jV_{BI}. \quad \ldots\ldots\ldots\ldots \quad (76)$$

In the example we put

$$\rho_A = 0{\cdot}88, \quad \kappa_A = -0{\cdot}0980, \quad V_A = 1{\cdot}337, \quad (\rho\kappa V')_{\kappa=0} = -0{\cdot}715,$$

and the real and imaginary parts of V and V', in the vicinity of the singularity become

$$\left.\begin{aligned} V_R &\simeq 0{\cdot}734 - 0{\cdot}2595 \ln|\kappa| \\ V_R' &\simeq -0{\cdot}715/(\rho\kappa) \end{aligned}\right\}, \quad \ldots\ldots \quad (77)$$

$$V_I \simeq -0{\cdot}815, \qquad V_I' = 0. \quad \ldots\ldots\ldots \quad (78)$$

We evaluate V_R and V_I separately. Using (77) and (78) we obtain the values in the first rows of tables 1 (*b*) and 1 (*c*) respectively, and then proceed as before until κ is effectively unity.

External to the column, $V_R = A_R'\rho + B_R'\rho^{-1}$, and, since $\kappa = 1$,

$$2A_R' = \kappa V_R/\rho + V_R', \qquad 2B_R' = \rho(V_R - \rho\kappa V_R'), \quad \ldots \quad (79)$$

and similarly for A_I' and B_I', where $A' = A_R' + jA_I'$, $B' = B_R' + jB_I'$. From the last rows of tables 1 (*b*) and 1 (*c*), we get $A_R' = 0{\cdot}073$, $B_R' = 0{\cdot}866$, $A_I' = -0{\cdot}376$, $B_I' = -0{\cdot}461$, hence $|B'/A'| = 2{\cdot}56$. Using (72) with $(\frac{1}{2})! = \sqrt{\pi}/2$ (for $s = 4$), we obtain $g_\perp/g_\parallel = 2{\cdot}89$.

The same procedure has been carried through for $s = 2$, and a wide range of values of f, leading to the values of A_R'/B_R', A_I'/B_R', B_I'/B_R', plotted in fig. 13. When f decreases towards unity, both A_I' and B_I' tend to infinity, however, it is not difficult to show that $A_I'/B_I' = A_R'/B_R'$ at $f = 1$. When $f < 1$, of course, both A_I' and B_I' are zero.

For other s, the solutions have been evaluated in the vicinity of the resonance and fig. 14 gives the values of A_I'/B_R', B_I'/B_R', for the resonant condition ($A_R' = 0$), as a function of s.

It is clear that the above method of numerical integration is generally applicable to the solution of (7) for all modes and for any electron density distribution which is a function only of radius.

APPENDIX II

Some Particular Electron Distributions Exhibiting Multipole Resonances

(*a*) *Stepped Cylindrical Column*

We will put $\kappa = \kappa_1$, when $0 < r < a$ and $\kappa = \kappa_2$ when $a < r < b$.

The solution of (7), external to the column, is $V_m = A_m r^m + B_m r^{-m}$, where

$$\frac{A_m}{B_m} = \frac{1}{b^{2m}} \frac{b^{2m}(\kappa_2+\kappa_1)(1+\kappa_2) + a^{2m}(\kappa_2-\kappa_1)(1-\kappa_2)}{b^{2m}(\kappa_2+\kappa_1)(1-\kappa_2) + a^{2m}(\kappa_2-\kappa_1)(1+\kappa_2)}. \quad \ldots \quad (80)$$

Eqn. (20) then gives the reflection coefficient for the various modes, and, if both κ_1 and κ_2 are real, resonance occurs when the numerator of (80) is zero.

This result may be useful in connection with laboratory experiments using discharge tubes since it enables account to be taken of the glass walls

Fig. 13

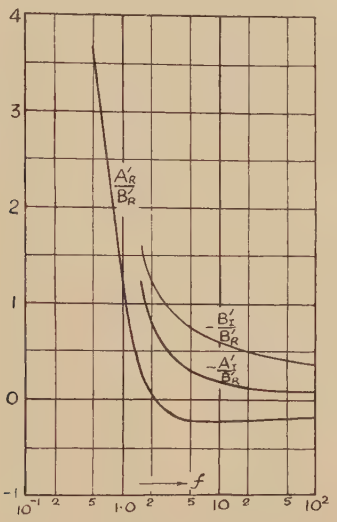

Fig. 14

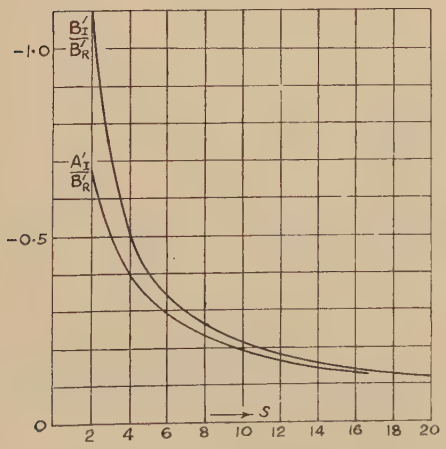

by making κ_2 the dielectric constant of the glass, a and b the inner and outer radii of the tube, and κ_1 the dielectric constant within the discharge. The presence of the glass walls has the effect of removing the degeneracy of the resonant modes, however the splitting would seem too small and in the wrong direction, to explain the subsidiary resonances observed by Romell (1950).

The case of $\kappa_1=1$, $\kappa_2=\kappa<1$, corresponding to a plasma confined between concentric tubes, is of some interest. We obtain

$$\frac{A_m}{B_m}=\frac{1}{b^{2m}}\frac{b^{2m}(1+\kappa)^2-a^{2m}(1-\kappa)^2}{(b^{2m}-a^{2m})(1-\kappa^2)}, \quad \ldots\ldots \quad (81)$$

and resonance occurs when $\kappa=\kappa_a$ and $\kappa=\kappa_b$ where

$$\kappa_a=\kappa_b{}^{-1}=(a^m-b^m)/(a^m+b^m), \quad \ldots\ldots \quad (82)$$

i.e. there are two resonances for each mode, $0>\kappa_a>-1$, and $-1>\kappa_b>-\infty$ and as $m\to\infty$ they crowd towards $\kappa=-1$. The degeneracy is again removed and, when b/a approaches unity, considerable separation of the first few resonant modes may be expected. The values of κ at resonance are given, for the first few modes, in fig. 15, for $b/a=1{\cdot}5$.

Fig. 15

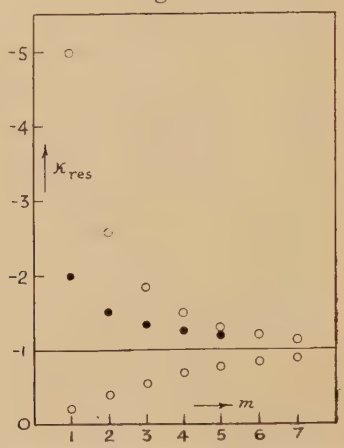

○—Multipole resonance conditions for an ionized annular cylinder having external and internal radii in the ratio 3/2.

●—Multipole resonance conditions for a diffuse spherical distribution of ionization.

The above result suggests an experiment (see § 7) to determine the magnitude of the disputed Lorentz term in the expression for κ, namely

$$\kappa=1-\frac{4\pi n\boldsymbol{e}^2}{k^2\boldsymbol{mc}^2+p4\pi n\boldsymbol{e}^2}. \quad \ldots\ldots \quad (83)$$

The factor p, which we have taken as zero, is given the value 1/3 by some authors. From (83), we see that when $n\to\infty$, $\kappa\to 1-p^{-1}$, i.e. if $p=1/3$, $\kappa\not<-2$. If p is finite then, as b/a is increased towards unity, the resonance defined by κ_b in (82) will, at some point, disappear, even for the highest electron densities.

(*b*) *Spherical Electron Cloud*

An approximate solution of the scattering of an electromagnetic wave from a small ($(kr)^2\ll 1$) spherical cloud of electrons may be obtained by a similar technique to that used above for cylinders. We will give only an outline of the method.

We consider, first, a sphere of dielectric constant, $\kappa(r)$, centred at the origin of spherical coordinates. If the incident wave is propagated along the z-axis and polarized parallel to the x-axis, the appropriate potential function is

$$V=\Sigma V_m \cos\phi P_m^1(\cos\theta), \quad \ldots\ldots \quad (84)$$

where P_m^1 is an associate Legendre Function and V_m is the solution of

$$\frac{d}{dr}\left(\kappa r^2 \frac{dV_m}{dr}\right)=m(m+1)\kappa V_m. \quad \ldots\ldots \quad (85)$$

These correspond to the eqns. (8) and (7) for the cylinder and (85) may be integrated numerically for any given $\kappa(r)$ in a similar manner to (7) (see Appendix I).

External to the sphere, $\kappa=1$, and we find

$$V_m=A_m r^m+B_m r^{-(m+1)}. \quad \ldots\ldots \quad (86)$$

The exact form of the solution external to the sphere is more difficult to obtain than before since the phase of the incident wave is not independent of any coordinate and we need to express a unit vector plane wave as a set of spherical waves. The total electric field components external to the sphere are given by Stratton (1941). Replacing the spherical Bessel functions in Stratton's expressions by their approximate values when $(kr)^2 \ll 1$ and comparing the result with the field components derived from (86), we obtain the following expression for the reflection coefficient, a_m.

$$-\frac{1}{a_m}\simeq 1+j\frac{m(2m)\,!\,(2m+1)\,!}{4^m(m+1)(m\,!)^2k^{2m+1}}\frac{A_m}{B_m}. \quad \ldots\ldots \quad (87)$$

The total reflection coefficient for backward scattering is now

$$g=\sum_1^\infty (m+\tfrac{1}{2})\,|\,a_m\,|, \quad \ldots\ldots \quad (88)$$

and the backward scattering cross-section is

$$\sigma=g^2\lambda^2/\pi. \quad \ldots\ldots \quad (89)$$

For a diffuse spherical cloud, using the Herlofson model, we obtain, for a sphere of radius a,

$$\frac{A_m}{B_m}=\frac{m+1}{ma^{2m+1}}\frac{m[\kappa/(a\kappa')](j\pi-\ln|\kappa|)+[1+m\kappa/(m+1)]}{m[\kappa/(a\kappa')](j\pi-\ln|\kappa|)+(1-\kappa)}, \quad \ldots \quad (90)$$

where κ' is the gradient of κ at $\kappa=0$.

For a homogeneous sphere, $\kappa' \to \infty$, and

$$\frac{A_m}{B_m}=\frac{\kappa+(m+1)/m}{a^{2m+1}(1-\kappa)}. \quad \ldots\ldots \quad (91)$$

Resonance occurs when $\kappa=-(m+1)/m$, which is given, for the first few modes, in fig. 15.

We will define the magnitude of the resonance as the ratio of the resonant reflection coefficient to that of the same number of free electrons oscillating in the same phase ; it is thus equivalent to $g_\perp/g_\parallel$ for a resonant cylinder.

Denoting it by η and proceeding as in § 5 we get, for the diffuseness limited dipole resonance,

$$\eta \simeq \tfrac{1}{2}\left|\frac{3s \ln 3}{2(\ln 2 - j\pi)} + 1\right|, \quad \ldots\ldots \quad (92)$$

where the electron density, as before, is proportional to $\exp[-(r/r_0)^s]$. We have plotted η against s in fig. 16 and although the values derived from the Herlofson model may be somewhat less than the true ones (as in the cylindrical case), it is clear that the diffuseness of the boundary has a greater effect for the sphere than for the cylinder.

Fig. 16

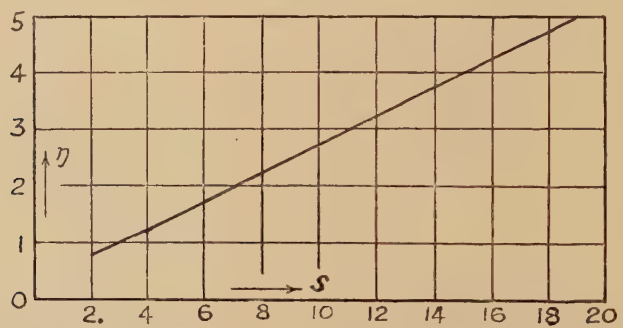

Magnitude of the dipole resonance for a diffuse spherical distribution of ionization.

II. *An Equation for a Particle with Two Mass States and Positive Charge Density*

By H. J. Bhabha, F.R.S.
Tata Institute of Fundamental Research, Bombay, India *

[Received September 21, 1951]

Summary

A relativistic wave equation in the canonical form (2) is given which describes a particle having two different rest masses. In one mass state the particle has a spin 3/2, in the other a spin 1/2. The free charge density is positive definite so that the equation can be quantized in the usual manner in accordance with the exclusion principle. The equation is irreducible.

This example establishes the principle that irreducible multi-mass equations exist which can be used to form the basis of a physical theory along the usual lines, contrary to the general prevalent view.

§1. Introduction

The purpose of this paper is to give an irreducible relativistic wave-equation in which the particle has states corresponding to two different values for its rest mass. Unlike all previously known equations of this type, however, the free charge density is positive definite, as for the Dirac equation, so that the equation can be quantized in accordance with the exclusion principle in the usual way. The equation is derivable by the variation principle from a Lagrangian density of the canonical form

$$\psi^\dagger D(\alpha^k p_k+\chi)\psi, \qquad (1)$$

where† $p_k=-i\partial/\partial x^k$ and χ is a constant of the same dimension as p_k. The matrices D and α^k have certain standard properties which will be stated in the next section. The wave equation has therefore the canonical form

$$(\alpha^k p_k+\chi)\psi=0 \qquad (2)$$

where the matrices α^k are defined in the next section.

Equations of the form (2) which have solutions for several different values of the invariant length $p^k p_k$ of the energy momentum vector p_k have been known for some time (cf. Bhabha 1945). But it has turned out that for all these equations neither the total charge nor the total energy is positive definite, so that it has not been possible to interpret the equations

* Communicated by the Author.

† x^0, x^1, x^2, x^3 are the coordinates and the metric tensor g_{kl} is taken in the form $g_{00}=-g_{11}=-g_{22}=-g_{33}=1$, $g_{kl}=0$ for $k\neq l$.

in the usual manner as describing particles with states of different rest mass. This has led to the general belief that irreducible equations describing a particle with several values of the rest mass cannot exist. Pais and Uhlenbeck (1950), basing their investigations on a much more limited form of the Lagrange function than (1), have shown that a physically sensible theory cannot be made for multi-mass equations due to the lack of positive definiteness of the energy and the charge. The present paper therefore proves that the generally held belief mentioned above is false, and that physically sensible theories can be constructed on the basis of multi-mass equations provided one works within the more general framework of Lagrange functions of the canonical form (1).

Whether the equation given in this paper will prove to describe an elementary particle actually found in Nature is not a question which can be answered now. The main importance of the present investigation in my opinion is that it establishes the principle that certainly one, and probably several, irreducible relativistic wave equations exist upon which can be based a physically sensible theory for particles having states corresponding to more than one value of the rest mass.

The new equation is defined in § 2. Its general properties are established in § 3. Its irreducibility is proved in § 4. An explicit representation of the matrices α^k is given in the Appendix.

§ 2. Definition of the Equation

The matrix D is by definition non-singular and hermitian. It is such that the four matrices $D\alpha^k$ are likewise hermitian.

The wave function ψ transforms according to a representation $\mathscr{R}$ of the Lorentz group, so that a transformation t of the coordinates :

$$x'^k = t_l^k x^l \quad . \quad . \quad . \quad . \quad . \quad . \quad . \quad . \quad . \quad (3)$$

causes a transformation of the wave-function given by

$$\psi' = T\psi, \quad . \quad . \quad . \quad . \quad . \quad . \quad . \quad . \quad . \quad (4\,a)$$

where T is the matrix representing t in $\mathscr{R}$. The invariance of the expression (1) then requires the five matrices D and α^k to transform according to

$$T^\dagger D T = D, \quad . \quad . \quad . \quad . \quad . \quad . \quad . \quad . \quad (4\,b)$$

$$T^{-1}\alpha^k T = t_l^k \alpha^l. \quad . \quad . \quad . \quad . \quad . \quad . \quad . \quad (4\,c)$$

The components of ψ, and in consequence the matrices of the representation $\mathscr{R}$, and the matrices D and α^k can always be subjected to simultaneous transformation by an arbitrary non-singular matrix s :

$$\psi \to \psi' = s^{-1}\psi, \quad . \quad . \quad . \quad . \quad . \quad . \quad . \quad (5\,a)$$

$$D \to D' = s^\dagger D s, \quad . \quad . \quad . \quad . \quad . \quad . \quad . \quad (5\,b)$$

$$\alpha^k \to \alpha'^k = s^{-1}\alpha^k s, \quad . \quad . \quad . \quad . \quad . \quad . \quad . \quad (5\,c)$$

$$T \to T' = s^{-1} T s, \quad . \quad . \quad . \quad . \quad . \quad . \quad . \quad (5\,d)$$

without changing anything in the theory. All such formulations are equivalent.

We take a ψ transforming according to the representation

$$\mathscr{R}=\mathscr{R}(\tfrac{3}{2},\tfrac{1}{2})+\mathscr{R}(\tfrac{1}{2},\tfrac{1}{2})+\mathscr{R}(\tfrac{1}{2},\tfrac{1}{2}), \quad . \quad . \quad . \quad . \quad . \quad (6)$$

where $\mathscr{R}(\frac{3}{2},\frac{1}{2})$ and $\mathscr{R}(\frac{1}{2},\frac{1}{2})$ denote two irreducible representations of the full Lorentz group in the usual notation. Under restriction to the proper Lorentz group the representation $\mathscr{R}(k+l, k-l)$, $k>l$ breaks up into two irreducible representations $\mathscr{D}(k, l)$ and $\mathscr{D}(l, k)$ of the proper Lorentz group. Thus, $\mathscr{R}(\frac{3}{2},\frac{1}{2})\sim\mathscr{D}(1,\frac{1}{2})+\mathscr{D}(\frac{1}{2}, 1)$, while $\mathscr{R}(\frac{1}{2},\frac{1}{2})\sim\mathscr{D}(\frac{1}{2}, 0)+\mathscr{D}(0,\frac{1}{2})$. The representation $\mathscr{D}(k, l)$ describes the transformation properties of a spinor $a_{\dot\alpha_1\ldots\dot\alpha_{2l}}^{\varrho_1\ldots\varrho_{2k}}$ symmetric in its $2k$ undotted indices and likewise symmetric in its $2l$ dotted ones. We assume that $\mathscr{R}$ is already in its fully reduced form with respect to the proper Lorentz group, and that its irreducible parts are arranged in the order

$$\mathscr{R}\sim\mathscr{D}(1,\tfrac{1}{2})+\mathscr{D}(0,\tfrac{1}{2})+\mathscr{D}(0,\tfrac{1}{2})+\mathscr{D}(\tfrac{1}{2}, 1)+\mathscr{D}(\tfrac{1}{2}, 0)+\mathscr{D}(\tfrac{1}{2}, 0).$$

Then

$$\psi=\left\{\begin{array}{c}\phi_\alpha^{\cdot\varrho\sigma}\\ \phi_\alpha^{\cdot(1)}\\ \phi_\alpha^{\cdot(2)}\\ \phi_{\alpha\dot\beta}^{\cdot\cdot\varrho}\\ \phi^{(1)\alpha}\\ \phi^{(2)\alpha}\end{array}\right\}. \quad . \quad . \quad . \quad . \quad . \quad . \quad . \quad . \quad (7)$$

Moreover, we arrange the six independent components of the first spinor in (7) in a column in the order $\phi_1^{\cdot 11}$, $\sqrt{2}\phi_1^{\cdot 12}$, $\phi_1^{\cdot 22}$, $\phi_2^{\cdot 11}$, $\sqrt{2}\phi_2^{\cdot 12}$, $\phi_2^{\cdot 22}$. Similarly, for the spinor $\phi_{\alpha\dot\beta}^{\cdot\cdot\varrho}$ we take the components in the order $\phi_{1\dot1}^{\cdot\cdot 1}$, $\sqrt{2}\phi_{1\dot2}^{\cdot\cdot 1}$, $\phi_{2\dot2}^{\cdot\cdot 1}$, etc. The second, third, fifth and sixth spinors have only two components each, and we take them in the order $\phi_1^{\cdot(1)}$, $\phi_2^{\cdot(1)}$, $\phi_1^{\cdot(2)}$, $\phi_2^{\cdot(2)}$, $\phi^{(1)_1}$, $\phi^{(1)_2}$, etc.

In a recent paper* (Bhabha 1951 a) I have investigated a class of Lagrange functions of the type (1) in which ψ transforms according to the representation $\mathscr{R}(\frac{3}{2},\frac{1}{2})+\mathscr{R}(\frac{1}{2},\frac{1}{2})$. We have only to repeat the methods and arguments of that paper to arrive at the general form of the matrices D and α^k in the present case. We first divide up the matrices D and α^k into submatrices corresponding to the subdivision of ψ into irreducible spinors as in (7). We then arrive at the result that the most general form of D, which is hermitian and satisfies (4 *b*), is

$$D=\begin{pmatrix}\cdot & D'\\ D' & \cdot\end{pmatrix}, \quad . \quad . \quad . \quad . \quad . \quad . \quad . \quad . \quad (8\,a)$$

where

$$D'=\left\{\begin{array}{ccc}d_1 1_{(6)} & \cdot & \cdot\\ \cdot & d_2 1_{(2)} & \cdot\\ \cdot & \cdot & d_3 1_{(2)}\end{array}\right\}. \quad . \quad . \quad . \quad . \quad . \quad . \quad (8\,b)$$

* Referred to here as (A).

$1_{(n)}$ stands for the unit matrix of n rows or columns, and d_1, d_2 and d_3 stand for either 1 or -1 independently of each other.

The most general form of the four matrices α^k satisfying (4 c) and the condition that the matrices $D\alpha^k$ shall all be hermitian is then

$$\alpha^0=\begin{pmatrix}\cdot & \alpha'^0\\ \alpha'^0 & \cdot\end{pmatrix}, \qquad \alpha^k=\begin{pmatrix}\cdot & \alpha'^k\\ -\alpha'^k & \cdot\end{pmatrix}, \qquad \text{for } k=1,\,2,\,3, \quad . \quad (9\,a)$$

where

$$\alpha'^k=\begin{Bmatrix} a_1u^k & d_1c_3v^k & d_1c_2v^k\\ d_2c_3w^k & a_2z^k & d_2c_1z^k\\ d_3c_2w^k & d_3\bar{c}_1z^k & a_3z^k\end{Bmatrix}. \quad . \quad . \quad . \quad . \quad . \quad (9\,b)$$

a_1, a_2, a_3, c_1, c_2 and c_3 are six arbitrary numbers of which a_1, a_2, a_3 must be real, while c_2 and c_3 can be taken to be real without loss of generality. For if they are not real, they can be made so by a similarity transformation of the type (5). The sets of matrices u^k, v^k, w^k and z^k are reduction matrices whose form is fixed, except for multiplication by arbitrary numerical factors, once the form of ψ is fixed as in (7).

The general form of the matrices D and α^k given by (8) and (9) is easily understood. A reflection turns an upper undotted spinor index into a lower dotted one, and vice versa. With the arrangement of the spinors in ψ given by (7) the transformation r which reverses the directions of the three space axes must be represented therefore by a matrix R having the form (8). By (4 b) the matrix D must commute with R since $R^\dagger=R=R^{-1}$. Moreover, taking the complex conjugate of a spinor turns an undotted index into a dotted one and vice versa. D must therefore have the form (8) with d_1, d_2, d_3 any real numbers. By a transformation of the type (5) we can then make the modules of these numbers 1. This settles the form of D given by (8).

Denoting by $(k', l' \mid \alpha^j \mid k, l)$ the submatrix of α^j which lies in the row corresponding to the representation $\mathscr{D}(k', l')$ and the column corresponding to the representation $\mathscr{D}(k, l)$, I have shown (Bhabha 1945, §5) that

$$(k', l' \mid \alpha^j \mid k, l)=0 \text{ unless } \begin{matrix}k'=k\pm\frac{1}{2}\\ l'=l\pm\frac{1}{2}\end{matrix} \text{ independently.} \quad . \quad (10)$$

Further, according to (4 c), R commutes with α^0 and anticommutes with α^k, $k=1, 2, 3$. This settles the form (9) of the α^k. Finally, the requirement that the four matrices $D\alpha^k$ shall be hermitian requires that a_1u^k, a_2z^k and a_3z^k shall be hermitian. Without loss of generality we can therefore take u^k and z^k to be hermitian, and a_1, a_2 and a_3 to be real numbers. Finally, we must have

$$w^k=v^{k\dagger}. \quad . \quad . \quad . \quad . \quad . \quad . \quad . \quad . \quad . \quad (11)$$

The actual form of the matrices u^k, v^k and z^k can be obtained in terms of the reduction matrices u'', v'', u'' and v'' introduced by Dirac (1936) and developed by Fierz (1939). An irreducible representation $\mathscr{D}(k, l)$ of the

proper Lorentz group is determined by its six infinitesimal transformations $I^{rs}(k, l)$. This set can be connected with two spinors $K^{\lambda\mu}$ and $L^{\dot{\lambda}\dot{\mu}}$ symmetric in their spinor indices through the relations

$$\left.\begin{aligned} K_1{}^1(k) &= -K_2{}^2(k) = I^{03} + iI^{12}, \\ K_2{}^1(k) &= (I^{01} + iI^{23}) - i(I^{02} + iI^{31}), \\ K_1{}^2(k) &= (I^{01} + iI^{23}) + i(I^{02} + iI^{31}), \end{aligned}\right\} \quad . \quad . \quad . \quad . \quad . \quad (12)$$

and

$$\left.\begin{aligned} L_1^{\dot{1}}(l) &= -L_2^{\dot{2}}(l) = I^{03} - iI^{12}, \\ L_2^{\dot{1}}(l) &= (I^{01} - iI^{23}) + i(I^{02} - iI^{31}), \\ L_1^{\dot{2}}(l) &= (I^{01} - iI^{23}) - i(I^{02} - iI^{31}). \end{aligned}\right\} \quad . \quad . \quad . \quad . \quad . \quad (13)$$

Then the two spinor matrices $u^{\mu}(k)$ having $2k+1$ rows and $2k$ columns and the two spinor matrices $v^{\mu}(k)$ having $2k$ rows and $2k+1$ columns satisfy, and are defined by, the equations*

$$\left.\begin{aligned} -u_{\mu}(k+\tfrac{1}{2})v^{\mu}(k+\tfrac{1}{2}) &= v_{\mu}(k)u^{\mu}(k) = 2k+1 \\ v_{\mu}(k)v^{\mu}(k+\tfrac{1}{2}) &= u_{\mu}(k+\tfrac{1}{2})u^{\mu}(k) = 0 \\ -v^{\mu}(k+\tfrac{1}{2})u_{\nu}(k+\tfrac{1}{2}) &= K_{\nu}{}^{\mu}(k) + (k+1)\delta_{\nu}{}^{\mu} \\ -u^{\mu}(k)v_{\nu}(k) &= K_{\nu}{}^{\mu}(k) - k\delta_{\nu}{}^{\mu} \end{aligned}\right\} \quad . \quad . \quad . \quad . \quad (14)$$

$u^{\dot{\mu}}$ and $v^{\dot{\mu}}$ satisfy similar equations with $L_{\dot{\nu}}^{\dot{\mu}}$ in place of $K_{\nu}{}^{\mu}$. One sees at once from (9) and (7) that u^k, v^k and z^k are just the submatrices

$$\left.\begin{aligned} u^k &= (1, \tfrac{1}{2} \mid \alpha^k \mid \tfrac{1}{2}, 1) \\ v^k &= (1, \tfrac{1}{2} \mid \alpha^k \mid \tfrac{1}{2}, 0) \\ z^k &= (\tfrac{1}{2}, 0 \mid \alpha^k \mid 0, \tfrac{1}{2}) \end{aligned}\right\} \quad . \quad . \quad . \quad . \quad . \quad . \quad (15)$$

Hence it follows from the form for these submatrices given in the paper quoted above (Bhabha 1945, formulae (66) and (67)), that we can take

$$\left.\begin{aligned} u^k &= \sigma_{\dot{\mu}\lambda}^{\;\;k} u^{\lambda}(1) v^{\dot{\mu}}(1) \\ v^k &= \sigma_{\dot{\mu}\lambda}^{\;\;k} u^{\lambda}(1) u^{\dot{\mu}}(\tfrac{1}{2}) \\ z^k &= \sigma_{\dot{\mu}\lambda}^{\;\;k} u^{\lambda}(\tfrac{1}{2}) v^{\dot{\mu}}(\tfrac{1}{2}) \end{aligned}\right\}, \quad . \quad . \quad . \quad . \quad . \quad . \quad (16)$$

where σ^0 stands for the 2×2 unit matrix, and σ^1, σ^2, σ^3 for the three Pauli matrices. The dotted index labels the rows and the undotted one the columns of these matrices. An explicit representation for the matrices u^k, v^k and z^k is given in the Appendix.

---

* cf. Bhabha (1945), §5.

We now maintain that the Lagrange function (1), *with the matrices* D *and* α^k *given by* (8) *and* (9), *and the constants* d, a *and* c *defined by*

$$d_1=-d_2=-d_3=1, \quad . \quad . \quad . \quad . \quad . \quad . \quad (17\,a)$$

$$a_1=1, \qquad a_2>\tfrac{1}{2}, \qquad a_3=\tfrac{1}{2}-a_2-|\lambda|, \quad . \quad . \quad . \quad (17\,b)$$

$$c_1=0, \qquad c_2{}^2=\tfrac{4}{3}a_3{}^2\left(\frac{a_2-\frac{1}{2}}{a_2-a_3}\right), \qquad c_3{}^2=\tfrac{4}{3}a_2{}^2\left(\frac{\frac{1}{2}-a_3}{a_2-a_3}\right), \quad . \quad (17\,c)$$

describes a particle having states of rest mass χ *and* $\chi/|\lambda|$ *and a positive definite free charge density. Its spin in the state of rest mass* χ *is* 3/2 *in the state of rest mass* $\chi/|\lambda|$ *it is* 1/2. *The equation is irreducible.*

Provided $a_1\neq 0$ we can always put $a_1=1$ without any specialization since this merely changes the definition of the mass in terms of χ. Moreover, the hermitian matrix

$$\begin{pmatrix} a_2 & c_1 \\ c_1 & a_3 \end{pmatrix},$$

which multiplies z^k in (9 b) when $d_2=d_3=\pm 1$ can always be brought to the diagonal form through a similarity transformation by a unitary matrix without changing the corresponding form of D'. Hence putting $c_1=0$ in (9 b) also represents no specialization when $d_2=d_3$. Finally, we note that c_2 and c_3 can be assumed to be purely real without any loss of generality. The sign of either is irrelevant since it can be changed by a transformation of the type (5). Thus (17 c) only defines the absolute magnitude of c_2 and c_3.

Introducing (16) into (9 b) and using (17) it can be shown without much difficulty that equation (2) is equivalent to the set of spinor equations

$$\tfrac{1}{2}(p^{\varrho\dot\beta}\phi_{\dot\alpha\dot\beta}{}^{\sigma}+p^{\sigma\dot\beta}\phi_{\dot\alpha\dot\beta}{}^{\varrho})-\frac{c_3}{2\sqrt{2}}(p_{\dot\alpha}{}^{\varrho}\phi^{(1)\sigma}+p_{\dot\alpha}{}^{\sigma}\phi^{(1)\varrho})$$

$$-\frac{c_2}{2\sqrt{2}}(p_{\dot\alpha}{}^{\varrho}\phi^{(2)\sigma}+p_{\dot\alpha}{}^{\sigma}\phi^{(2)\varrho})+\chi\phi_{\dot\alpha}{}^{\varrho\sigma}=0, \quad . \quad (18\,a)$$

$$-\frac{c_3}{\sqrt{2}}p_{\sigma}{}^{\dot\alpha}\phi_{\dot\alpha}{}^{\varrho\sigma}+a_2p^{\varrho\dot\alpha}\phi_{\dot\alpha}{}^{(1)}+\chi\phi^{(1)\varrho}=0, \quad . \quad (18\,b)$$

$$-\frac{c_2}{\sqrt{2}}p_{\sigma}{}^{\dot\alpha}\phi_{\dot\alpha}{}^{\varrho\sigma}+a_3p^{\varrho\dot\alpha}\phi_{\dot\alpha}{}^{(2)}+\chi\phi^{(2)}=0, \quad . \quad . \quad (18\,c)$$

$$\tfrac{1}{2}(p_{\dot\beta\sigma}\phi_{\dot\alpha}{}^{\varrho\sigma}+p_{\dot\alpha\sigma}\phi_{\dot\beta}{}^{\varrho\sigma})-\frac{c_3}{2\sqrt{2}}(p_{\dot\beta}{}^{\sigma}\phi_{\dot\alpha}{}^{(1)}+p_{\dot\alpha}{}^{\sigma}\phi_{\dot\beta}{}^{(1)})$$

$$-\frac{c_2}{2\sqrt{2}}(p_{\dot\beta}{}^{\sigma}\phi_{\dot\alpha}{}^{(2)}+p_{\dot\alpha}{}^{\sigma}\phi_{\dot\beta}{}^{(2)})+\chi\phi_{\dot\alpha\dot\beta}{}^{\varrho}=0, \quad . \quad (18\,d)$$

$$-\frac{c_3}{\sqrt{2}}p_{\varrho}{}^{\dot\beta}\phi_{\dot\alpha\dot\beta}{}^{\varrho}+a_2p_{\dot\alpha\varrho}\phi^{(1)\varrho}+\chi\phi_{\dot\alpha}{}^{(1)}=0, \quad . \quad (18\,e)$$

$$-\frac{c_2}{\sqrt{2}}p_{\varrho}{}^{\dot\beta}\phi_{\dot\alpha\dot\beta}{}^{\varrho}+a_3p_{\dot\alpha\varrho}\phi^{(2)\varrho}+\chi\phi_{\dot\alpha}{}^{(2)}=0. \quad . \quad (18\,f)$$

§3. Properties of the Equation

By Λ_r we denote in general a matrix having every element on the principal diagonal equal to λ_r, any element on the diagonal just above the principal diagonal equal to 0 or 1 independently of the others, and every other element zero. It is well known that every matrix, and in particular α^0, can be brought to the pseudo-diagonal form

$$\left\{\begin{matrix} \Lambda_1 & & & & \\ & \Lambda_2 & & & \\ & & \cdot & & \\ & & & \cdot & \\ & & & & \cdot \\ & & & & & \Lambda_n \end{matrix}\right\}, \quad \ldots\ldots \quad (19)$$

where $\lambda_1 \neq \lambda_2 \neq \ldots \neq \lambda_n$ are the eigenvalues of α^0.

We now note the following trivial :

Lemma 1. *H and Λ being two matrices such that H and $H\Lambda$ are both hermitian, all the submatrices $(i \mid H \mid j)$ are zero for $i \neq j$ if Λ is of the form* (19) *and all its eigenvalues are real.*

$(i \mid H \mid j)$ denotes the submatrix of H which lies in the row corresponding to Λ_i and the column corresponding to Λ_j. For the hermiticity of $H\Lambda$ requires that

$$\{(i \mid H \mid j)\Lambda_j\}^\dagger = (j \mid H \mid i)\Lambda_i.$$

Since $(i \mid H \mid j)^\dagger = (j \mid H \mid i)$, this requires

$$\Lambda_j^\dagger (j \mid H \mid i) = (j \mid H \mid i)\Lambda_i,$$

from which follows the statement of the lemma because $\overline{\lambda}_j = \lambda_j \neq \lambda_i$.

Lemma 2. *If the submatrix Λ_j in* (19) *be a multiple λ_j of the unit matrix, then the corresponding submatrix $(j \mid H \mid j)$ of H can be brought to the diagonal form without changing the form of Λ_j.*

For $(j \mid H \mid j)$ being hermitian, it can be brought to the diagonal form by a unitary matrix u : $u^{-1}(j \mid H \mid j)u = u^\dagger (j \mid H \mid j)u$ is diagonal. But $u^{-1}\Lambda_j u = \Lambda_j$ since Λ_j is a multiple of the unit matrix.

If Λ' be a matrix of n rows or columns having all elements on the principal diagonal equal to λ, all elements on the diagonal above the principal diagonal equal to 1, and all other elements 0, then we can prove :

Lemma 3. *H and Λ' being two matrices such that H and $H\Lambda'$ are hermitian and λ a real number, H must have the form*

$$\left\{\begin{matrix} \cdot & \cdot & \cdot & \cdot & \cdot & \cdot & \cdot & \cdot & h_1 \\ \cdot & \cdot & \cdot & \cdot & \cdot & \cdot & \cdot & h_1 & h_2 \\ \cdot & \cdot & \cdot & \cdot & \cdot & \cdot & h_1 & h_2 & h_3 \\ \cdot & \cdot & \cdot & \cdot & \cdot & \cdot & \cdot & \cdot & \cdot \\ \cdot & \cdot & h_1 & \cdot & \cdot & \cdot & \cdot & \cdot & \cdot \\ \cdot & h_1 & h_2 & \cdot & \cdot & \cdot & \cdot & h_{n-2} & h_{n-1} \\ h_1 & h_2 & h_3 & \cdot & \cdot & \cdot & \cdot & h_{n-1} & h_n \end{matrix}\right\}, \quad . \quad (20)$$

where $h_1, h_2, \ldots h_n$ are real numbers.

All elements on the principal transverse diagonal are h_1, all elements on the transverse diagonal below this h_2, and so on. For from the hermiticity of $H\Lambda'$ follows

$$\{(2\,|\,H\,|\,1)\lambda\}^\dagger=(1\,|\,H\,|\,1)+(1\,|\,H\,|\,2)\lambda,$$

whence

$$\lambda(1\,|\,H\,|\,2)=(1\,|\,H\,|\,1)+(1\,|\,H\,|\,2)\lambda,$$

or $(1\,|\,H\,|\,1)=0$. Proceeding in this way we can prove that $(1\,|\,H\,|\,r)=0$ for $r<n$. Hence $(r\,|\,H\,|\,1)$ is likewise zero for $r<n$. Taking the next column we can then prove that $(2\,|\,H\,|\,r)=(r\,|\,H\,|\,2)=0$ for $r<n-1$, while $(n-1\,|\,H\,|\,2)=(n\,|\,H\,|\,1)=h_1$ say. We eventually arrive at (20). The hermiticity of H then requires $h_1, h_2, \ldots h_n$ to be real numbers.

Consider now the matrix equation

$$(\Lambda' p_0+\chi)\psi=0, \quad . \ . \ . \ . \ . \ . \ . \ . \quad (21\,a)$$

where p_0 and χ are numbers and $\chi=0$. ψ is a column matrix with the elements $\psi_1, \psi_2, \ldots \psi_n$. This equation is equivalent to the set

$$\left.\begin{array}{l} (\lambda p_0+\chi)\psi_1+p_0\psi_2=0 \\ (\lambda p_0+\chi)\psi_2+p_0\psi_3=0 \\ \ldots\ldots\ldots\ldots \\ (\lambda p_0+\chi)\psi_{n-1}+p_0\psi_n=0 \\ (\lambda p_0+\chi)\psi_n \qquad\quad =0 \end{array}\right\} \ldots\ldots\ldots \quad (21\,b)$$

If $\lambda p_0+\chi\neq 0$ the only solution of this set is $\psi=0$. If $\lambda p_0+\chi=0$ there is only one non-vanishing solution, namely

$$\psi_1 \text{ arbitrary}, \qquad \psi_2=\psi_3=\ldots=\psi_n=0. \ . \ . \ . \quad (22)$$

If $\lambda=0$, then $\lambda p_0+\chi$ cannot be zero, and there is no solution of the type (22).

We now return to eqn. (2). It has been proved generally (cf. Bhabha 1949) that the rest masses of the particle are connected with the eigenvalues of α^0 if $\chi\neq 0$. Indeed, when $\chi\neq 0$ one can define a value of the rest mass as the value of $|\,p_0\,|$ for which a non-vanishing solution of

$$(\alpha^0 p_0+\chi)\psi=0 \quad . \ . \ . \ . \ . \ . \ . \ . \quad (23)$$

exists. Our first step is therefore to bring α^0 to its diagonal or pseudo-diagonal form (19), from which all the mass states of the particle can be determined.

In all equations derivable from the Lagrange function (1), the charge-current density vector is $\psi^\dagger D\alpha^k\psi$. The charge density is therefore

$$\psi^\dagger D\alpha^0\psi. \quad . \ . \ . \ . \ . \ . \ . \ . \ . \quad (24)$$

In the Dirac equation $D\alpha^0$ is a positive definite matrix. This requirement is however too stringent, and it is only necessary for a sensible physical interpretation that the expression (24) shall be positive for every free wave solution of (2). When this is so, we say that the free charge density is positive definite. This will be so from relativistic invariance if it is so for

every solution of (23) corresponding to a particle at rest. We have therefore to follow through the transformation of D under a transformation of the type (5 b) when α^0 undergoes a transformation of the type (5 c).

We first note that a transformation of the type (5) with an s given by

$$s = \frac{1}{\sqrt{2}} \begin{pmatrix} -1_{(10)} & 1_{(10)} \\ 1_{(10)} & 1_{(10)} \end{pmatrix}, \quad \ldots\ldots \quad (25)$$

immediately changes D and the α^k to

$$D \to \begin{pmatrix} -D' & \cdot \\ \cdot & D' \end{pmatrix}, \qquad \alpha^0 \to \begin{pmatrix} -\alpha'^0 & \cdot \\ \cdot & \alpha'^0 \end{pmatrix}, \quad \ldots \quad (26\,a)$$

$$\alpha^k \to \begin{pmatrix} \cdot & -\alpha'^k \\ \alpha'^k & \cdot \end{pmatrix}, \; k = 1, 2, 3. \quad \ldots \quad (26\,b)$$

Introducing the representation for the matrices u^0, v^0 and z^0 given in the Appendix into (9 b), and giving the constants the values (17), we get

$\alpha'^0 =$

$$\left[\begin{array}{cccccc|cc|cc}
1 & \cdot & \cdot & \cdot & \cdot & \cdot & \cdot & \cdot & \cdot & \cdot \\
\cdot & \tfrac{1}{2} & \cdot & \frac{1}{\sqrt{2}} & \cdot & \cdot & \tfrac{1}{2}c_3 & \cdot & \tfrac{1}{2}c_2 & \cdot \\
\cdot & \cdot & \cdot & \cdot & \frac{1}{\sqrt{2}} & \cdot & \cdot & \frac{1}{\sqrt{2}}c_3 & \cdot & \frac{1}{\sqrt{2}}c_2 \\
\cdot & \frac{1}{\sqrt{2}} & \cdot & \cdot & \cdot & \cdot & -\frac{1}{\sqrt{2}}c_3 & \cdot & -\frac{1}{\sqrt{2}}c_2 & \cdot \\
\cdot & \cdot & \frac{1}{\sqrt{2}} & \cdot & \tfrac{1}{2} & \cdot & \cdot & -\tfrac{1}{2}c_3 & \cdot & -\tfrac{1}{2}c_2 \\
\cdot & \cdot & \cdot & \cdot & \cdot & 1 & \cdot & \cdot & \cdot & \cdot \\
\hline
\cdot & -\tfrac{1}{2}c_3 & \cdot & \frac{1}{\sqrt{2}}c_3 & \cdot & \cdot & a_2 & \cdot & \cdot & \cdot \\
\cdot & \cdot & -\frac{1}{\sqrt{2}}c_3 & \cdot & \tfrac{1}{2}c_3 & \cdot & \cdot & a_2 & \cdot & \cdot \\
\hline
\cdot & -\tfrac{1}{2}c_2 & \cdot & \frac{1}{\sqrt{2}}c_2 & \cdot & \cdot & \cdot & \cdot & a_3 & \cdot \\
\cdot & \cdot & -\frac{1}{\sqrt{2}}c_2 & \cdot & \tfrac{1}{2}c_2 & \cdot & \cdot & \cdot & \cdot & a_3
\end{array}\right] \quad \ldots \quad (27)$$

This matrix becomes precisely the matrix dealt with in the preceding paper ((A) formula (26)) if we omit its last two rows and columns. We can therefore deal with it exactly like the matrix in that paper*. By a simple

* cf. also Bhabha 1951 b, *Report of an International Conference on Elementary Particles*, Bombay, 1950.

re-arrangement of the rows and columns of (27) we can bring it to the form

$$\alpha'^0 \to \begin{Bmatrix} 1_{(2)} & . & . \\ . & \alpha'' & . \\ . & . & \alpha'' \end{Bmatrix} \text{ where } \alpha''= \begin{bmatrix} \frac{1}{2} & \frac{1}{\sqrt{2}} & \frac{1}{2}c_3 & \frac{1}{2}c_2 \\ \frac{1}{2} & . & -\frac{1}{\sqrt{2}}c_3 & -\frac{1}{\sqrt{2}}c_2 \\ -\frac{1}{2}c_3 & \frac{1}{\sqrt{2}}c_3 & a_2 & . \\ -\frac{1}{2}c_2 & \frac{1}{\sqrt{2}}c_2 & . & a_3 \end{bmatrix}, \quad . \; . \; . \; (28)$$

while D' is brought simultaneously to the form

$$D' \to \begin{bmatrix} 1_{(2)} & . & . \\ . & D'' & . \\ . & . & D'' \end{bmatrix} \text{ where } D''= \begin{bmatrix} 1 & . & . & . \\ . & 1 & . & . \\ . & . & -1 & . \\ . & . & . & -1 \end{bmatrix}. \quad . \; . \; . \; (29)$$

It is clear that as in (A), the matrix α'^0 must have the eigenvalue 1 four times, for the component ϕ_1^{11} of the first spinor in (7), which is a component of the wave-function belonging to the eigenvalue 1 of α'^0, transforms according to the representation $\mathscr{D}_{\frac{3}{2}}$ of the three dimensional rotation group which is of degree 4. Indeed, a transformation of D'' and α'' of the type (5 *b*) and (5 *c*) by a matrix

$$s= \left[\begin{array}{cc|cc} \sqrt{\frac{2}{3}} & \sqrt{\frac{1}{3}} & . & . \\ \sqrt{\frac{1}{3}} & -\sqrt{\frac{2}{3}} & . & . \\ \hline . & . & 1 & . \\ . & . & . & 1 \end{array}\right], \quad . \; . \; . \; . \; . \; . \; (30)$$

immediately diagonalizes the eigenvalue 1 of α'^0 without changing the form of D''. Hence D' and α^0 are transformed simultaneously to

$$D' \to \begin{bmatrix} 1_{(4)} & . & . \\ . & \eta & . \\ . & . & \eta \end{bmatrix}, \qquad \alpha'^0 \to \begin{bmatrix} 1_{(4)} & . & . \\ . & \zeta & . \\ . & . & \zeta \end{bmatrix}, \quad . \; . \; . \; (31)$$

where

$$\eta= \begin{bmatrix} 1 & . & . \\ . & -1 & . \\ . & . & -1 \end{bmatrix}, \qquad \zeta= \begin{bmatrix} -\frac{1}{2} & \frac{\sqrt{3}}{2}c_3 & \frac{\sqrt{3}}{2}c_2 \\ -\frac{\sqrt{3}}{2}c_3 & a_2 & . \\ -\frac{\sqrt{3}}{2}c_2 & . & a_3 \end{bmatrix}. \quad . \; . \; . \; (32)$$

The matrix ζ has the characteristic equation

$$|\lambda-\zeta|=\{\lambda-(a_2+a_3-\tfrac{1}{2})\}\lambda^2=0. \quad . \quad . \quad . \quad . \quad . \quad . \quad (33)$$

Hence it has the two roots

$$\lambda=a_2+a_3-\tfrac{1}{2} \quad . \quad . \quad . \quad . \quad . \quad . \quad . \quad . \quad . \quad (34)$$

and zero. Moreover zero is a double root since ζ does not satisfy the equation $\{\lambda-(a_2+a_3-\frac{1}{2})\}\lambda=0$. Hence the pseudo-diagonal form of ζ is

$$\Lambda=\begin{bmatrix}\lambda & . & . \\ . & . & 1 \\ . & . & .\end{bmatrix}. \quad . \quad . \quad . \quad . \quad . \quad . \quad . \quad (35)$$

When ζ is transformed to the form Λ by a matrix s:

$$s^{-1}\zeta s=\Lambda, \quad . \quad . \quad . \quad . \quad . \quad . \quad . \quad . \quad . \quad (36)$$

η is transformed to

$$\eta'=s^{\dagger}\eta s, \quad . \quad . \quad . \quad . \quad . \quad . \quad . \quad . \quad . \quad (37)$$

and it follows from lemma 1 and 3 that η' must have the form

$$\eta'=\begin{bmatrix}\eta_1' & . & . \\ . & . & \eta_2' \\ . & \eta_2' & \eta_3'\end{bmatrix}. \quad . \quad . \quad . \quad . \quad . \quad . \quad (38)$$

It follows from the statement made immediately after (22) that the equation

$$(\Lambda p_0+\chi)\psi=0$$

has only one non-vanishing solution, namely

$$\psi_1 \text{ arbitrary}, \qquad \psi_2=\psi_3=0,$$

and this is possible only if

$$p_0=-\frac{\chi}{|\lambda|}. \quad . \quad . \quad . \quad . \quad . \quad . \quad . \quad . \quad . \quad (39)$$

For this solution the charge density (24) is

$$\bar{\psi}_1\eta_1'\lambda\psi_1=\eta_1'\lambda\bar{\psi}_1\psi_1. \quad . \quad . \quad . \quad . \quad . \quad . \quad . \quad (40)$$

It is therefore only necessary to calculate η_1'.

Denoting by s_1 the first column of the matrices in (36), it follows from (32) and (37) that

$$\left.\begin{aligned}\eta_1' &= s_1^{\dagger}\eta s_1 \\ &= |s_{11}|^2-|s_{21}|^2-|s_{31}|^2\end{aligned}\right\}, \quad . \quad . \quad . \quad . \quad . \quad (41)$$

where s_{11}, s_{21} and s_{31} are the three components of s_1. But by (36) s_1 satisfies

$$\zeta s_1=s_1\lambda.$$

From this it follows that but for an arbitrary multiplying factor

$$s_{11}=\frac{2}{\sqrt{3}}\frac{1}{c_2c_3}, \qquad s_{21}=\frac{1}{c_2(a_3-\frac{1}{2})}, \qquad s_{31}=\frac{1}{c_3(a_2-\frac{1}{2})} \quad . \quad (42)$$

Substituting this in (41) and inserting the values (17 c) for c_2 and c_3 we get

$$\eta_1' = -\frac{3}{4}\frac{(a_2-a_3)^2(a_2+a_3-\frac{1}{2})^2}{a_2^2 a_3^2(a_2-\frac{1}{2})^2(a_3-\frac{1}{2})^2} < 0, \quad \ldots \quad (43)$$

a_2 and a_3 being real, η_1' is always negative. Hence, if a_3 is so chosen that $\lambda<0$, the charge density (40) for the state of rest mass $\chi/|\lambda|$ is positive.

The equation also has a mass state χ which arises from the eigenvalue 1 of α'^0 in (31). The charge density is clearly seen from (31) to be positive for this state.

We have therefore proved that the equation (2) determined by the values (17) of the constants has two mass states χ and $\chi/|\lambda|$, and a positive definite free charge density.

The spin in the state of mass χ is 3/2. This follows from the fact that one of the components of ψ corresponding to this value of the mass is ϕ_1^{11}, which transforms according to the representation $\mathscr{D}_{\frac{3}{2}}$ of the three dimensional rotation group. Since the eigenvalue 1 only occurs four times in (31), there can be no other spin value for this mass state.

The eigenvalue λ occurs only once in ζ, but ζ occurs twice in α'^0 as seen from (31). Hence in the state of rest mass $\chi/|\lambda|$ the spin must be 1/2, for the representation $\mathscr{D}_{\frac{1}{2}}$ of the rotation group has just two components. (Spin zero is excluded by the fact that we are dealing exclusively with spinors having one or three spinor indices.)

§4. Irreducibility of the Equation

We shall now prove that the four matrices form an indecomposable set, that is, they cannot be decomposed into a direct sum of such sets. Suppose this is not so, and let the set be decomposable into the sum of a number of indecomposable sets

$$\alpha^k = \alpha^{(1)k} + \alpha^{(2)k} + \ldots \quad (44)$$

In the rest of this section we simply drop the index k for convenience. Now we have to consider cases of two types. Either the representation $\mathscr{R}$ is not correspondingly decomposable, or it is already correspondingly decomposed.

A case of the former type was investigated in (A). There the α-matrices decomposed into a direct sum of four sets of Dirac matrices although ψ transformed according to representation $\mathscr{R}(\frac{3}{2},\frac{1}{2})+\mathscr{R}(\frac{1}{2},\frac{1}{2})$. This is because a ψ transforming in this way can always be written as the direct product of a Dirac wave-function times a four vector. In the present case a ψ transforming according to the representation (6) can be written as the direct product of a Dirac wave-function times a four vector plus a scalar. Thus, if a contingency of the first type arises either the α's decompose into a direct sum of five sets of Dirac α-matrices or a direct sum of four sets of β-matrices, where by β-matrices I mean the set of four matrices given by Kemmer which occurs in the scalar meson wave-equation. In the former case the eigenvalues of α^0 must all be ± 1, in the latter ± 1 and zero. Since α^0 determined by (17) does not possess these eigenvalues we have proved that the first type of decomposition cannot occur.

We have therefore to consider the case in which the α's decompose as in (44) and the representation $\mathscr{R}$ decomposes correspondingly. Now either the part of $\mathscr{R}$ corresponding to one of the sets say, $\alpha^{(1)}$, in (44) only contains the representation $\mathscr{R}(\frac{3}{2}, \frac{1}{2})$, or it contains the representation $\mathscr{R}(\frac{3}{2}, \frac{1}{2})+\mathscr{R}(\frac{1}{2}, \frac{1}{2})$. It follows from the investigation in (A) that the former alternative is excluded since otherwise the eigenvalue of the corresponding matrix α^0 would be different from those of α^0 given by (17), and the free charge density would also not be positive definite. The second possibility needs further consideration, for it includes the case in which our equation might decompose into a direct sum of the canonical form of the Dirac–Fierz–Pauli equation for a particle of spin 3/2 given in (A), and the Dirac equation. Any other possibility is excluded because the free charge density would not be positive definite, as proved in (A), whereas it is positive definite for our equation.

It remains to prove, therefore, that our equation does not decompose into the direct sum of the canonical form of the Dirac–Fierz–Pauli equation for a particle of spin 3/2 plus the Dirac equation. Suppose such a decomposition were possible. Then α^k must be transformable through a transformation of the type (5 *c*) to the form

$$\left\{\begin{array}{c|c} \gamma^k & \cdot \\ \hline \cdot & \alpha^{(D)k} \end{array}\right\}, \qquad \ldots\ldots\ldots \quad (45)$$

where γ^k are the four matrices of the former equation and $\alpha^{(D)k}$ stands for the four Dirac matrices. Without changing the form (45) we can bring $\mathscr{R}$ to the form

$$\left[\begin{array}{cc|c} \mathscr{R}(\frac{3}{2}, \frac{1}{2}) & & \\ & \mathscr{R}(\frac{1}{2}, \frac{1}{2}) & \\ \hline & & \mathscr{R}(\frac{1}{2}, \frac{1}{2}) \end{array}\right], \qquad \ldots\ldots \quad (46)$$

the first two representations corresponding to the γ^k. Now we can write the α's of our equation (2) in the form

$$\alpha^k = \left[\begin{array}{cc|c} U^k & c_3 V^k & c_2 V^k \\ -c_3 W^k & a_2 \alpha^{(D)k} & \cdot \\ \hline -c_2 W^k & \cdot & a_3 \alpha^{(D)k} \end{array}\right], \qquad \ldots\ldots \quad (47)$$

with the representation $\mathscr{R}$ in precisely the form (46). Thus the matrix s which transforms (47) to (45) must commute with (46). It must therefore have the form

$$s = \left[\begin{array}{ccc} s_{11}\mathbf{1}_{(12)} & \cdot & \cdot \\ \cdot & s_{22}\mathbf{1}_{(4)} & s_{23}\mathbf{1}_{(4)} \\ \cdot & s_{32}\mathbf{1}_{(4)} & s_{33}\mathbf{1}_{(4)} \end{array}\right], \qquad \ldots\ldots \quad (48)$$

where the elements s_{ab} are numbers. Certain submatrices in (48) have to be zero since $\mathscr{R}(\frac{3}{2}, \frac{1}{2})$ and $\mathscr{R}(\frac{1}{2}, \frac{1}{2})$ are inequivalent representations. Now

the top right-hand element in $s^{-1}\alpha^k s$ is $s_{11}{}^{-1}(c_3 s_{23}+c_2 c_{33})V^k$. This must vanish since it does so in (45). Hence, multiplying by s_{11} which is certainly not zero since s is non-singular,

$$c_3 s_{23}+c_2 s_{33}=0. \quad \ldots\ldots\ldots \quad (49)$$

Moreover, the zero in the last column of (47) must remain unchanged by this transformation. Hence

$$(s^{-1})_{22}a_2 s_{23}+(s^{-1})_{23}a_3 s_{33}=0.$$

But by definition

$$(s^{-1})_{22}s_{23}+(s^{-1})_{23}s_{33}=0.$$

Since neither a_2 nor a_3 are zero, it follows that

$$(s^{-1})_{22}s_{23}=0 \qquad \text{and} \qquad (s^{-1})_{23}s_{33}=0.$$

But s_{23} and s_{33} cannot both be zero since s is non-singular. Nor can $(s^{-1})_{22}$ and $(s^{-1})_{23}$ both be zero. Hence, either

$$s_{23}=0, \qquad s_{33}\neq 0$$

or

$$s_{23}\neq 0, \qquad s_{33}=0.$$

But this leads to a contradiction with (49) since neither c_2 nor c_3 are zero. This rules out the case we are considering and proves that the equation defined by (17) is indecomposable.

APPENDIX

An explicit representation of the matrices u^k, v^k_l and z^k is provided by

$$u^0=\begin{bmatrix} 1 & . & . & . & . & . \\ . & \frac{1}{2} & . & \frac{1}{\sqrt{2}} & . & . \\ . & . & . & . & \frac{1}{\sqrt{2}} & . \\ . & \frac{1}{\sqrt{2}} & . & . & . & . \\ . & . & \frac{1}{\sqrt{2}} & . & \frac{1}{2} & . \\ . & . & . & . & . & 1 \end{bmatrix}, \qquad \sqrt{2}v^0=\begin{bmatrix} . & . \\ \frac{1}{\sqrt{2}} & . \\ . & 1 \\ -1 & . \\ . & -\frac{1}{\sqrt{2}} \\ . & . \end{bmatrix},$$

$$u^3=-\begin{bmatrix} 1 & . & . & . & . & . \\ . & -\frac{1}{2} & . & \frac{1}{\sqrt{2}} & . & . \\ . & . & . & . & -\frac{1}{\sqrt{2}} & . \\ . & \frac{1}{\sqrt{2}} & . & . & . & . \\ . & . & -\frac{1}{\sqrt{2}} & . & \frac{1}{2} & . \\ . & . & . & . & . & -1 \end{bmatrix}, \qquad \sqrt{2}v^3=\begin{bmatrix} . & . \\ \frac{1}{\sqrt{2}} & . \\ . & 1 \\ 1 & . \\ . & \frac{1}{\sqrt{2}} \\ . & . \end{bmatrix},$$

$$u^1 = -\begin{bmatrix} \cdot & \frac{1}{\sqrt{2}} & \cdot & \cdot & \cdot & \cdot \\ \frac{1}{\sqrt{2}} & \cdot & \cdot & \cdot & \frac{1}{2} & \cdot \\ \cdot & \cdot & \cdot & 1 & \cdot & \cdot \\ \cdot & \cdot & 1 & \cdot & \cdot & \cdot \\ \cdot & \frac{1}{2} & \cdot & \cdot & \cdot & \frac{1}{\sqrt{2}} \\ \cdot & \cdot & \cdot & \cdot & \frac{1}{\sqrt{2}} & \cdot \end{bmatrix}, \qquad \sqrt{2}v^1 = \begin{bmatrix} -1 & \cdot \\ \cdot & -\frac{1}{\sqrt{2}} \\ \cdot & \cdot \\ \cdot & \cdot \\ \frac{1}{\sqrt{2}} & \cdot \\ \cdot & 1 \end{bmatrix},$$

$$u^2 = -\begin{bmatrix} \cdot & -\frac{i}{\sqrt{2}} & \cdot & \cdot & \cdot & \cdot \\ \frac{i}{\sqrt{2}} & \cdot & \cdot & \cdot & -\frac{i}{2} & \cdot \\ \cdot & \cdot & \cdot & i & \cdot & \cdot \\ \cdot & \cdot & -i & \cdot & \cdot & \cdot \\ \cdot & \frac{i}{2} & \cdot & \cdot & \cdot & -\frac{i}{\sqrt{2}} \\ \cdot & \cdot & \cdot & \cdot & \frac{i}{\sqrt{2}} & \cdot \end{bmatrix}, \qquad \sqrt{2}v^2 = \begin{bmatrix} i & \cdot \\ \cdot & \frac{i}{\sqrt{2}} \\ \cdot & \cdot \\ \cdot & \cdot \\ \frac{i}{\sqrt{2}} & \cdot \\ \cdot & i \end{bmatrix},$$

$$z^0 = \begin{pmatrix} 1 & \cdot \\ \cdot & 1 \end{pmatrix}, \qquad z^1 = \begin{pmatrix} \cdot & 1 \\ 1 & \cdot \end{pmatrix}, \qquad z^2 = \begin{pmatrix} \cdot & -i \\ i & \cdot \end{pmatrix}, \qquad z^3 = \begin{pmatrix} 1 & \cdot \\ \cdot & -1 \end{pmatrix}.$$

References

Bhabha, H. J., 1945, *Rev. Mod. Phys.*, **17,** 200–216 ; 1949, *Ibid.*, **21,** 451–462 ; 1951 a, *Proc. Ind. Acad. Sci.* A (in course of publication) ; 1951 b, *Report of an International Conference on Elementary Particles* (Bombay, 1950).

Dirac, P. A. M., 1936, *Proc. Roy. Soc.* A, **155,** 447–459.

Fierz, M., 1939, *Helv. phys. Acta*, **12,** 3–37.

Pais, A., and Uhlenbeck, E., 1950, *Phys. Rev.*, **79,** 145–165.

III. *Second Sound and the Thermo-Mechanical Effect at very low Temperatures*

By J. C. Ward and J. Wilks
Clarendon Laboratory, Oxford*

[Received September 5, 1951]

Summary

At very low temperatures the phenomena of second sound and the thermo-mechanical effect in liquid helium may be described by using a phonon model independently of two fluid concepts.

§1. Introduction

Second sound in liquid helium was first predicted by Tisza and Landau on the basis of the two fluid theory. While this has been successful in correlating the velocity of second sound and the viscosity measured by oscillating disc experiments, it is still only a phenomenological theory with no satisfactory theoretical basis.

Recent work by Kramers (1951) has confirmed what had before been only suspected, namely, that at sufficiently low temperatures ($<0{\cdot}5^{\circ}$) liquid helium has a specific heat which varies as the cube of the temperature and is about the magnitude to be expected in a Debye type continuum in which only longitudinal waves are permitted. The present authors (1951) have already shown that a consideration of a Debye type model leads directly without any recourse to a two fluid theory to a velocity of second sound equal to the velocity of first sound divided by $\sqrt{3}$ as predicted by Landau. Experiments by Atkins and Osborne (1950) had shown that at very low temperatures this value is approximately correct, but as the temperature is raised it decreases considerably. This fall is no doubt due to deviations from the behaviour of the ideal model, but so far there is no satisfactory quantum theory of the liquid state to indicate what form these must take. In the meantime it may be profitable to consider a little more closely the phenomena of second sound in the very low temperature region. The object of this paper is to present the ideas underlying our previous note and also briefly to remark on the thermo-mechanical effect in liquid helium.

§2. The Velocity of Second Sound

Consider a Debye type model in which the elementary excitations are quanta of longitudinal sound waves or phonons. Associated with a phonon there is an energy E and a momentum p related by $E=pc$ where

* Communicated by the Authors.

c is the group velocity (or the velocity of ordinary sound). The sound waves are not independent as otherwise thermal equilibrium could never be established; in all cases there must be interactions between the waves. These interactions give rise to the possibility of a periodic variation in the phonon distribution function being propagated through the system with a definite wave velocity. For this to occur we must assume that the interactions conserve energy and momentum since it is only under these conditions that an undamped thermal wave can be propagated. Collisions in which the momentum is not conserved lead to a thermal resistance and to the heat diffusing in the usual way.

We previously derived the velocity of second sound by postulating a density wave in a phonon gas, and by making use of results already available for a photon gas. However, it is possible to show rather more generally that second sound should exist with the correct velocity. We first write down the Boltzmann equation which describes the process of transference of energy and momentum in the liquid. If $f(x^i, p^i)$ is the distribution function for the phonons, which are treated as localized phonons as in the usual approximations of the theory of thermal conductivity of solids, we have:

$$\frac{\partial f}{\partial t}+\frac{cp^i}{p}\frac{\partial f}{\partial x^i}=\Delta_c f, \qquad (p=|\,p^i\,|).$$

All the phonons are assumed to travel with a constant velocity c and $\Delta_c f$ is the rate of change of f due to collisions. Assuming conservation of energy and momentum in collisions, we then find at once the equations

$$\frac{\partial E}{\partial t}+c\frac{\partial P^i}{\partial x^i}=0, \qquad \frac{\partial P^i}{\partial t}+c\frac{\partial T^{ik}}{\partial x^k}=0$$

where

$$E=\int pf d^3p, \qquad P^i=\int p^i f d^3p, \qquad T^{ik}=\int\frac{p^ip^k}{p}f\,d^3p.$$

In writing these integrals we have made the assumption that many interactions (or phonon collisions) occur in a distance equal to the wavelength of any disturbance that may be propagated. This is quite essential, for to take an analogy from gas kinetics, it is impossible to propagate a density wave in a gas at so low a pressure that it is in the Knudsen region. Finally, on remarking that $T^{ik}=\frac{1}{3}\delta^{ik}E$ for a distribution function f disturbed only slightly from spherical symmetry, these equations give directly:

$$\frac{\partial^2 E}{\partial t^2}=\frac{c^2}{3}\frac{d^2E}{dx^{i2}}$$

which is the required result. This proof applies equally to the velocity of sound in a relativistic gas, and perhaps clarifies our previous argument. We should also mention that we have heard recently from Professor H. A. Kramers that he too has devised a proof which though differing from this in details is essentially similar.

§3. The Thermo-Mechanical Effect

Quite apart from second sound there seems to be another consequence of this phonon type of representation. Let us consider a liquid with a Debye type excitation spectrum and suppose that it has a vanishingly small viscosity. The phonons can be regarded as exerting an osmotic pressure in the liquid; this should be observable if one could find a suitable semi-permeable membrane, which would be permeable to the liquid but not to the thermal waves in the liquid. This requirement expressed in the language of two fluid theory means that the membrane is to be permeable only to helium at absolute zero, that is to the superfluid. It seems that an effective membrane is a slot or capillary whose smallest dimension is of the order of the wavelengths of the phonons. The most striking example of the way in which heat may be filtered off is seen when liquid helium is forced through very fine channels; heat is developed at the entrance to the channels and the liquid emerges from them at a lower temperature.

Consider now two reservoirs A and B containing liquid helium at temperatures T and $T+\Delta T$ and connected by a narrow capillary. There will be a difference ΔP in the osmotic pressure (P) of the phonons in A and B, and since the capillary acts as a semi-permeable membrane a difference in the levels of liquid in A and B will be set up equal to ΔP. To calculate ΔP we express the pressure P in terms of the internal energy E per unit volume and the specific heat per unit volume (C) as aT^3 so that

$$\Delta P=\tfrac{1}{3}\Delta E=\tfrac{1}{3}C\,\Delta T=\tfrac{1}{3}aT^3\Delta T.$$

This is in agreement with H. London's formula

$$\Delta P=S\,.\,\Delta T$$

where S is the entropy per unit volume. (Of course any satisfactory kinetic description of the thermo-mechanical effort must lead to London's formula as this is known to be a general thermo-dynamic result (De Groot 1950).)

References

Atkins, K. R., and Osborne, D. V., 1950, *Phil. Mag.*, **41**, 1078.

De Groot, 1950, *Thermodynamics of Irreversible Processes* (Amsterdam: North Holland Publishing Co.).

Kramers, H. C., 1951, *Report to the Oxford Low Temperature Conference.*

Ward, J. C., and Wilks, J., 1951, *Phil. Mag.*, **42**, 314.

IV. *Space Charge Smoothing of Microwave Shot Noise in Electron Beams*

By F. N. H. Robinson
Clarendon Laboratory, Oxford*

[Received September 14, 1951]

Summary

A theoretical analysis is given which takes account of both space charge interaction between electrons and the multi-valued nature of the flow due to the Maxwellian distribution of initial velocities. The theory is in agreement with the experimental results of Cutler and Quate (1950) and makes possible a coherent account of shot noise at all frequencies.

Recent work on the travelling wave tube as a signal amplifier (Kompfner 1947, Pierce 1947, 1950, Robinson and Kompfner 1951) makes it desirable to have a theoretical account of shot noise in electron beams at frequencies in excess of 2000 Mc/s. In order to be rigorous such a theory must take account not only of space charge interaction of electrons throughout their flow but also of the multi-velocitied nature of the flow, due to its origin at a thermionic cathode.

We are concerned to calculate the fluctuating component at frequency $\omega/2\pi$ of the convection current in a cylindrical electron beam from a gun similar to that shown in fig. 1. The shape of the electrodes is arranged to cause electron flow in trajectories normal to the cathode. Pierce (1940) has shown that the steady state conditions, then obtaining within the beam, are similar to those within a planar diode of infinite extent having the same current density and anode voltage. In analysing the gun system it is therefore, in the first approximation, permissible to treat it as a diode whose anode is permeable to electrons.

MacDonald (1949, 1950) has considered the *growth* of shot noise in an initially smooth electron beam as it passes through regions where the potential is constant or varies according to certain laws. He considers only the noise generated by the random variation of the transit times of electrons due to the velocity distribution and neglects the effect of the fluctuating space charge interaction, although this is included in a more recent paper (MacDonald 1951) on the equilibrium noise in an electron beam. When his theory is applied to an electron gun system used in travelling wave tubes it predicts values of noise considerably in excess of those found experimentally by Robinson and Kompfner (1951). Clearly space charge interaction must play a considerable part in determining the noise content of such a beam.

---

* Communicated by Dr. K. MacDonald.

Pierce (1950) applies Llewellyn's (1941) analysis of the diode to the gun system and following Rack (1938) assumes that the effect of the Maxwellian distribution of initial velocities can be represented by an equivalent fluctuation in time of the average velocity of all electrons at the potential minimum. This procedure takes account of space charge interaction but depends for its validity on the assumption that the electron velocity is effectively a single valued function of position and time at points beyond the potential minimum. Rack (1938) showed that this is a legitimate assumption if the spread in transit time from the potential minimum to the anode is a negligible fraction of a cycle at the frequency concerned. This has generally been held to be the case, but MacDonald (1950) shows that in fact it is not so. Considering a diode in which the potential varies as the 4/3rd power of the distance, he finds an expression for the transit time $\tau(E)$ of an electron with initial kinetic energy E at the minimum,

$$\tau(E)=\tau(0)\left\{1-0{\cdot}85\left(\frac{E}{e\phi}\right)^{1/4}\right\}, \quad . \quad . \quad . \quad . \quad . \quad (1)$$

Fig. 1

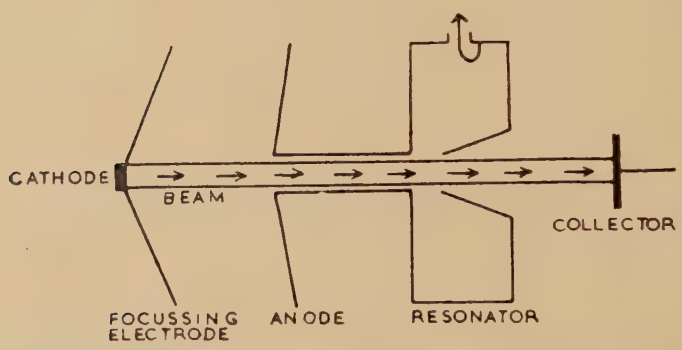

Experimental arrangement for microwave noise study.

where $\tau(0)$ is the transit time of an electron with zero initial energy, and ϕ is the anode potential. Typical figures for $\tau(0)$ and ϕ for an electron gun used at 3000 Mc/s might be 4 cycles and 1000 volts. If we put $E=kT$, the mean energy of electrons originating at a cathode at 1000° K, we find

$$\tau(0)-\tau(E)=\tfrac{1}{3} \text{ cycle}=2\pi/3 \text{ radians}.$$

This will be the order of the spread in transit angle due to thermal velocities and is clearly not negligible.

We are therefore faced with the necessity of finding a theory which, while including the effect of space charge interaction, does not neglect the multi-valued nature of the electron flow.

The device of replacing the velocity distribution by an equivalent fluctuation will be valid in any region provided that the spread in transit angle from one boundary of the region to the other is small. If, therefore,

proceeding from the cathode towards the anode we can find a plane such that in the region bounded by this plane and the anode this condition is fulfilled then we may apply a single valued analysis of this type to this region.

That we can in fact find such a plane follows from eqn. (1). If we consider four electrons with initial energies 0, kT, $2kT$, $3kT$, their transit times (in the numerical example quoted above) are τ_0, $0{\cdot}915\tau_0$, $0{\cdot}898\tau_0$, $0{\cdot}888\tau_0$. The difference in transit angle between the first two electrons is $0{\cdot}67\pi$, between the second two is $0{\cdot}13\pi$, and between the last two $0{\cdot}08\pi$. While $0{\cdot}67\pi$ is certainly not negligible $0{\cdot}13\pi$ and $0{\cdot}08\pi$ may well be, since the effect of a spread $\Delta\omega\tau$ in transit angle will manifest itself as a difference in the phases of the various components of the fluctuation due to individual electrons and will be of the order of $1-\cos\Delta\omega\tau$. This suggests that if we choose a plane whose potential is $\alpha kT/e$ (where $\alpha\sim1$) so that the slowest electrons have kinetic energy αkT at this plane; then the spread in transit angle from this plane, which we shall refer to as the 'α' plane, will be small enough for it to be permissible to use the single-valued analysis in the region beyond it. Direct calculation of the mean reduction in transit time from the 'α' plane due to the thermal velocities and of the root mean square deviation of the transit time shows that this is indeed so. The calculation is laborious and it will suffice to note that the situation is in fact slightly more favourable to the application of the single-valued theory than is indicated by the estimate obtained above.

Consideration of the results obtained by MacDonald (1949) also makes it apparent that the single-valued theory will apply to the region of free drift which the electrons enter on passing the anode of the gun. The initial velocities will not cause any appreciable spread in transit angle in this region until some hundreds of cycles have elapsed.

We, therefore, propose to calculate the shot noise content of the beam emerging from the gun on the assumption that it is legitimate to apply a single-valued analysis to the region beyond the 'α' plane. We shall also assume that at the 'α' plane the current and velocity fluctuations are those appropriate to a fully random beam emitted from a cathode at temperature T. This appears to be a reasonable assumption, since there is no *a priori* reason for supposing that the potential minimum exerts any smoothing action on the components of noise at these frequencies. We shall find that the result gives agreement with experiment and that it is relatively insensitive to the particular choice of 'α'. This latter fact gives us some confidence that the device of dividing the analysis at the 'α' plane is sound. In fig. 2 we show the form of the potential distribution within the diode and the position of the 'α' plane.

We write the mean square value of the current fluctuation at the 'α' plane in the form

$$\overline{c_\alpha^2}=2eI_0B, \qquad (2)$$

where I_0 is the d.c. beam current and B is the bandwidth over which the noise will finally be measured.

We make use of the result derived in the Appendix to calculate $\overline{v_\alpha^2}$ the mean square value of the equivalent velocity fluctuation at the 'α' plane. If the mean number of electrons crossing any plane in time T is NT, where $N=I_0/e$, then the mean square derivation of their average velocity observed in time T from the long term average is

$$\overline{(\delta\widetilde{v^{\mathrm{T}}})^2}=(N\mathrm{T})^{-1}[\widetilde{v^2}-(\tilde{v})^2], \quad . \quad . \quad . \quad . \quad . \quad . \quad . \quad . \quad (3)$$

where $\widetilde{v^2}$ and $\tilde{v}$ are the mean square and mean of the velocity averaged over the velocity distribution.

Fig. 2

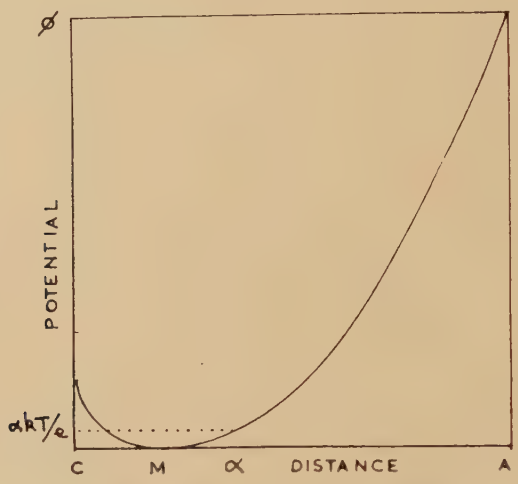

Potential distribution and position of the 'α' plane in a space charge limited diode.

By a theorem due to MacDonald (1949) we may then obtain the power spectrum $w(f)$ of the velocity fluctuations.

$$w(f)=4\pi f\int_0^\infty \frac{\partial\Psi}{\partial\mathrm{T}}\sin 2\pi f\mathrm{T}\,d\mathrm{T}, \quad . \quad . \quad . \quad . \quad . \quad . \quad . \quad . \quad (4)$$

where

$$\Psi=\mathrm{T}^2\overline{(\delta\widetilde{v^{\mathrm{T}}})^2}. \quad . \quad . \quad . \quad . \quad . \quad . \quad . \quad . \quad . \quad (5)$$

The mean square equivalent velocity fluctuation is then

$$\overline{v_\alpha^2}=w(f)\,.\,B. \quad . \quad . \quad . \quad . \quad . \quad . \quad . \quad . \quad . \quad (6)$$

At the 'α' plane

$$\widetilde{v^2}=\int_0^\infty\left(\frac{2E+2\alpha kT}{m}\right)\exp(-E/kT)\frac{dE}{kT}, \quad . \quad . \quad . \quad . \quad (7)$$

$$\tilde{v}=\int_0^\infty\left(\frac{2E+2\alpha kT}{m}\right)^{1/2}\exp(-E/kT)\frac{dE}{kT}. \quad . \quad . \quad . \quad (8)$$

Evaluating these expressions and substituting the results in equations (3), (4), (5) and (6) there results

$$\overline{v_\alpha^2} = \frac{e}{m} \cdot \frac{4kTB}{I_0} f(\alpha), \quad \ldots \ldots \ldots \quad (9)$$

where

$$f(\alpha) = 1 + \alpha - [\alpha^{1/2} + \tfrac{1}{2} e^{\alpha} \pi^{1/2} (1 - \operatorname{erf} \alpha^{1/2})]^2 \quad \ldots \quad (10)$$

and

$$\operatorname{erf} x \equiv 2\pi^{-1/2} \int_0^x e^{-t^2}\, dt.$$

We tabulate $f(\alpha)$ for a range of values of α in table 1.

$$\left.\begin{array}{ll} \text{for } \alpha > 20 & f(\alpha) \sim (4\alpha)^{-1}, \\ \text{for } \alpha = 0 & f(\alpha) = 1 - \pi/4, \end{array}\right\} \quad \ldots \ldots \quad (10\,a)$$

and eqn. (9) reduces to the expression found by Rack (1938) by a less direct and more intuitive method.

Table 1

α	$f(\alpha)$	α	$f(\alpha)$	α	$f(\alpha)$	α	$f(\alpha)$
0	0·215	0·8	0·109	2·5	0·060	10	0·020
0·1	0·182	1·0	0·099	3·0	0·053	13	0·016
0·2	0·162	1·3	0·087	4·0	0·043	16	0·014
0·4	0·140	1·6	0·079	5·0	0·036	20	0·011
0·6	0·123	2·0	0·069	7·0	0·028		

Expressions have been given by Llewellyn (1941) based on a single-valued analysis for the fluctuating components of potential V, convection current c and velocity v at any plane in the diode in terms of their values at an earlier plane (which we shall identify with the 'α' plane). V_α, c_α and v_α.

$$\left.\begin{aligned} V - V_\alpha &= A_{11} I_1 + A_{12} v_\alpha + A_{13} c_\alpha \\ v &= A_{21} I_1 + A_{22} v_\alpha + A_{23} c_\alpha \\ c &= A_{31} I_1 + A_{32} v_\alpha + A_{33} c_\alpha \end{aligned}\right\}, \quad \ldots \quad (11)$$

where I_1 is the fluctuating component of total (sum of convection and displacement) current and the coefficients A are functions of frequency, d.c. current density and the coordinates of the two planes.

At lower frequencies (<100 Mc/s) shot noise is observed in a circuit connected between the anode and cathode of the diode and the measured quantity is I_1 or V. In the experiments with which we are concerned the noise is observed by measuring the voltage induced in a resonator or helix when the beam passes through it after leaving the gun. The observed quantity is the fluctuation c in the convection current. Fluctuations in anode potential (V) and total current (I_1) are not therefore of interest. Moreover it may be shown that if the total transit time across the diode is greater than two cycles the error involved in neglecting terms in V and I_1

is less than 3%. We can therefore simplify equations (11) considerably and also do not have to consider the effect of any external impedance connected between the anode and cathode of the gun.

Eqns. (11) are thus reduced to

$$\left.\begin{aligned} v&=A_{22}v_\alpha+A_{23}c_\alpha \\ c&=A_{32}v_\alpha+A_{33}c_\alpha \end{aligned}\right\} \quad . \quad . \quad . \quad . \quad . \quad . \quad . \quad (12)$$

It is convenient to express the coefficients A in terms of I_0 the steady diode current, T the cathode temperature, ω the angular frequency, τ_0 the transit time of an electron from the potential minimum to the anode in the absence of any initial velocities and the normalized potentials α and $\eta=e\phi/(kT)$ of the 'α' plane and the anode. We then have

$$\left.\begin{aligned} A_{22}&=F_1(\alpha,\eta), \qquad A_{23}=-K^{-1}F_2(\alpha,\eta), \\ A_{32}&=KF_3(\alpha,\eta), \qquad A_{33}=F_4(\alpha,\eta), \end{aligned}\right\} \quad . \quad . \quad (13)$$

where

$$K=j\omega\tau_0 I_0(2kT/m)^{-1/2}, \quad . \quad . \quad . \quad . \quad . \quad . \quad . \quad (14)$$

$$F_1=1-2[\eta](1+\eta)^{-1/2}\{[\eta]-[\alpha]\}, \quad . \quad . \quad . \quad . \quad . \quad (15\,a)$$

$$F_2=(1+\eta)^{-1/4}\{1+[\alpha][\eta]\}\{[\eta]-[\alpha]\}, \quad . \quad . \quad . \quad . \quad . \quad (15\,b)$$

$$F_3=(1+\eta)^{-3/4}\{[\eta]-[\alpha]\}, \quad . \quad . \quad . \quad . \quad . \quad . \quad . \quad (15\,c)$$

$$F_4=1-(1+\eta)^{-1/2}\{[\eta]-[\alpha]\}^2, \quad . \quad . \quad . \quad . \quad . \quad (15\,d)$$

and

$$\left.\begin{aligned} [\alpha]&\equiv[(\alpha+1)^{1/2}-1]^{1/2}, \\ [\eta]&\equiv[(\eta+1)^{1/2}-1]^{1/2}. \end{aligned}\right\} \quad . \quad . \quad . \quad . \quad . \quad (16)$$

Now in using eqns. (12) to evaluate the fluctuating currents and velocities at the anode we must bear in mind that c_α and v_α are uncorrelated. Their contributions must therefore be calculated separately and then summed as squares.

Denoting by c_1 and v_1 those components of c and v derived from c_α and by c_2 and v_2 those derived from v_α we have

$$\overline{c^2}=\overline{c_1^2}+\overline{c_2^2}, \quad . \quad . \quad . \quad . \quad . \quad . \quad . \quad . \quad (17)$$

with a similar equation for $\overline{v^2}$.

From eqns. (2), (9), (12) and (13),

$$c_1=F_4(2eI_0B)^{1/2}, \quad . \quad . \quad . \quad . \quad . \quad . \quad . \quad . \quad (18\,a)$$

$$v_1=-K^{-1}F_2(2eI_0B)^{1/2}, \quad . \quad . \quad . \quad . \quad . \quad . \quad . \quad (18\,b)$$

$$c_2=KF_3(e/m)^{1/2}(4kTBf(\alpha)/I_0)^{1/2}, \quad . \quad . \quad . \quad . \quad (18\,c)$$

$$v_2=F_1(e/m)^{1/2}(4kTBf(\alpha)/I_0)^{1/2}. \quad . \quad . \quad . \quad . \quad (18\,d)$$

Expressing $\overline{c^2}$ in the form

$$\overline{c^2}=\Gamma^2 \,.\, 2eI_0B, \quad . \quad . \quad . \quad . \quad . \quad . \quad . \quad (19)$$

and using eqn. (14) there results, after some re-arrangement, an expression for the space charge smoothing factor Γ^2 at the anode of the diode.

$$\Gamma^2=F_4^2+(\omega\tau_0)^2f(\alpha)F_3^2, \quad \ldots\ldots (20)$$

where F_3, F_4 and $f(\alpha)$ are defined in eqns. (15) and (10).

We may also calculate the value Γ_D^2 of the space charge factor which will be found after the beam has drifted for a time τ_D in a field free space beyond the anode of the gun. The current fluctuation c_D is then given in terms of the current and velocity fluctuations c and v at the anode by

$$c_D=c\cos\omega_0\tau_D-j(\omega/\omega_0)I_0(v/u)\sin\omega_0\tau_D, \quad \ldots (21)$$

where u is the steady beam velocity and ω_0 is the plasma frequency in the beam (Ramo 1939).

In applying equation (21) we use the relations

$$u=(2kT/m)^{1/2}(1+\eta)^{1/2}, \quad \ldots\ldots (22)$$

$$\omega_0\tau_0=\sqrt{2}. \quad \ldots\ldots (23)$$

Again evaluating contributions due to c_x and v_x separately and taking the sum of squares there results :

$$\Gamma_D^2=\{F_4^2+\tfrac{1}{2}F_2^2(1+\eta)^{-1}\}\sin^2(\omega_0\tau_D+\chi_1)$$
$$+(\omega\tau_0)^2f(\alpha)\{F_3^2+\tfrac{1}{2}F_1^2(1+\eta)^{-1}\}\sin^2(\omega_0\tau_D+\chi_2), \quad (24)$$

where

$$\left.\begin{aligned}\tan\chi_1&=\sqrt{2}(1+\eta)^{1/2}F_4/F_2\\ \tan\chi_2&=-\sqrt{2}(1+\eta)^{1/2}F_3/F_1\end{aligned}\right\} \quad \ldots\ldots (25)$$

The dependence of Γ_D^2 on the arbitrary parameter α is not in eqn. (24) very perspicuous ; we may note, however, that for $\alpha=0$ and η large, eqn. (24) reduces to the equation derived by Pierce (1940) on the basis of an entirely single-valued theory, namely,

$$\Gamma_D^2=\tfrac{3}{2}kT/(e\phi)(\omega\tau_0)^2(1-\pi/4)\sin^2(\omega_0\tau_D+\chi). \quad \ldots (26)$$

In order to elucidate further the dependence on α we shall use as a numerical example the experimental data of Cutler and Quate (1950). These authors explored the variation with τ_D of Γ_D^2 using a gun which had a cathode temperature $T=2000°$ K, transit angle $\omega\tau_0=32$ radians and anode potential $\phi=900$ volts. Writing eqn. (24) in the form

$$\Gamma_D^2=A\sin^2(\omega_0\tau_D+\chi_1)+B\sin^2(\omega_0\tau_D+\chi_2), \quad \ldots (24\,a)$$

we tabulate A, B, χ_1 and χ_2 for a range of values of α for this gun in table 2. In the last row we have tabulated the amplitude of Γ_D^2 neglecting the small difference between χ_1 and χ_2 which alters $|\Gamma_D^2|$ by less than 1% and also gives rise to a small constant term of the order of 10^{-4}. It is immediately apparent, as we predicted, that the result obtained is not critically dependent on the particular value of α between 0 and 4.

The experimental values found by Cutler and Quate can be written in the form

$$\Gamma_D^2=0{\cdot}055\sin^2(\omega_0\tau_D+66°)+0{\cdot}01. \quad \ldots\ldots (27)$$

The small constant term is attributed by these authors to partition noise. When we bear in mind that microwave noise measurements are seldom more accurate than 5% and that the type of experiment carried out by Cutler and Quate would tend to overestimate the magnitude of Γ_D^2 the agreement with the results in table 2 appears to be satisfactory.

Table 2

$\alpha=$	0	$\frac{1}{4}$	$\frac{1}{2}$	1	2	4	η
$A=$	0·0003	0·010	0·0172	0·0283	0·0451	0·0737	1
$B=$	0·061	0·0405	0·0316	0·0231	0·0128	0·0070	0
$\chi_1=$	55·3°	68·5°	69·7°	70°	70·2°	71·2°	90°
$\chi_2=$	55·5°	56·7°	56·9°	57·9°	58·7°	59·7°	0°
$\lvert\Gamma_D^2\rvert=$	0·061	0·051	0·049	0·051	0·058	0·081	1

However, in carrying out the analysis we have neglected the effect of the finite size of the beam. It is possible (Ramo 1939) to introduce a correction for this in the field-free drift region and in interpreting their results in the light of Pierce's theory Cutler and Quate did this. In this region the finite size of the beam results in a reduction of the effective plasma frequency ω_0. Inspection of eqn. (21) shows that this results in an increase in the contribution to Γ_D^2 from velocity fluctuations at the anode and a decrease in χ. Making this correction Cutler and Quate found good agreement with the experimental value of the periodicity ω_0 ; but on the basis of Pierce's equation (26) they obtained a theoretical value

$$\Gamma_D^2=0{\cdot}089\sin^2(\omega_0\tau_D+42^\circ), \quad . \quad . \quad . \quad . \quad . \quad (27\,a)$$

which is outside the limits of experimental error. The present theory with the most favourable value of α is capable of yielding a value $\lvert\Gamma_D^2\rvert=0{\cdot}065$ when these corrections are made but the discrepancy in the value of χ still remains.

Cutler and Quate suggest that this is due to the neglect in the analysis of the finite beam size within the gun. Although an exact treatment of this region has not yet been attempted, a qualitative estimate does indeed suggest that the effect of finite beam size will there tend to compensate the effect on $\lvert\Gamma_D^2\rvert$, χ_1 and χ_2 of the corrections applied in the region of free drift. In the absence of a complete theory of this effect the agreement obtained is as good as can be expected.

At very low frequencies eqn. (20) predicts that $\Gamma^2\to kT_l/(e\phi)$. The discrepancy between this result and the value $\Gamma^2=0{\cdot}644kT_l/e\phi$ obtained by Thomson, North and Harris (1940) by a quasi-static analysis, arises from the neglect of terms in I_1 in eqn. (11) which is only permissible for frequencies such that $\omega\tau_0>4\pi$.

At extremely high frequencies Pierce's (1950) single-valued analysis leads to the conclusion that Γ^2 can increase indefinitely as ω increases and reach values in excess of unity. In the present theory this difficulty does not occur, since as the frequency increases the region, within which a single-valued analysis applies, contracts. That is to say, that in order for

the mean spread in transit angle $\Delta\omega\tau$ to be less than any pre-assigned value larger and larger values of 'α' have to be taken until finally the 'α' plane coincides with the anode when eqn. (20) predicts that $\Gamma^2=1$.

If the assigned value of the permissible spread in transit angle is Δ, then from eqn. (1) α is determined by

$$0{\cdot}85\Delta^{-1}\omega\tau_0\{kT/(e\phi)\}^{1/4}\{(\alpha+1)^{1/4}-\alpha^{1/4}\}=1. \quad . \quad . \quad (28)$$

We have only qualitative considerations to guide us in the choice of Δ. If $\Delta \leqslant \pi/2$ space charge interaction will already play a considerable part

Fig. 3

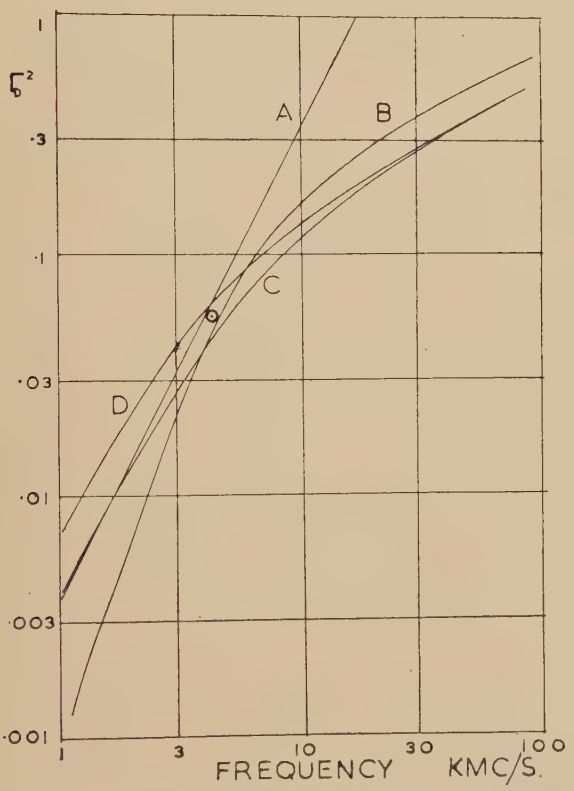

Space charge smoothing factor as a function of frequency.
A. Pierce's theory. B, C, D. Present theory with $\Delta=\pi/2$, $\pi/4$ and $\pi/8$.

in determining the noise content of the beam, but the single-valued analysis will give only a very rough account of the behaviour in the region beyond the 'α' plane. If on the other hand $\Delta \leqslant \pi/8$, the single-valued analysis will be a very good approximation to the behaviour beyond the 'α' plane but we shall have neglected any ordering of the beam which may have taken place before the 'α' plane is reached. It, therefore, appears reasonable to expect that a correct description will be found with $\pi/8<\Delta<\pi/2$. In fig. 3 we plot $|\Gamma_D{}^2|$ as a function of frequency between

1000 and 100 000 Mc/s for $\Delta=\pi/8$, $\pi/4$ and $\pi/2$. The values of τ_0 and η are those appropriate to the gun used by Cutler and Quate discussed above. For the purpose of comparison we also give the value of $|\Gamma_D^2|$ from Pierce's equation (26) and Cutler and Quate's experimental result. Throughout this region the difference between χ_1 and χ_2 is less than 12° and is neglected.

It is satisfying that it is possible to show that the existence of electron beams showing a considerable degree of space charge smoothing at micro-wave frequencies does not imply that the potential minimum exerts any smoothing action on such high frequency components of shot noise. It is indeed difficult to see how this could occur, at frequencies so high that the transit of electrons from cathode to minimum occupies several cycles. We have in fact assumed that the stream of electrons emerging from the potential minimum is entirely random. In a forthcoming paper Kompfner (1951) will show how the interpretation of micro-wave partition noise given by Robinson and Kompfner (1951) and depending on the compensating action of the potential minimum, can be adapted to the view of the space charge smoothing process given above.

The theory we have obtained differs from earlier theories (Pierce 1950) chiefly in the interpretation it affords and in eliminating the possibility of Γ^2 exceeding unity at sufficiently high frequencies ; but at least one practical consequence is worthy of note.

The fact that the current and velocity fluctuations consist of two uncorrelated components whose minima do not coincide ($\chi_1 \neq \chi_2$) limits the reduction in noise possible by the method proposed by Field, Tien and Watkins (1951). In this method the beam is suddenly accelerated and then at a later point decelerated, the points of acceleration and deceleration coinciding with the minima of the current and velocity fluctuations respectively. In the simplest case when the amplitude of the two components associated with χ_1 and χ_2 are equal in magnitude the greatest reduction in noise possible will be approximately $\sin 2(\chi_1-\chi_2)$.

In conclusion it may be instructive to give a brief account of the course of fluctuations in a beam of electrons from the time it leaves the cathode. Between the cathode and the potential minimum and beyond the potential minimum to the region of the ' α ' plane the behaviour is dominated by the Maxwellian velocity distribution and the beam remains effectively random. From the ' α ' plane to the anode the flow becomes effectively single-valued and Llewellyn's (1941) analysis correctly describes the influence of space charge interaction which is here the dominant feature of the flow. Beyond the anode the flow is also at first effectively single-valued, a treatment such as that of Ramo (1939) is appropriate, and in this region the amplitude of the fluctuations varies periodically with distance. Eventually, however, since the flow is not strictly single-valued the velocity distribution will again dominate and the periodic variations will decay until finally the current and velocity fluctuations reach the equilibrium value predicted by MacDonald (1951) on thermodynamic

grounds. This final transition to the equilibrium state has not been analysed but it appears plausible to assume that it will occur after a transit angle such that the spread in transit angle due to the Maxwellian distribution becomes comparable with π. According to MacDonald (1949) this will require a total drift time of some hundreds of cycles in even the most favourable case.

APPENDIX

We consider electrons crossing a fixed plane at a mean rate N per second, with an average distribution in velocity $n(v)$ so that the long term average velocity is

$$\tilde{v}=\frac{\sum_i n_i v_i}{\sum_i n_i}. \qquad \text{(A 1)}$$

If we observe the electrons over a period T during which time the actual distribution is $n_i+\nu_i$ say, then the average velocity observed in this interval will be

$$\widetilde{v^{\mathrm{T}}}=\frac{\sum_i (n_i+\nu_i)v_i}{\sum_i n_i+\nu_i}. \qquad \text{(A 2)}$$

Now if electrons in each velocity class v_i are emitted independently and at random,

$$\overline{(\mathrm{T}\nu_i)^2}=\mathrm{T}n_i, \qquad \text{(A 3)}$$

where the average is over many periods T.

Provided T is long enough and the subdivision into velocity classes is coarse enough so that $\mathrm{T}n_i$ is large, ν_i will be much small than n_i and we can expand (A 2) as

$$\widetilde{v^{\mathrm{T}}}=\frac{1}{N}\left\{\sum_i (n_i+\nu_i)v_i\right\}\left\{1-\frac{1}{N}\sum_i \nu_i\right\},$$

and so

$$\delta\widetilde{v^{\mathrm{T}}}=\widetilde{v^{\mathrm{T}}}-\tilde{v}=\frac{1}{N}\left\{\sum_i \nu_i v_i-\tilde{v}\sum_i \nu_i\right\}. \qquad \text{(A 4)}$$

We now average $(\delta\widetilde{v^{\mathrm{T}}})^2$ over many periods T and obtain

$$\begin{aligned}\overline{(\delta\widetilde{v^{\mathrm{T}}})^2}&=N^{-2}\overline{\left\{\sum_i \nu_i v_i-\tilde{v}\sum_i \nu_i\right\}^2}\\ &=N^{-2}\overline{\sum_i\sum_j \nu_i v_i \nu_j v_j}-2\tilde{v}\overline{\sum_i\sum_j \nu_i\nu_j v_i}+(\tilde{v})^2\overline{\sum_i\sum_j \nu_i\nu_j}.\end{aligned} \qquad \text{(A 5)}$$

Since the fluctuations in each velocity class are independent this reduces to

$$\overline{(\delta\widetilde{v^{\mathrm{T}}})^2}=N^{-2}\overline{\left\{\sum_i \nu_i^2 v_i^2-2\tilde{v}\sum_i \nu_i^2 v_i+(\tilde{v})^2\sum_i \nu_i^2\right\}}. \qquad \text{(A 6)}$$

We now make use of eqn. (A 3) to obtain

$$\overline{(\delta\widetilde{v}^{\mathrm{T}})^2}=(N^2\mathrm{T})^{-1}\left\{\sum_i n_i v_i^2-2\tilde{v}\sum_i n_i v_i+(\tilde{v})^2\sum_i n_i\right\}$$

$$=(N\mathrm{T})^{-1}\{\widetilde{v^2}-(\tilde{v})^2\}, \quad . \quad . \quad . \quad . \quad . \quad . \quad . \quad . \quad . \quad . \quad (\mathrm{A}\,7)$$

which is the result used in the text.

Acknowledgments

It is a pleasure to thank Dr. R. Kompfner and Dr. D. K. C. MacDonald for their helpful criticism and encouragement. I am particularly indebted to Dr. MacDonald for suggesting the approach used in the Appendix. I am also indebted to the Nuffield Foundation for a Research Fellowship.

References

Cutler, C. C., and Quate, C. F., 1950, *Phys. Rev.*, **80,** 875.
Field, L., Tien, P. K., and Watkins, D., 1951, *Proc. I.R.E.*, **39,** 194.
Kompfner, R., 1947, *Wireless Engnr.*, **24,** 255 ; 1951, to be published.
Llewellyn, F. B., 1941, *Electron Inertia Effects* (Cambridge : University Press).
MacDonald, D. K. C., 1949, *Phil. Mag.* [7], **40,** 561 ; 1950, *Ibid.*, **41,** 863 ; 1951, *Ibid.*, **42,** 515.
Pierce, J. R., 1940, *J. Appl. Phys.*, **11,** 548 ; 1947, *Proc. I.R.E.*, **35,** 111 ; 1950, *Travelling Wave Tubes* (New York : Van Nostrand).
Rack, A. J., 1938, *Bell. Syst. Tech. J.*, **17,** 592.
Ramo, S., 1939, *Phys. Rev.*, **56,** 276.
Robinson, F. N. H., and Kompfner, R., 1951, *Proc. I.R.E.*, **39,** 918.
Thomson, B. J., North, D. O., and Harris, W. A., 1940, *R.C.A. Review*, **5,** 371.

V. *The Coulomb Scattering of Charged Particles in Nuclear Emulsions*

By W. Bosley and H. Muirhead
Department of Natural Philosophy, University of Glasgow*

[Received September 14, 1951]

Summary

Measurements have been made on the multiple coulomb scattering of electrons and protons in normal and diluted Ilford G5 emulsions. Empirical constants are given relating the mean angle of scattering to the product momentum × velocity for particles of unit charge.

§1. Introduction

The nature and energy of a charged particle traversing a nuclear emulsion may be established by making observations on any two of the following three characteristics of its track :—

(*a*) The residual range.

(*b*) The multiple coulomb scattering.

(*c*) The ionization (grain density or delta rays).

The grain density produced by a charged particle is partially dependent upon the method of processing of the emulsion, and can vary from one batch of plates to another despite apparently rigid conditions of development. For an emulsion of a given composition the residual range and the magnitude of the coulomb scattering of particles with the same mass, velocity and charge are always the same, however, within the limits imposed by statistical deviations. These two properties may, therefore, be regarded as the ' constants ' of a nuclear emulsion, and their values will depend upon its atomic composition.

The extremely sensitive nuclear emulsions employed in recent years have contained a very high silver halide to gelatine ratio. Their sensitivity was mainly dependent upon this feature. Recently, however, Dodds and Waller (1951) have introduced new types of emulsions, which, whilst capable of recording the passage of particles at minimum ionization, possess a much smaller silver halide content. These are known as diluted Ilford G5 emulsions.

In this paper values will be given for the ' scattering constants ' of normal, × 2 and × 4 G5 emulsions (that is, emulsions with the normal gelatine to silver halide ratio and with twice and four times the normal value of this ratio). A later paper from this laboratory will give range–energy relationships for the diluted emulsions.

* Communicated by Professor P. I. Dee, F.R.S.

§2. Method

Measurements have been carried out using protons with kinetic energies of 58, 77 and 146 Mev, and electrons with energies of 9·5, 13·5 and 18·5 Mev. Thus the coulomb scattering has been examined for particles of unit charge over a wide range of velocities and masses.

The proton tracks were measured in plates exposed to the external uncollimated beam of the Harwell cyclotron, and the two lower energies obtained by interposing aluminium absorbers in the path of the beam. The electron tracks were obtained by pair production in the x-ray beam of the smaller Glasgow University synchrotron. Electrons with the required momenta were selected by means of a magnetic channel.

The proton scattering measurements were carried out over track segments $8000\,\mu$ in length. Segments of $1500\,\mu$ were used for the electrons. The scattering measurements were performed on a Cooke M.4000 microscope with a $\times 45$ objective and $\times 15$ eyepieces, using the coordinate technique developed by Fowler (1950).

Grain-density determinations were also carried out on the proton tracks in both normal and diluted emulsions in order to examine the variation of grain-density with change of velocity. For these measurements a $\times 95$ objective was used.

§3. Results

(i) *Presentation*

A review of the theories of multiple coulomb scattering of charged particles has recently been given by the Bristol group (Gottstein *et al.* 1951. We are grateful to the authors for making their results available to us before publication). Using the notation adopted by these authors, the mean angle of scattering may be given as

$$\langle\Phi\rangle_{\text{chord}}=\frac{2e^2(NZ^2)^{1/2}t^{1/2}z}{p\beta c}\times L, \qquad (1)$$

where $\langle\Phi\rangle_{\text{chord}}$ is the mean angle of scattering measured by the coordinate method. N, Z, t are the number of scattering atoms per cm^3, their atomic number and the thickness of the medium in microns (in our case the cell-size). ze, p, βc are the charge, momentum, and velocity of the scattered particle. L is a slowly varying function of N, Z, t and β.

Values of L as a function of t and β have been given in graphical form by Goldschmidt-Clermont (1950), using the Molière theory (1948).

Eqn. (1) may be reformulated as

$$\langle\Phi\rangle_{\text{chord}}\times\frac{p\beta c}{z}\times\left(\frac{100}{t}\right)^{1/2}=2e^2(NZ^2)^{1/2}L(100)^{1/2}=K, \qquad (2)$$

where K is termed the 'scattering constant' of the medium. It is usually expressed in units of degrees Mev $(100\,\mu)^{-1/2}$, and we shall employ this convention.

We shall also use a parameter K_c—the scattering constant determined from a restricted selection of the experimental values of Φ_{chord}. This parameter is of particular importance in the determination of the energies of very fast particles traversing the emulsion. In such determinations comparatively few angular measurements can be made on a single track, and the presence of one large angle single scattering can appreciably alter the mean value of the scattering angle. In the present work we have employed the convention that angles greater than four times the median value are not included in the determination of K_c.

In our presentation of the results corrections have been made for the following effects :—

(*a*) Spurious scattering introduced by observational and microscope errors (Levi Setti 1951).

(*b*) The inclination of the track to the coordinate axes employed for measurement. (This correction was necessary only for the electron tracks.)

Table 1

Kinetic energy (after correction for loss)	K				
	$t=25\,\mu$	50	100	200	400
8·7 Mev	28·2±0·6	27·1±0·8	26·5±1·2	25·8±1·7	25·3±2·6
13·4	—	27·4±0·8	27·3±1·2	28·4±1·7	26·5±2·5
17·2	—	28·3±0·8	26·5±1·0	25·7±1·5	24·9±2·2
	K_c				
8·7	21·4±0·5	21·9±0·7	23·5±0·9	24·5±1·7	25·3±2·6
13·4	—	23·3±0·7	24·5±1·1	23·2±1·6	26·5±2·5
17·2	—	23·2±0·7	24·9±1·0	22·4±1·6	24·9±2·2

(*c*) Energy losses by the particles in passing through the emulsion (Rossi and Greisen 1941, Smith 1947, Montgomery 1949, Bradner *et al.* 1950).

(*d*) Distortion of the electron tracks in the ×4 emulsion. A frequency distribution of the algebraic values of Φ_{chord} was plotted, and it was found that the median was appreciably displaced from the zero position (Menon *et al.* 1951). The displacement was assumed to represent the distortion, and its value was added algebraically to the individual measurements of Φ_{chord}. Tests on the proton tracks in the ×4 emulsion, and on electron and proton tracks in normal and ×2 emulsions indicated that distortion was negligible.

(ii) *Experimental Results for Normal* G5 *Emulsions*

The experimental values of K and K_c for electrons are shown for various energies and cell-sizes in table 1 : the errors quoted are the statistical

' probable errors '. It can be seen that, within the limits imposed by the statistical error, K and K_c are independent of energy, in accordance with theoretical predictions. The values of $\langle\Phi\rangle_{\text{chord}} \times p\beta c$ as a function of $p\beta c$ are given in fig. 1.

Fig. 1

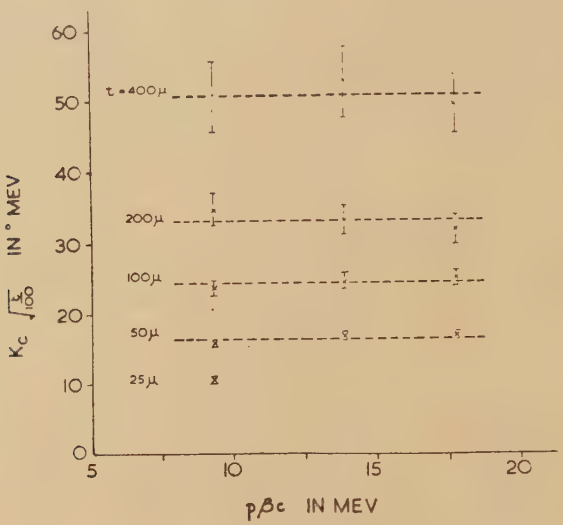

$\langle\Phi\rangle_{\text{chord } c} \times p\beta c = K_c\left(\frac{t}{100}\right)^{1/2}$ versus $p\beta c$ as a function of cell-size. The horizontal lines represent the weighted mean values of $\langle\Phi\rangle_{\text{chord } c} \times p\beta c$.

Fig. 2

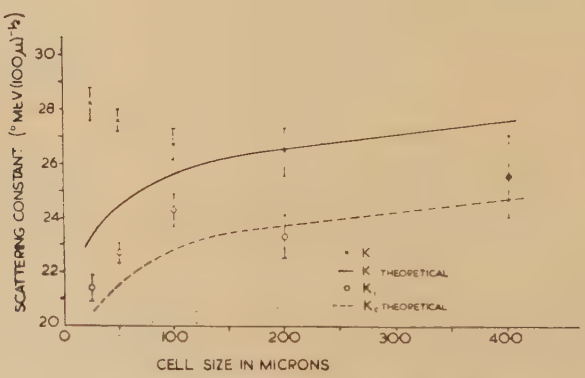

Comparison of experimental results for the electrons with Molière's theory of multiple scattering.

In fig. 2 the weighted mean values of K and K_c for the three energies are plotted as a function of cell-size ; the theoretical curves for K and K_c, derived from Goldschmidt's paper and the Molière distribution function, are included in this diagram. It can be seen that the experimental and theoretical values of K do not agree for small cell-sizes. This lack of

agreement can possibly be explained by a small difference in the theoretical and experimental frequency distributions of the values of Φ_{chord} for large scattering angles. Better agreement is obtained between the experimental and theoretical values of K_c.

The value of K at a cell-size of $100\,\mu$ is in good agreement with that obtained by other workers (Gottstein *et al.* 1951, Corson 1951, Voyvodic and Pickup 1951).

Table 2

Kinetic energy (after correction for loss)	K		
	$t=200\,\mu$	400	800
140 MeV	—	$30{\cdot}0\pm0{\cdot}8$	$32{\cdot}0\pm1{\cdot}2$
66	$33{\cdot}0\pm0{\cdot}6$	$31{\cdot}9\pm0{\cdot}8$	$31{\cdot}7\pm1{\cdot}2$
47*	$27{\cdot}1\pm0{\cdot}7$	$26{\cdot}2\pm1{\cdot}0$	$27{\cdot}8\pm1{\cdot}4$
	K_c		
140 MeV	—	$28{\cdot}6\pm0{\cdot}8$	$29{\cdot}0\pm1{\cdot}1$
66	$28{\cdot}3\pm0{\cdot}6$	$28{\cdot}6\pm0{\cdot}8$	$29{\cdot}0\pm1{\cdot}1$
47*	$24{\cdot}2\pm0{\cdot}7$	$24{\cdot}2\pm0{\cdot}9$	$27{\cdot}0\pm1{\cdot}4$

* This value is based on residual range measurements of protons in the emulsion (Bradner *et al.* 1950).

Table 3

Type of particle	Kinetic energy (after correction for loss)	K				
		$t=50\,\mu$	100	200	400	800
Electrons	18·9 MeV	$22{\cdot}7\pm0{\cdot}7$	$21{\cdot}0\pm0{\cdot}9$	$21{\cdot}7\pm1{\cdot}3$	$22{\cdot}5\pm2{\cdot}4$	—
Protons	141	—	—	—	$23{\cdot}4\pm0{\cdot}8$	$22{\cdot}2\pm1{\cdot}2$
	69	—	—	$24{\cdot}7\pm0{\cdot}6$	$22{\cdot}6\pm0{\cdot}7$	$20{\cdot}7\pm1{\cdot}0$
	49	—	—	$27{\cdot}9\pm0{\cdot}6$	$25{\cdot}7\pm0{\cdot}9$	$25{\cdot}0\pm1{\cdot}1$
		K_c				
Electrons	18·9	$16{\cdot}7\pm0{\cdot}5$	$16{\cdot}8\pm0{\cdot}7$	$20{\cdot}0\pm1{\cdot}2$	$22{\cdot}5\pm2{\cdot}4$	—
Protons	141	—	—	—	$21{\cdot}5\pm0{\cdot}8$	$22{\cdot}0\pm1{\cdot}2$
	69	—	—	$21{\cdot}9\pm0{\cdot}5$	$21{\cdot}3\pm0{\cdot}7$	$19{\cdot}8\pm1{\cdot}0$
	49	—	—	$24{\cdot}9\pm0{\cdot}8$	$23{\cdot}3\pm1{\cdot}0$	$25{\cdot}0\pm1{\cdot}6$

The value of K and K_c for protons with mean kinetic energies of 140, 66 and 47 MeV (after correction for ionization losses in the emulsion) are given in table 2. There is good agreement with the theoretical values but the expected small increase in K with increasing cell-size is too small to observe in this case.

(iii) *Diluted Emulsions*

The experimental values of K and K_c for $\times 2$ and $\times 4$ diluted emulsions are given in tables 3 and 4. It can be seen that there is little or no variation of K with cell-size.

The values of K and K_c for the electrons in the $\times 4$ emulsions cannot be considered as reliable as those for electrons in the other emulsions. In addition to the distortion mentioned previously great difficulty was experienced in following the widely spaced grains which marked the passage of the electrons in these emulsions.

Table 4

Type of particle	Kinetic energy (after correction for loss)	K				
		$t=50\,\mu$	100	200	400	800
Electrons	19·1 MEV	—	19·2±0·9	17·6±1·3	20·4±2·3	—
Protons	142	—	—	—	23·1±0·8	21·7±1·1
	69	—	—	19·9±0·7	19·8±0·7	18·4±1·0
	50	—	—	22·6±0·6	19·9±0·9	18·8±1·1
		K_c				
Electrons	19·1	—	13·6±0·7	13·8±1·1	20·4±2·3	—
Protons	142	—	—	—	17·3±0·7	19·4±1·1
	69	—	—	16·1±0·4	18·6±0·6	17·5±0·9
	50	—	—	18·4±0·5	17·9±0·7	18·6±1·0

Table 5

Emulsion		Protons, $t=400\,\mu$			Electrons, $t=100\,\mu$
		141 MEV	68	49	>5 MEV
Normal	Experiment	30·0±0·8	31·9±0·8	26·2±1·0	26·7±0·6
	Theory	28·6	28·9	29·0	25·5
×2	Experiment	23·4±0·8	22·6±0·7	25·7±0·9	21·0±0·9
	Theory	23·4	23·7	23·8	20·7
×4	Experiment	23·1±0·8	19·8±0·8	19·9±0·8	19·2±0·9
	Theory	19·5	19·6	19·7	17·1

(iv) *Summary of Scattering Results*

In table 5 the values of K for electrons and protons in the three emulsions are compared with those calculated from the Molière theory ;

there is good overall agreement. The cell-sizes were chosen so that the statistical accuracy is high and any residual effects due to spurious scattering are negligible.

Empirical formulae relating $\langle\Phi\rangle_{\text{chord } c}$, the mean angle of scattering with cut-off, to the product of momentum and velocity are given in table 6. These take into account only the variation of K_c with β. The rapid change in the value of K_c for electrons using cell-sizes smaller than $100\,\mu$ has been neglected since considerably larger cell-sizes are normally used for experiments which apply the scattering technique. In presenting these formulae we have taken into account the data of Gottstein *et al.* for the scattering of protons with energies of 10–20 Mev and 340 Mev in normal G5 emulsions.

Table 6

$$\langle\Phi\rangle_{\text{chord } c}=K_c\left(\frac{t}{100}\right)^{1/2}\frac{z}{p\beta c}\text{ degrees.}$$

Emulsion	
Normal	$\langle\Phi\rangle_{\text{chord } c}=[27{\cdot}5-3{\cdot}5f(\beta)]\left(\frac{t}{100}\right)^{1/2}\times\frac{z}{p\beta c}$
×2	$=[22{\cdot}5-4f(\beta)]\left(\frac{t}{100}\right)^{1/2}\times\frac{z}{p\beta c}$
×4	$=[17{\cdot}5-3f(\beta)]\left(\frac{t}{100}\right)^{1/2}\times\frac{z}{p\beta c}$

$f(\beta)\sim 0$, $\beta=0\rightarrow 0{\cdot}7$,
$f(\beta)\sim 1$, $\beta\sim 1$.

(v) *Variation of Grain Density with Velocity*

An investigation was carried out on the variation of grain density in the proton tracks as a function of the velocity of the proton for the three types of emulsion. In addition to measurements on the grain density of the proton tracks, values were obtained for $g_{\min}$, the grain density at minimum ionization in the plates. The tracks of cosmic ray particles of great energy and identifiable fast electrons were used for the latter determinations.

The results are presented in table 7 as the ratio of grain density at a velocity βc to that at minimum ionization ; figures for the latter quantity are given in the final column of the table. It should be noted that the values of $g_{\min}$ do not enable a comparison to be made of the sensitivity of the different emulsions, since it was found necessary to employ a stronger developer for the diluted emulsions than for the normal ones.

The statistical errors only are quoted in the above table, in addition ystematic errors can arise as mentioned in the introduction to this paper.

It can be seen, however, that for a given value of the velocity the grain density ratios are reasonably constant for the three types of emulsion. In fig. 3 the weighted mean values of the ratios are plotted as a function of

Table 7

Emulsion	141 MEV $\beta c=0{\cdot}495c$	68 $\beta c=0{\cdot}36c$	49 $\beta c=0{\cdot}31c$	$g_{\min}$*
Normal	$2{\cdot}8\pm0{\cdot}1$	$5{\cdot}2\pm0{\cdot}1$	$6{\cdot}9\pm0{\cdot}2$	$14{\cdot}9\pm0{\cdot}3$
$\times2$	$3{\cdot}1\pm0{\cdot}1$	$4{\cdot}3\pm0{\cdot}1$	$5{\cdot}8\pm0{\cdot}2$	$10{\cdot}0\pm0{\cdot}2$
$\times4$	$3{\cdot}1\pm0{\cdot}1$	$5{\cdot}2\pm0{\cdot}2$	$6{\cdot}2\pm0{\cdot}2$	$5{\cdot}7\pm0{\cdot}15$

* $g_{\min}$=grain density at minimum ionization in grains per 50 μ.

Fig. 3

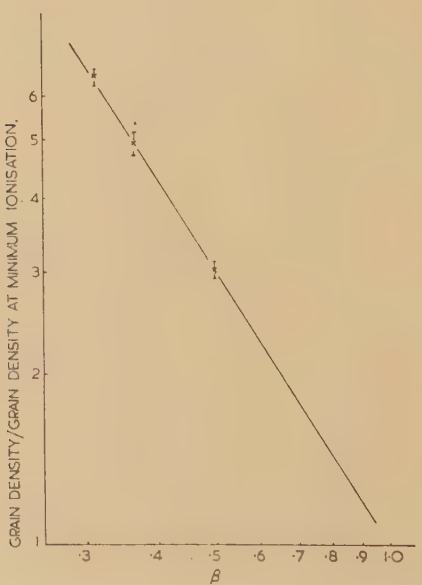

The variation of grain density at a velocity βc to that at minimum ionization as a function of β.

the velocity on a logarithmic scale ; in the velocity range $\beta c=(0{\cdot}3\rightarrow0{\cdot}5)c$ the data may be represented by the relation

$$\frac{\text{Grain density at velocity } \beta c}{g_{\min}} \sim \beta^{-1{\cdot}58}.$$

ACKNOWLEDGMENTS

The authors wish to express their gratitude to Professor P. I. Dee, F.R.S., for his interest and encouragement during the course of this work, and to Sir John Cockcroft, F.R.S., for his kindness in providing the

facilities of the Harwell cyclotron. We are especially grateful to Dr. T. G. Pickavance and the members of the cyclotron group at Harwell, and to Miss C. F. Lees of this laboratory for carrying out the proton exposures. Generous aid was also given by Mr. J. M. Reid and Dr. D. Greene of this laboratory during the synchrotron exposures. Lastly, we wish to thank Mrs. J. Muirhead for her assistance with the measurements.

One of us (W.B.) is grateful to the Nuffield Foundation for the award of a grant which has enabled him to carry out this research.

References

Bradner, Smith, Barkas and Bishop, 1950, *Phys. Rev.*, **77,** 462.
Corson, 1951, *Phys. Rev.*, **83,** 217.
Dodds and Waller, 1951, 'Photographic Sensitivity', *Bristol Conference Report*, p. 266.
Fowler, 1950, *Phil. Mag.*, **41,** 169.
Goldschmidt-Clermont, 1950, *Nuovo Cim.*, **7,** 331.
Gottstein, Menon, Mulvey, O'Ceallaigh and Rochat, 1951, *Phil. Mag.*, **42,** 708.
Levi Setti, 1951, *Nuovo Cim.*, **8,** 96.
Menon, O'Ceallaigh and Rochat, 1951, *Phil. Mag.*, **42,** 932.
Molière, 1948, *Z. für Naturforschung*, **3***a*, 78.
Montgomery, 1949, 'Cosmic Ray Physics'.
Rossi and Greisen, 1941, *Rev. Mod. Phys.*, **13,** 240.
Smith, 1947, *Phys. Rev.*, **71,** 32.
Voyvodic and Pickup, 1951, *Phys. Rev.*, **81,** 890.

VI. *The Growth of Cadmium Iodide Crystals: I—Dislocations and Spiral Growth*

By A. J. Forty
H. H. Wills Physical Laboratory, University of Bristol*

[Received October 22, 1951].

Summary

Evidence is given that cadmium iodide crystals grow from a low degree of supersaturation by the dislocation mechanism. Sequences of photographs illustrate the stages in the growth of the crystal plates. The screw dislocations are not simple but are *groups* of simple dislocations. The kinking of step-lines is explained by the interaction of screw dislocation groups of different strengths. The properties of large screw dislocation groups in the crystal plates are discussed.

§ 1. Introduction

The growth of cadmium iodide crystals from aqueous solution has been reported earlier in a preliminary note (Forty 1951). It has been found that, at low degrees of supersaturation, the crystal plates develop in thickness by the dislocation mechanism of spiral growth, proposed by F. C. Frank (1949, 1950; see also N. F. Mott 1949). The successive stages of growth of the crystals can be studied under the optical microscope. This paper gives a more detailed account of some of the observations.

§ 2. Methods of Observing the Growing Crystals

The crystals are grown between a microscope slide and coverslip from a drop of solution, just saturated at 60° c and allowed to cool slowly to room temperature. The crystal surfaces are observed in reflection, using an ordinary optical metallurgical microscope. The step-heights of the growth layers are usually large (up to 2000 Å high; a study of step-heights on cadmium iodide crystals is described in Paper II) and the step-lines have a high visibility. Several methods for observing the step-lines have been employed.

(1) *Vertical, Bright Field Illumination*

The growing surfaces are observed in reflection; the refractive index of the crystals is high and hence the reflectivity is considerable. By 'stopping-down' the illuminating beam to a narrow pencil, step visibility is improved (Griffin 1951). Figs. 5–10, 14–23, 24, 26 (Plates I, II and III†) are photographs using this method.

---

* Communicated by Professor N. F. Mott, F.R.S.

† For plates see end of issue.

(2) *Bright Field : Double Transmission*

When the steps are high, some contrast may be sacrificed to obtain stronger illumination for short exposures of photographs. This is simply achieved by placing a mirror behind the crystal. Figs. 11–13, 25 (Plates I, III) are microphotographs taken in this way.

(3) *Reflection Phase Contrast Illumination*

This mode of illumination is found especially useful for observing small steps on dry crystals with fairly simple surface structure. Fig. 27 (Plate IV) is a microphotograph of a dry, unsilvered crystal taken with Cooke, Troughton and Simms metallographic reflection phase-contrast equipment.

§3. Observations and Some Deductions

(1) *Growth Sequences*

After nucleation, the crystals grow in the form of extremely thin, hexagonal or triangular plates. The well-developed (0001) faces, growing parallel to the cover-slip are normally observed. The initially rapid lateral growth of the plates may well take place without the aid of dislocations. on the less closely packed prism faces of the hexagonal structure; the initial degree of supersaturation of the solution is about 50%. The rapid growth of a large number of small crystals lowers the degree of supersaturation and the lateral growth of the plates soon decreases. Then growth in thickness is observed by the appearance of several small hills near the edges of the plate. Eventually these are near the centre of the crystal as a result of continuing lateral growth. As the growth rate decreases, the hills can be resolved into step-line patterns centred on systems of screw dislocations emerging on the (0001) faces.

The structure and behaviour of growth hills agree with the theoretical predictions (F. C. Frank 1949, 1950 ; Burton *et al.* 1951), but it must be emphasized that the growth layers in this case are not ' monomolecular '. Sequences of photographs can be taken to illustrate the stages in the growth of these crystals.

(a) *Growth based on a Single Screw Dislocation Group*

The step-line terminating on the emergence of the dislocation group on the (0001) surface winds itself into a spiral. Figs. 5–10 (Plate I) are photographs taken at intervals of ten minutes to illustrate the development of the spiral step-line about a screw dislocation group as the growth proceeds.

(b) *Growth based on Two Screw Dislocation Groups of the same hand*

Figs. 11–13 (Plate I) are photographs at 10-minute intervals illustrating this type of growth centre. The co-operation of two screw dislocation groups of the same hand produces a step-line pattern of a pair of spirals, one following the other. The two cases described by Burton

et al. (1951), namely for the distance between dislocations $l > 2\pi\rho_c$ and for $l < 2\pi\rho_c$, where ρ_c is the radius of the critical nucleus for growth to occur, have been observed. The difference between these two cases is the interchange of step-lines away from the centre. If the screw dislocation groups are very close together, the resultant step-line pattern appears to be a double spiral with a single centre, as in figs. 11–13 (Plate I).

(c) *Growth based on Two Screw Dislocation Groups of opposite hand*

Figs. 14–18 (Plate II) (taken at 12-minute intervals) and figs. 19–23 (Plate II) (taken at 60-minute intervals) show the stages in the expansion of the terrace between two screw dislocation groups of opposite hand, dominating the growth of a crystal face. The outward growth of the terrace generates a closed loop and a new terrace. This cycle is repeated indefinitely and the crystal thickens at the rate of one layer thickness per cycle.

(d) *More Complex Growth Centres*

Growth centres of many screw dislocation groups have been observed. All show that the thickening of the crystal plates is due solely to the dislocation mechanism of growth. Fig. 24 (Plate III) is part of a surface of a crystal containing many screw dislocation groups. At the top of the photograph there are at least three independently active groups, not all of the same strength (or Burgers vector normal to the face). On the right there is growth from a pair of screw dislocation groups of the same hand, and in the centre there is an irregular spiral based on a single screw dislocation group.

The turns of this spiral are more closely spaced and were seen to be advancing faster than the others (fast enough to blur the image slightly in the 75 second exposure). Many other smaller dislocation groups are present, producing kinks in the step-lines (see later, (5)). It is interesting to note that the central spiral eventually spread over the whole surface and figs. 5–10 (Plate I) are a sequence of its growth twenty-four hours later; the layers becoming polyhedral as the growth rate decreased.

(2) *The Shape of Growth Layers*

It is always observed that, when the dislocation type of growth commences, the step-lines are curvilinear, the layers becoming polyhedral as the growth rate decreases with the fall in degree of supersaturation. From many observations of growth, the phenomena can be summarized :—

Initial fast growth from a high degree of supersaturation	*Final slow growth*
(*a*) Steps close together	Steps widely spaced.
(*b*) Fast rotation of step-line about screw dislocation	Slow rotation of step-line.
(*c*) Step-lines are curvilinear.....	Layers polyhedral.

The shape of the polygonal layers displays the symmetry of the crystal surface. This is trigonal for a basal surface of cadmium iodide. In figs. 14–18 (Plate II) the polygonal growth steps have the angles of a regular hexagon but the sides are alternately short and long. In figs. 19–23 (Plate II) which show the same crystal at a later and slower stage of growth the short sides of the hexagons have undergone a rotation of 30 degrees so that alternate angles are close to 150 degrees and 90 degrees. Though the step-lines are straight and parallel their directions do not apparently correspond to low crystallographic indices.

(3) *Cross-Laced Patterns on Cadmium Iodide*

Fig. 27 (Plate IV) shows a phenomenon similar to one observed by Verma (1951 : fig. 13). Disregarding for the moment the supplementary pyramid on the lower slope of the main pyramid, it is seen that the terraces are ' cross-laced ' along each pyramid edge. Frank (1951 a) gave an explanation of this case. The slowest growing monolayer in the stack of monolayers which comprise one repetition of the crystal is a different one for two different orientations 60° apart. In each orientation, succeeding monolayers pile up behind the one with slowest advance, and since this is a different one in adjacent pyramid faces, the pyramid edges are cross-laced. Conditions for the same theory to apply can exist in a cadmium iodide crystal having a suitable ' polytypic ' variant of the standard structure. It is difficult to see how this behaviour could be accounted for without polytypism. Further evidence for polytypism in cadmium iodide will be presented in Paper II.

(4) *The Origin and Shape of the Big Screw Dislocation Groups*

As already reported (Forty 1951), the step-heights of the growth layers in cadmium iodide are often large : those in the photographs are between 500 Å and 1000 Å. This indicates that the crystals are growing from screw dislocation groups of large Burgers' vector, and that groups of practically any strength are possible.

A possible explanation of the origin of these large screw dislocation groups has been put forward by F. C. Frank (1951 a). The non-uniform distribution of impurities should be sufficient to stress the extremely thin plates beyond the theoretical yield stress for the ideal structure. A ' buckle ' followed by slip of the sandwiches (close-packed layers of cadmium ions between close-packed layers of iodine ions) past one another in the [0001] direction, produces the large screw dislocation groups. The plate immediately begins to thicken by ' spiral growth ' on the groups so formed.

Observations of the growth of pure lead iodide crystals (these have a structure similar to that of cadmium iodide) show that only very small screw dislocations occur. Screw dislocation groups of larger Burgers' vector can be produced by adding a small amount of camium iodide as impurity in the solution. This indicates the importance of impurities in the formation of the groups. The results of a study of step-heights

on growing cadmium iodide crystals, given in Paper II, provide some confirmation of the ' buckle, followed by slip ' process.

It is somewhat surprising that such large dislocation groups are possible, since enormous strain energy in the crystal lattice might be associated with them. Frank (1951 b) has suggested that since the unit Burgers' vector for carborundum is greater than 10 A, the core of a screw dislocation in carborundum is a hollow tube about one or two microns in diameter. This effectively relieves the strain energy around the dislocation. He expects large dislocation groups in carborundum to have a hollow core consisting of many such tubes. It is only occasionally (e.g. figs. 11–13 (Plate I) and 25 (Plate III)) that there are indications of a hollow core for dislocations in cadmium iodide.

Figs. 14–18 (Plate II), 19–23 (Plate II) and other photographs taken throughout the growth of this crystal show a persistent line about 3 microns long at the centre of the spirals. If the dislocation group of total strength 750 A is distributed along this line, making a ribbon of dislocation passing through the crystal, the portions of the lattice on either side of this ribbon are rotated only $1\frac{1}{2}$ degrees with respect to each other. In this arrangement the strain energy density would not be excessive.

(5) *Effect of Dominated Dislocation Groups on Growth Fronts*

(a) *The ' Cross-linking ' Type of Interaction*

Since the large screw dislocation groups can have practically any size, more than one group of exactly the same strength is rarely found on a given crystal face. For this reason, the ' cross-linking ' type of interaction of advancing step-lines with a dominated dislocation group, whose Burgers' vector equals the step-height of advancing layer, is seldom observed. (This is the normal type of interaction on Beryl where all the screw dislocations have unit Burgers' vector (Griffin 1950, 1951).)

(b) *The Formation of Kinks in Step-lines**

A step-line of height equal to the normal component of the Burgers' vector extends in the surface from each point of emergence of a screw dislocation group. The growth of a particular face is normally dominated by one or a few groups. The step-lines from a dominating growth centre develop kinks where they pass over other dislocation groups of different strength.

What can be called the fundamental crystal structure of cadmium iodide (G. Hägg 1948) consists of a layer lattice in which the unit cell contains two sandwiches each consisting of a layer of cadmium ions between two layers of iodine ions. Disordered variants of this structure have been reported. If the crystal has the fundamental cadmium iodide structure of two sandwich layers and the Burgers' vectors of all dislocations present are multiples of the fundamental period, the dislocations are perfect and the crystal structure is continuously ' good '

* I am greatly indebted to Dr. Frank for these explanations of the kinking.

except in the dislocations. Some, however, may have Burgers' vectors corresponding to an odd number of minimal sandwich layers. These may be called ' odd ' dislocations for brevity. These are imperfect dislocations if the dominating dislocation group is even, so that the resulting structure is the fundamental one. If the dominating dislocation group is odd, the resulting structure is a polytype (see Paper II for the discussion of polytypism) and all the other dislocation groups, odd or even, are almost certainly imperfect. A surface of lattice discontinuity extends from every imperfect dislocation. Step-lines terminating on imperfect dislocations therefore mark fault surfaces and cannot move as easily as steps extending from perfect dislocations.

A geometrically possible configuration for the interaction of a smaller dislocation group with dominating growth layers is shown in fig. 1 (a, b).

Fig. 1

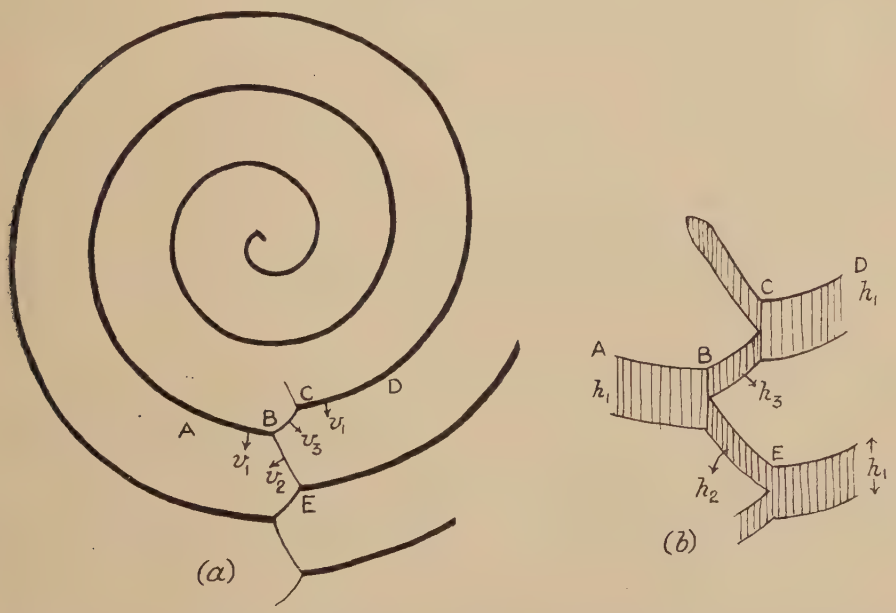

It can easily be shown that such a pattern can only be recurrent (in the sense that it reproduces itself after a cycle of rotation of the dominating spiral) if the approximately radial steps advance slower than the main spiral step. This can be the case if, and only if, the dominated dislocation is an imperfect dislocation of the structure resulting from the dominating one, so that the radial step approximately follows the trace of a fault surface in the crystal. Depending on the degree of misfit at the fault, various degrees of hindrance in the passage of a growth step over it may be anticipated. In the extreme case of complete hindrance we would expect a figure such as 2 (a). Then any excess of supersaturation on either side of the fault line will lead to different rates of advance of the main steps on either side, producing configurations like fig. 2 (b). This

Fig. 2

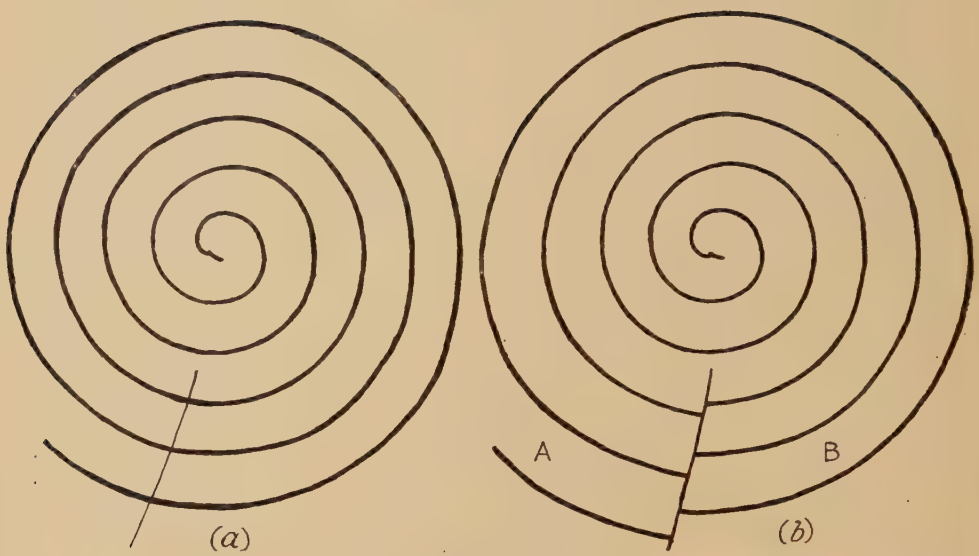

in its essentials, is the commonest form of interaction observed. (cf. figs. 5–10, 19–23, 26). (Plates I, II, III.)

If the main growth layers dominate a pair of co-operating screw dislocation groups, other forms of interaction are possible. Fig. 3 represents the formation of a possible configuration if a pair of smaller

Fig. 3

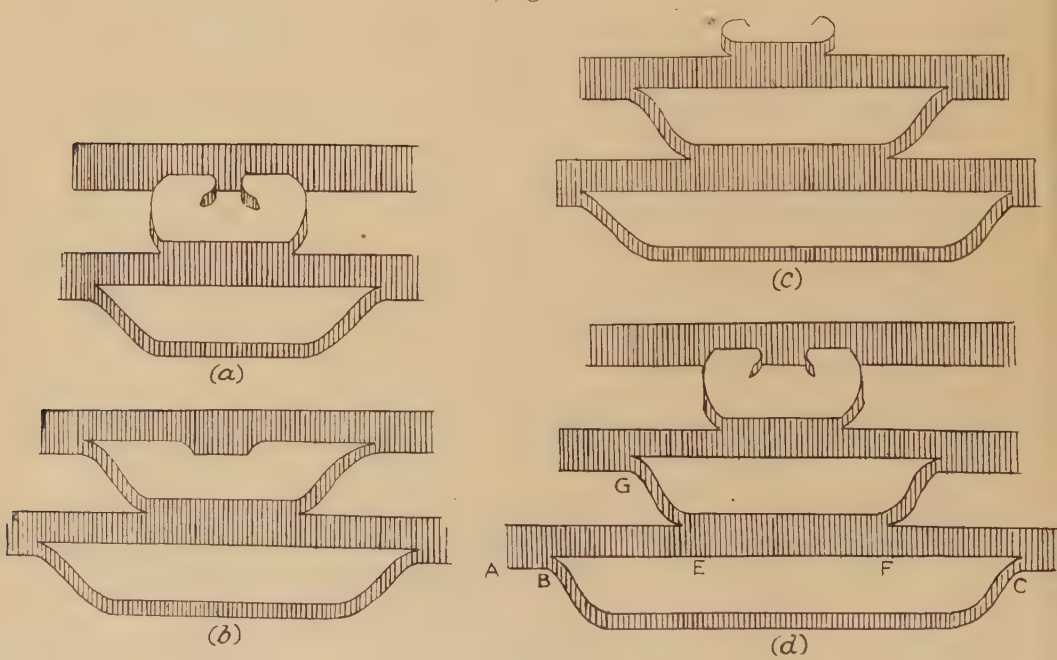

co-operating screw dislocations of opposite hand are dominated. If the rate of growth of a composite layer is governed by its lowest member, then it is likely that the rate of advance of step EF will be different from that of AB, CD although these sections have the same step-heights. This leads to a ' fan-shaped ' region, radiating from the dominated dislocations, inside which the steps advance at a rate different from those over the rest of the hill. If the strength of the dominated dislocation groups is small, the steps such as GE might not be observed but the ' fan ' will be obvious from the two rows of kinks radiating from the pair of dislocations. It is thought that this type of interaction occurs in the growth hill photographed in fig. 27 (Plate IV) where the two dominated dislocation groups are close together. Measurements have shown that the thickness of growth layers inside the fan-shaped region is equal to that of the layers on the rest of the hill.

The interaction described in fig. 4 can occur if the directions of the

Fig. 4

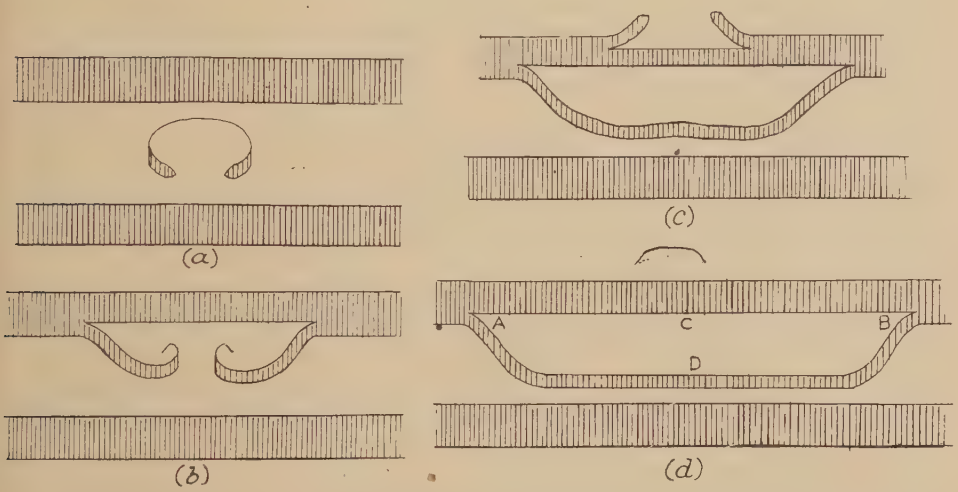

dominated pair of screw dislocation groups are opposite to those in the case described above. A thinner layer formed by the co-operation of the pair of smaller dominated dislocation groups is ' pushed ' ahead of each dominating growth layer. In this case there is not necessarily a connecting step between the main growth layers unless the rate of advance of a layer such as ADB is greater than the rate of advance of a layer ACB. This form of interaction appears on the crystal photographed in figs. 14–18 (Plate II) where the main growth centre dominates the pair of small co-operating dislocation groups on its left.

(6) *Kinking of Step Lines due to Growth from Two Unequal Co-operating Dislocation Groups*

Usually, when two co-operating dislocation groups are large, they do not have exactly the same strength. Hence, a step equal to the difference

of the Burgers' vectors extends from the larger dislocation group to the edge of the crystal. The step-lines of the growth layers propagated from the two co-operating dislocation groups, usually become kinked across this line in a manner essentially similar to that of the domination of a single smaller dislocation group by another distant group. The same explanation holds in principle for the formation of rows of kinks from growth centres of any number of dislocations, of either hand. Figs. 14–18, 19–23 (Plate II) are photographs illustrating this type of kinking for growth from two unequal dislocation groups of opposite hand.

(7) *The Penetration of the Screw Dislocation Group through the Crystal*

The ' double-transmission ' method is particularly useful for observing both surfaces of the crystal plates at the same time. It is found that the screw dislocation groups penetrate the plates, to emerge on both surfaces. If growth occurs on only one surface of a plate containing a single screw dislocation group a spiral step-line is observed on that surface and a radial step-line on the other (see fig. 25 (Plate III)). If growth takes place on both surfaces, a spiral step-line is observed on both, centred on the same screw dislocation group. Fig. 26 (Plate III) illustrates such a case ; the rates of growth of the two surfaces are obviously different, indicated by the difference in spacing of the step-lines.

The cadmium iodide structure is polar (see Paper II). Upper and lower surfaces of the plate differ from each other and both have trigonal symmetry. Hence with similar degrees of supersaturation on the two surfaces it would not be surprising to find that the trigonal shapes of the polygonal spirals, centred on the same dislocation group, were rotated through 60 degrees of arc with respect to each other. Actually, it is always observed that the rotation is $(60 \pm \theta)$ degrees, where θ is a small angle of 5 or 10 degrees of arc. This demonstrates that the segments of the polygonal growth spirals do not have orientations corresponding strictly to simple crystallographic indices. A proper understanding of the phenomenon has not yet been reached.

According to Eshelby and Stroh (1951), the repulsion between like screw dislocations in a crystal plate falls off rapidly at distances greater than the thickness of the plate. Therefore, if the large dislocation groups disintegrate by internal repulsions, the components should not move far apart. Usually, the group remains as a unit through the plate (by the internal interference method described in Paper II, the step-lines of the two surfaces have been shown to be of equal height). However, in a few cases, growth on a single screw dislocation group produces a single spiral step-line on one surface, and two or more smaller, radial or spiral step-lines on the other surface. This could be interpreted as meaning that repulsion between parts of the screw dislocation group causes a separation which increases through the plate. This separation should become more pronounced as the crystal thickens, but this has not yet been observed.

Acknowledgments

I wish to thank Dr. F. C. Frank for his help and interest in all stages of this work. I am grateful for a maintenance grant from the Department of Scientific and Industrial Research.

References

Burton, W. K., Cabrera, N., and Frank, F. C., 1951, *Phil. Trans. Roy. Soc.* A, **243,** 299–358.

Eshelby, J. D., and Stroh, A. N., 1951, *Phil. Mag.*, **42,** 1401.

Forty, A. J., 1951, *Phil. Mag.*, **42,** 670.

Frank, F. C., 1949, Discussions of the Faraday Society, No. 5, 'Crystal Growth', **48**; 1950, *Phil Mag.*, **41,** 200; 1951 a, *Ibid.*, **42,** 1014; 1951 b, *Acta Crystallographica* (submitted for publication).

Griffin, L. J., 1950, *Phil. Mag.*, **41,** 196; 1951, *Ibid.*, **42,** 775.

Hägg, G., 1948, *Colloques Internationaux du centre national de la recherche scientifique*, 10 (Paris, 1948).

Mott, N. F., 1949, *Nature*, **165,** 295.

Verma, A. R., 1951, *Phil. Mag.*, **42,** 1005.

VII. *The Natural Radioactivity of Rubidium*

By S. C. Curran, D. Dixon, and H. W. Wilson
Department of Natural Philosophy, The University, Glasgow, W.2*

[Received August 15, 1951]

Abstract

The mode of decay of ^{87}Rb is investigated chiefly by means of a shielded proportional tube operating as a spectrometer. It is shown to consist simply of a β-transition between the ground states of ^{87}Rb and ^{87}Sr the limiting energy of the particles being 275 kev and the average energy 44 kev. The spectrum, which was investigated using sources of thickness 1 mg/cm^2 and 0·128 mg/cm^2, shows no maximum, differs very considerably from that for an allowed transition and is in agreement qualitatively with that for a third forbidden transition with parity change, $\Delta I=3$, yes. The period is found to be $\tau=6{\cdot}15\times10^{10}$ yr. No γ-rays, x-rays or internal conversion electrons ascribable to the decay process are emitted in appreciable intensity. It is suggested that the established natural radio-elements with $Z<80$ form a well-defined and isolated group with log ft.$=18$ approximately.

Introductory

The radioactivity of rubidium has been the subject of many investigations since its discovery by J. J. Thomson in 1906 yet the nature of the decay was far from clear at the beginning of the present study. Thomson established the fact that the particles were negatively charged and later Campbell and Wood (1908) showed that the radiation was heterogeneous and less penetrating than that of potassium. The results achieved by more modern techniques are summarized in table 1 which gives the source thickness in mg/cm^2, the half-life in 10^{10} yr., the end-point energy E_0 and the gamma ray energy $h\nu$ in mev.

The period τ is very important in connection with the age of the earth and mineral deposits and separate studies have been concerned with its evaluation. Hemmendinger and Smythe (1937) established the identity of the radioactive isotope of rubidium, viz. ^{87}Rb by isotope separation while Hahn, Strassman and Walling (1937) showed that strontium was the decay product, Mattauch (1937) identifying the particular isotope, ^{87}Sr. Strassman and Walling (1938) estimated the period by the uranium-lead method, giving the value $6{\cdot}3\times10^{10}$ yr.

Table 1 indicates the considerable uncertainty and disagreement in the results with the most consistent data appearing for τ. It has to be

* Communicated by the Authors.

noted that Muhlhoff could not allow for the abundance of the radioactive isotope. Haxel *et al.* consider that Eklund's value of τ is fortuitously nearly correct. The same authors stress the importance of agreement in τ values as obtained by purely radioactive measurements and the uranium-lead method. Anticipating our own findings we can eliminate their suggestion that the source emits two electrons (one decay type and one from photo-conversion) per disintegration, so that it is desirable that their value of τ should be confirmed or amended.

Table 1

Author	mg/cm²	τ	E_0	$h\nu$	Remarks
Muhlhoff, 1930	1·5 to 3·0	12	~1·1	—	Comparison of absorption with RaE
Klemperer 1935	1·5 to 3·0	—	0·25	—	Examination of Muhlhoff data
Libby and Lee 1939	?	—	0·132	—	Screen-wall counter
Ollano 1941	thick	—	~0·13	0·034 0·053 0·082 0·102 0·129	Gamma rays deduced from conversion photoelectrons
Saha 1946	300	—	0·144	—	Modified Libby device
Eklund 1946	0·1	5·8	—	—	Counter with internal source
Fazzini and Franchetti 1948	?	—	0·56	—	Cloud chamber
Haxel and Houtermans, 1948	~0·1	6·9	~0·01	~0·135	Coincidences in G.M. tubes
Haxel, Houtermans and Kemmerich 1948	~0·1	6·0	~0·01	~0·135	Tentative allocation of decay β rays and electrons
Kemmerich 1949	0·03	6·0	—	—	Study of effect of source thickness

From the stand-point of beta decay theory the transition $^{87}Rb \rightarrow {}^{87}Sr + \beta^-$ is of special interest. The spins of the grounds states of both nuclei are known ($^{87}Rb = 3/2$, $^{87}Sr = 9/2$, Jackson 1933, Heyden and Kopfermann 1938, Millman and Kusch 1940) giving a spin change $\Delta I = 3$ in the ground state to ground state transition and the calculated ft. value (Feingold

1951) is 16·5 corresponding to a third forbidden transition. This probably unique case offers a searching test of theory, as Wu (1950) has already pointed out.

Our experience in the past with large proportional counters operating as β- and γ-ray spectrographs assured us that the spectra of sources of moderate energy could be analysed successfully even when the specific intensity was extremely low. The large acceptance angles, 4π for internal sources, 2π for wall mounting make the instrument ideally suited to investigations of weak radioactivities such as that of ^{87}Rb. A large source area can be utilized, $\sim 10^3$ cm^2, so that a mass of 1 g say yields a source thickness of 1 mg/cm^2. The ' background ' spectrum of a large counter at high pressure (5 to 7 atm) is spread out more or less uniformly,

Fig. 1

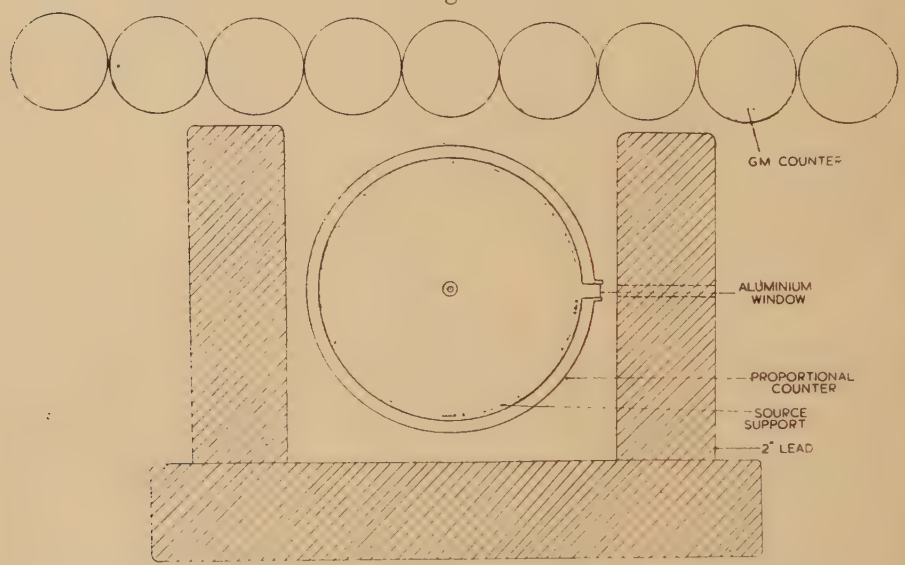

Proportional counter with lead and anti-coincidence counter shielding.

over an energy range $\sim$0·5 MeV. Hence for a K-capture source, whose radiation is concentrated in a range of less than say 5 kev, the sensitivity of the tube is $\sim$100 times better than that of a Geiger-Müller. The same is true for sources decaying by emission of γ-radiation or X-radiation and internal conversion electrons. For normal β-decay sources the position is somewhat altered but generally very favourable. Frequently the radiation from weakly active sources is of low energy and it covers therefore a relatively small part of the total energy range of the instrument. Within this restricted range the ratio of counting rate with source present to rate in its absence is enhanced. For example, if the β-spectrum covers 50 kev the ratio is increased by a factor $\sim$10 and near the maximum of the β-spectrum the factor is very much greater.

The present investigation is part of a general study of the weak natural radio-elements of $Z < 80$.

Experimental Arrangement

The schematic diagram of the spectrometer is shown in fig. 1. A large proportional tube of diameter 5·5 in., provided with field tubes to give a fully effective length of 10 in. (Cockroft and Curran 1951), is surrounded with a lead shield, thickness 2 in. An array of Geiger tubes, 2 in. diameter, operates in anti-coincidence with the proportional counter and serves to eliminate most of the background due to cosmic rays. For photographic recording of the spectrum the Geiger impulses, suitably shaped are fed to the ' black-out ' electrode of the cathode ray tube on which the amplified output pulses of the spectrometer are displayed. Alternatively the output pulses of an anti-coincidence circuit are used to quench the time-coincident pulses from the spectrometer tube before they are applied to an electronic ' kick-sorter '. Both electronic and photographic analysis of the spectrum were employed in the present work. Fluorescence x-rays of silver were used to calibrate the spectrometer, the x-radiation entering the counter when necessary through an aluminium window. The proportional tube was maintained at a pressure of 5 atm of argon+20 cm of methane.

The source consisted of spectroscopically pure RbCl deposited on the inner surface of an aluminium cylinder which was inserted into the tube and served as cathode. Two thicknesses were employed, namely 1·5 mg/cm^2 and 0·128 mg/cm^2, the former laid down smoothly with a fine brush as a hot water solution and the latter with the help of a specially prepared glass wiper. Both appeared uniform in thickness and care was taken to keep them within the effective length of the tube.

Results

(*a*) Spectrum Analysis. With the thicker source the spectrum was analysed at different gain-settings and the overlapping portions coincided smoothly to give the shape shown in fig. 2. The region of low energy, below 40 kev was examined separately using the thin source (0·128 mg/cm^2) with the results shown in fig. 3. The curve thus obtained was fitted to the curve for the thicker source and smooth coincidence from 40 kev to about 30 kev observed, as seen in fig. 2.

Below about 20 kev there is clearly a serious absorption of β-particles in the thicker source (curve indicated by dashed line). The final form of the complete spectrogram, full line in fig. 2, is believed to be accurate down to about 10 kev and over the whole range from 10 kev to the end-point at 275 kev no maximum appears on the curve. The curve near the end-point is shown in more detail in the inset figure. The curve falls very steeply at first with increasing energy and it shows an extremely long ' tail '. No doubt the very unusual form of the spectrum explains much of the difficulty of earlier workers.

The Fermi plot is shown in fig. 4. The curve departs very remarkably from the straight line form given by an allowed transition. The extrapolation of the Fermi curve in the vicinity of E_0, assuming it linear over a short range gives E_0=275 kev in agreement with direct observation.

(*b*) Gamma Radiation and Conversion. The non-appearance of conversion lines on the spectrum seemed remarkable in view of Ollano's results and a sensitive method of searching for internal conversion was adopted. The thick source (1·5 mg/cm^2) of RbCl was covered with sufficient aluminium to stop the β-rays (58 mg/cm^2). This cover reduces the intensity of K x-radiation of Sr to about 50%. The average efficiency of the counter, at 2 atm pressure, for such rays was assessed at 84%.

Fig. 2

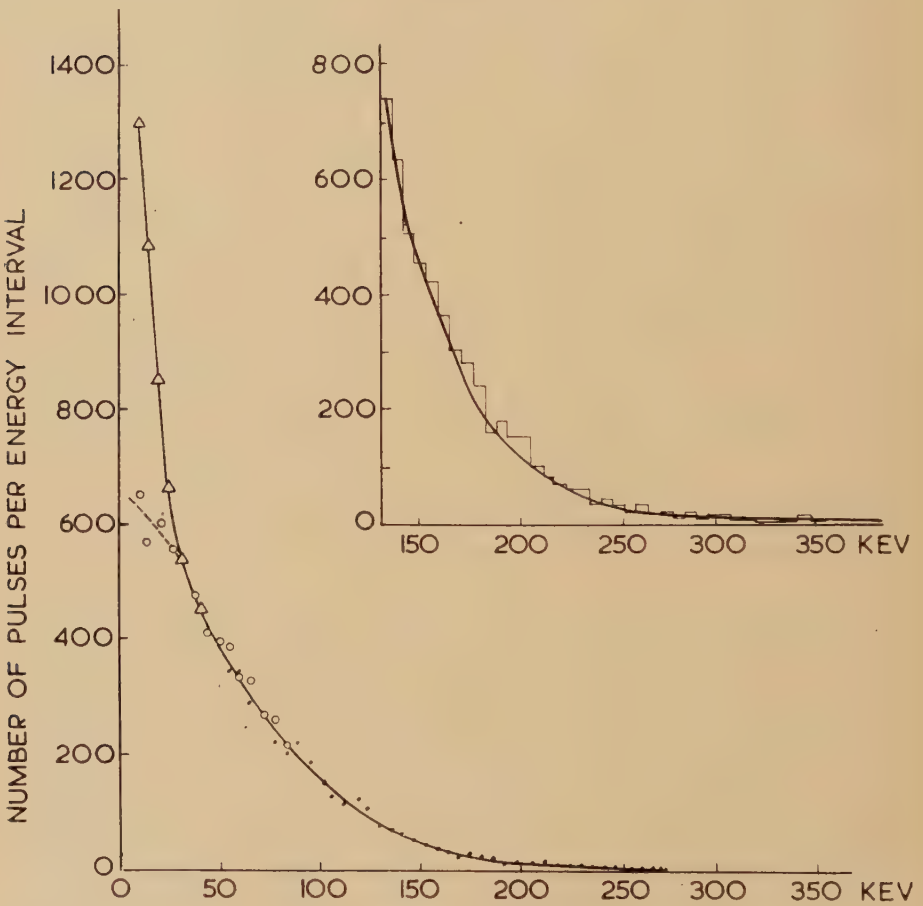

β-spectrum of ^{87}Rb.

The results of our search are shown in fig. 5. The total number of x-rays emitted per unit time was determined from the histogram and comparison with the β-rays from the source showed that the x-rays were down in intensity relative to the β-rays by a factor of more than 500. The extremely low intensity of x-radiation made accurate definition of energy difficult but as indicated in fig. 5, allocation to Sr seems slightly preferable to Rb. On the other hand the intensity is not inconsistent with the view that the x-rays are generated by bombardment of the rubidium by the

Fig. 3

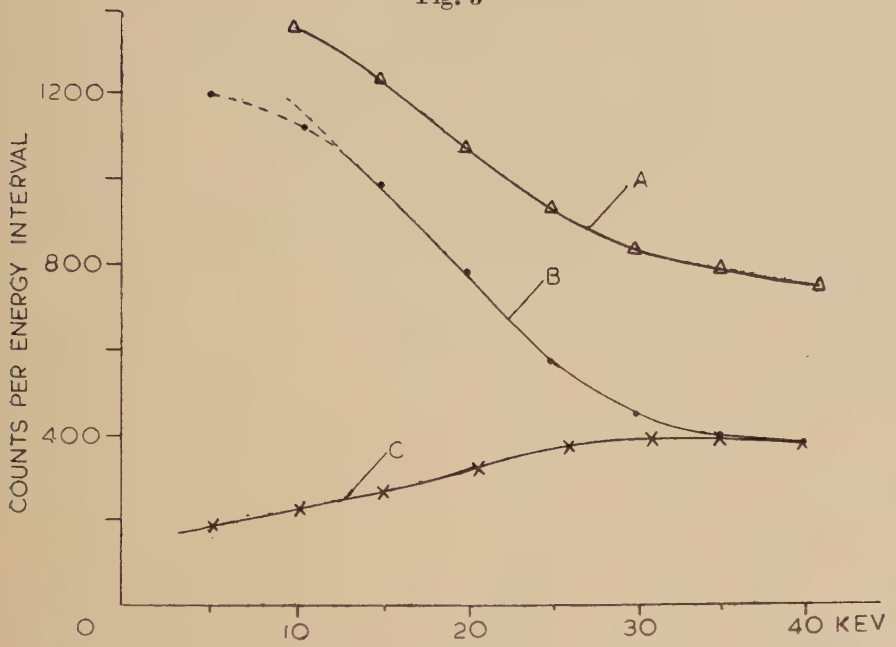

β-spectrum of ^{87}Rb, using 0·128 mg/cm^2 source. Curve A is the spectrum including background; curve B, the spectrum with background subtracted and curve C, the background of the counter.

Fig. 4

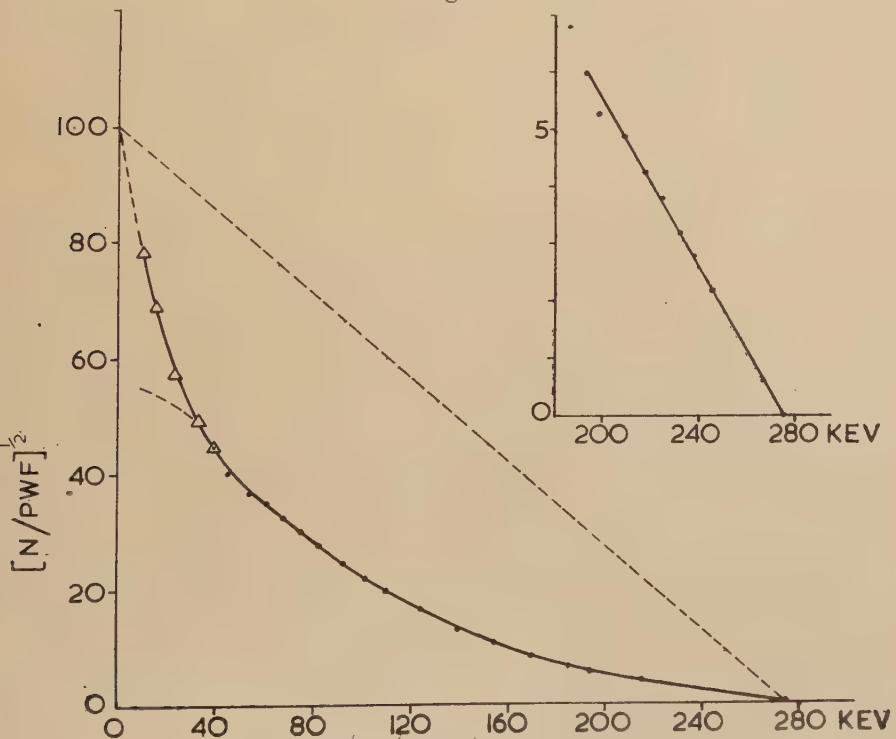

Fermi Plot of β-spectrum of ^{87}Rb.

β-rays. In any case it appears certain that internal conversion in the K-shell of ^{87}Sr does not occur in more than 0·2% of the disintegrations. This result completely contradicts the conclusions of Ollano and we are forced to the view that his electron groups are spurious and the result of unfortunate statistical fluctuations.

A separate search for L x-ray quanta was carried through since there was a remote possibility that γ-radiation might convert in the L shell only. The low energy of L-radiation ($\sim$ 1·8 kev) prohibited the use of the β-absorbing screen of aluminium. Using x-rays of Ga (9·2 kev)

Fig. 5

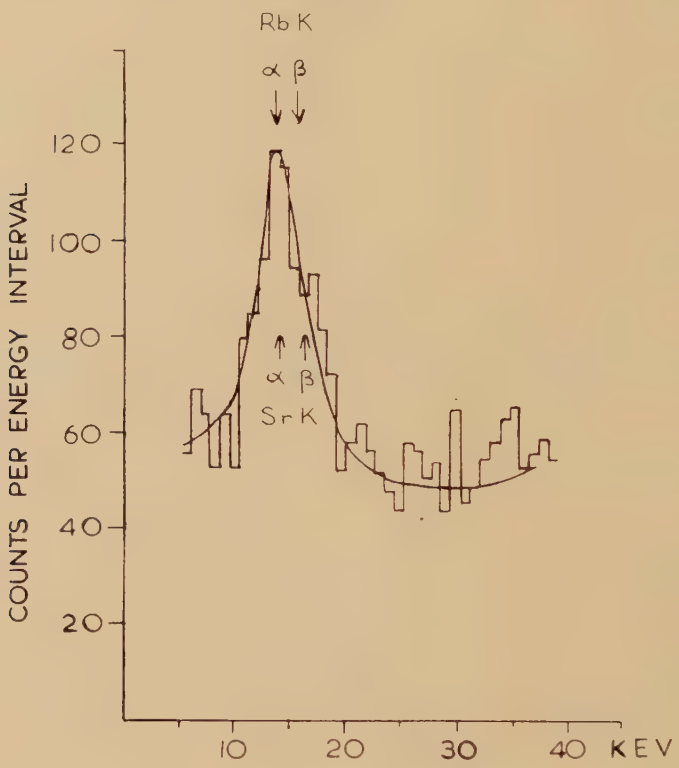

K x-rays observed with ^{87}Rb.

emitted from ^{71}Ge, the threshold energy for detection, as defined by a discriminator, could be varied over a wide range, above and below the value of 1·8 kev. Now if x-rays are emitted in some disintegrations, in 50% of such cases the x-ray will not be detected in coincidence with a β-particle. Hence a relatively sharp rise in counting rate, could be expected as the threshold energy is reduced through the value 1·8 kev. The results of fig. 6 show that no appreciable discontinuity can be found. Even if the slow rise on the curve is distorted to create a discontinuity as shown by the dashed line on the figure an upper limit of about 3% is found. It is much more likely however that the upper limit is not greater

than that for the K-radiation namely 0·2%. Thus there is no real evidence of conversion of γ-radiation in either K or L shells in more than 0·2% of the disintegrations.

Finally, a sensitive search for γ-radiation was carried out by Mr. Bannerman of this Department, with a scintillation counter operating as a spectrometer. About 5·6 g of RbCl was packed round the scintillator (NaI, Tl) and the counter detected an additional 10 counts/min. The crystal was shielded from the β-rays with aluminium. There was no indication of homogeneity in the pulses produced and they were almost certainly excited by the passage of the β-rays through the absorber-bremsstrahlung. Whatever the origin we can conclude that γ-quanta in the range 20 to 100 kev cannot be released in more than one per 5×10^3 disintegrations and in more than one per 10^3 disintegrations in the range 100 to 300 kev.

Fig. 6

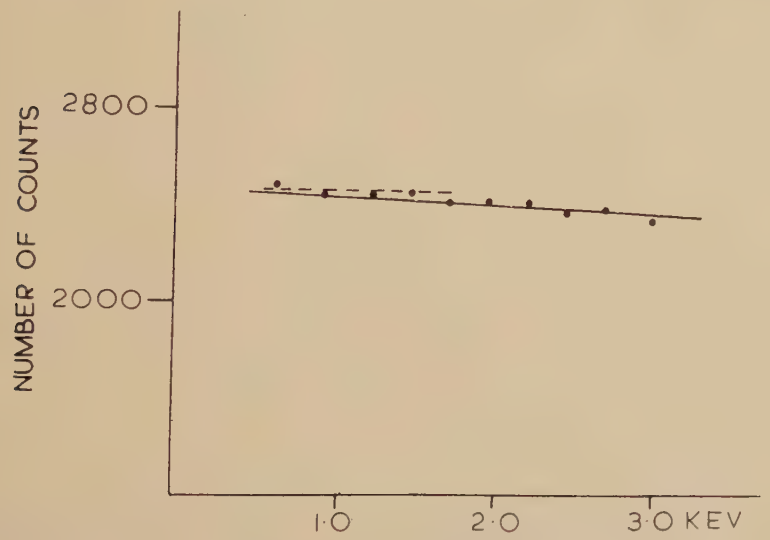

Search for L x-rays. Counting rate as discriminator bias is varied over range including the L-radiation.

It would appear certain from this search for γ-quanta, K and L x-rays that the probability of the β-decay leaving the nucleus ^{87}Sr excited is negligibly small. The decay process consists in the transition by β-decay between the ground states of ^{87}Rb and ^{87}Sr.

The Period τ

The conclusion that the β-decay of ^{87}Rb is simple raises some issues concerning τ. The most recent accurate work of Haxel, Houtermans and Kemmerich (1948, 1949) was based on false assumptions regarding the decay scheme since they assumed that two electrons were emitted in each disintegration. Clearly the unusually high intensity of the continuous spectrum at low energies explains to some extent their observations, but

we are forced to suggest that the coincidences observed in their double counter probably had their origin in reflexion at the counter walls. However, as they themselves pointed out, their method of deducing the number of disintegrations gives a result which is independent of their assumptions regarding the nature of the coincidences. Indeed in our view it amounts to correcting for reflexion by materials near the source. We were interested to compare our value of τ with theirs.

Accurate measurements of the counting rate at high gain showed that the rate was practically independent of the voltage over a range of some hundreds of volts. The difference count with and without the source (0·128 mg/cm^2) was 1477 counts per min for the total mass of 0·10075 g of RbCl, measured to a statistical accuracy better than 1%. Allowing for the 2π geometry, chemical composition and isotopic abundance this gives directly $\tau = 5{\cdot}95 \times 10^{10}$ yr.

Two corrections have to be applied for (*a*) the reflexion of particles in the source and support and (*b*) the self-absorption of the source. To estimate (*a*) we made use of data due to both Yaffe and Burtt (1950). These workers are in fairly close agreement but both plot the variation of reflexion coefficient as a function of E_0. Due to the remarkable shape of the spectrum of ^{87}Rb it is probably more desirable for us to estimate the reflexion in terms of the average energy, $\bar{E}$ of the β-rays. Thus we find $\bar{E}$ for ^{87}Rb is 44 kev, less than the values 52 and 54 kev for ^{14}C and ^{35}S respectively although E_0 for ^{87}Rb considerably exceeds E_0 for both ^{14}C and ^{35}S. In the region involved here the reflexion seems to vary rapidly with the energy of the β-rays, further complicating the estimation. The value which we adopt is 7·5%. Regarding (*b*) we take the source as equivalent in thickness to the range of a β-particle of energy 5 kev. We deduce from fig. 2, extrapolated portion between 10 kev and zero energy, that the self-absorption reduces the counting rate by 4·5%. Hence the overall contribution to the counting rate conists of an increase of (7·5—4·5)%. The final value for τ is therefore $5{\cdot}95 \times 1{\cdot}03$ or $6{\cdot}15 \times 10^{10}$ yr. The chief uncertainties in this value arise from the estimation of the corrections and together with statistical fluctuations in counting we consider an error of $\pm 4\%$ is possible. With these rather conservative limits our value for τ becomes $\tau = 6{\cdot}15 \pm 0{\cdot}3 \times 10^{10}$ yr.

Discussion and Conclusions

The experiments establish that the β-decay of ^{87}Rb is a simple process involving transition from ground state to ground state with a maximum energy $E_0 = 275$ kev. The Kurie plot lies very markedly below the straight line corresponding to an allowed transition and seems consistent with $\Delta I = 3$ with change of parity according to present theoretical views. The calculation of the correction factor C_{3T} given by Greuling (1942) and containing an adjustable factor (the ratio of the matrix elements $Q_3(\beta\alpha, r)$ and $Q_3(\beta\sigma \times r, r)$ in Greuling's notation) is exceedingly laborious but it is probable that adjustment can be made. We have not attempted to complete this task.

The degree of agreement of our τ value with the most recent measurement and the geological estimate gives considerable confidence.

The new value of E_0, 275 kev leads to the value 17·6 for log ft. A remarkable degree of agreement in ft. value is now apparent among four of the best established natural radioactivities as shown in table 2. Now it is to be noted that a considerable gap exists between the value 17·6 for ^{87}Rb and the next well-established value 13·65 for ^{10}Be although there is a fairly uniform distribution below this latter value (see the data due to Feingold 1951). The Table shows ^{150}Nd as an obvious exception on the assumption that $E_0=11$ kev and $\tau=5\times10^{10}$ yr. Some preliminary work with the equipment already described has shown that these values (Libby 1934) are almost certainly erroneous* since the necessary number of low energy β-rays could not be detected with the counter. The period may be underestimated but assuming that it is very approximately correct and that E_0 is in error, the calculation shows that log *ft* for ^{150}Nd can be made approximately equal to that for the other elements of the group

Table 2

Source	E_0 MEV	10^{10} yr.	log ft.
Rb^{87}	0·275	6·15	17·6
K^{40}	1·36	0·11	18·05
Lu^{176}	0·215	2·4	18·02
	0·4		or 18·91
Re^{187}	0·043	4·0	17·73
Nd^{150}	0·011	5	13·73

when $E_0=250$ kev (see Feenberg and Trigg 1950 for Log f as function of energy and Z). Further work is contemplated but at present it appears that such a value is not entirely ruled out by our results. If this should prove to be the case the natural radio-elements with $Z<80$ will form a narrow group with log *ft* close to 18.

We wish to record our gratitude to Professor P. I. Dee, F.R.S., for his interest and encouragement in this work.

References

Campbell, N. R., and Wood, A., 1908, *Proc. Camb. Phil. Soc.*, **14**, 15.
Cockroft, A. L., and Curran, S. C., 1951, *Rev. Sci. Instrum.*, **22**, 37.
Eklund, S., 1946, *Arkiv. Mat. Astron. Fysik*, **33A**, 60.
Fazzini, T., and Franchetti, S., 1948, *Nuovo Cimento*, **5**, 311.
Feenberg, E., and Trigg, G., 1950, *Rev. Mod. Phys.*, **22**, 399.
Feingold, A. M., 1951, *Rev. Mod. Phys.*, **23**, 10.

* We are informed privately by Professsor T. P. Kohman that work on natural radio-elements which he is carrying out independently with much the same system as that described here has not confirmed Libby's data.

Greuling, E., 1942, *Phys. Rev.*, **61,** 568.
Hahn, O., Strassman, F., and Walling, E., 1937, *Naturw.*, **25,** 189.
Haxel, O., and Houtermans, F. G., 1948, *Zeits. f. Physik*, **124,** 705.
Haxel, O., Houtermans, F. G., and Kemmerich, M., 1948, *Phys. Rev.*, **74,** 1886.
Hemmendinger, A. H., and Smythe, W. R., 1937, *Phys. Rev.*, **51,** 1052.
Heyden, M., and Kopfermann, H., 1938, *Zeits. f. Physik*, **108,** 232.
Jackson, D. A., 1933, *Proc. Roy. Soc.* A, **139,** 673.
Kemmerich, M., 1949, *Zeits. f. Physik*, **126,** 399.
Klemperer, O., 1935, *Proc. Roy. Soc.* A, **148,** 638.
Libby, W. F., 1934, *Phys. Rev.*, **46,** 196.
Libby, W. F., and Lee, D. D., 1939, *Phys. Rev.*, **55,** 245.
Mattauch, J., 1937, *Naturw.*, **25,** 189 and *Phys. Z. S.*, **38,** 951.
Millman, S., and Kusch, P., 1940, *Phys. Rev.*, **58,** 438.
Muhlhoff, W., 1930, *Ann. Physik*, **7,** 205.
Ollano, Z., 1941, *Nuovo Cimento*, **18,** 11.
Saha, A. K., 1946, *Proc. Nat. Inst. Sci. Ind.*, **12,** 159.
Strassman, F., and Walling, E., 1938, *Ber. d. d. Chem. Ges.*, **71,** 1.
Thomson, J. J., 1906, *Phil. Mag.*, **10,** 584.
Wu, C. S., 1950, *Rev. Mod. Phys.*, **22,** 386.
Yaffe, L., and Burtt, B. P., 1950, Separate contributions to Conference on Absolute β Counting, Nuclear Science Series, *Prelim. Report No.* 8.

VIII. *The Prediction of Uranium Deformation Textures*

By E. A. Calnan and C. J. B. Clews
National Physical Laboratory*

[Received September 26, 1951]

Summary

Tension, compression and rolling textures have been derived for the orthorhombic metal α-uranium. From a consideration of the relative importance of the slip and twinning mechanisms it is possible to differentiate between the textures developed after slight and severe deformations at both room and elevated temperatures.

§1. Introduction

A method has recently been proposed by which the preferred orientation developed in metals as a result of various mechanical operations may be derived from a knowledge of the deformation modes of their single crystals (Calnan and Clews 1950, 1951 a, b). The treatment has been applied successfully to the prediction of tension, compression, rolling and drawing textures of face-centred cubic, body-centred cubic and hexagonal metals, and the purpose of the present paper is to extend it to the orthorhombic structure, α-uranium. For this metal both the detailed crystal structure (Jacob and Warren 1937) and the deformation modes (Cahn 1951 a) have been established.

§2. Fundamental Principles

The slip and twinning systems observed by Cahn are listed in table 1. He concludes that at room temperature twinning is the predominating mechanism, the relative importance of the twinning systems being in the order listed, and that at temperatures above about 300° c (Cahn 1951 b) slip plays a larger part. The slip system (*a*) is by far the more important. Since the amount of deformation associated with twinning is limited, considerable slip must occur at all temperatures if high deformations are attained.

Consider now an isolated single crystal of uranium deforming only on the slip system (*a*) under a single tensile stress whose orientation is represented by the point *P* on the standard stereographic projection, fig. 1. The resolved shear stress on the most favourable slip system, namely the direction [100] on the plane (010), varies with the orientation of the stress direction in the manner illustrated by the contours in this figure. Thus the resolved shear stress corresponding to an applied stress direction *P* is 0·3 of the applied stress, T_a, and slip occurs when $0{\cdot}3T_a$

* Communication from the National Physical Laboratory.

reaches a critical value. In a polycrystalline aggregate, however, slip will not generally occur when this condition is satisfied owing to the constraints imposed by the neighbouring grains. This implies that the critical value has not been attained on this slip system and that the effective stress, T_e, may be represented by a point on a lower contour.

Table 1. Slip and Twinning Modes in Uranium

Slip	Plane	Direction		
a	(010)	[100]		
b	(110)	?		
Twinning	K_1	K_2	η_1	η_2
c	(130)	$(1\bar{1}0)$	$[3\bar{1}0]$	[110]
d	Irrational ~(172)	$(1\bar{1}2)$	$[3\bar{1}2]$	Irrational
e	$(1\bar{1}2)$	Irrational ~(172)	Irrational	$[3\bar{1}2]$

Fig. 1

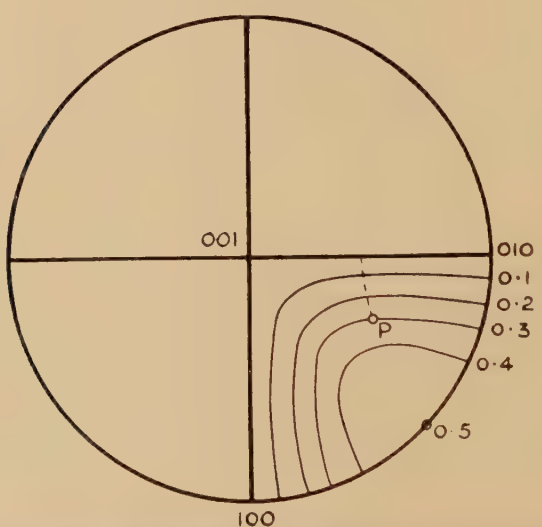

Standard stereographic projection of α-uranium showing resolved shear stress contours for slip on the (010)[100] system.

T_e may continue to move down the contours until it reaches the (001)—(010) boundary where the resolved shear stress on either of the $\{010\}\langle 100\rangle$ systems is zero, after which no further movement of T_e is possible and no slip occurs. The resolved shear stress for stress axis orientations on the (001)—(100) boundary also is zero. Thus it will be seen that no duplex or multiple slip is possible and that slip on one

system only with associated single crystal rotation can occur. This rotation moves the stress axis orientation along the great circle towards the slip direction [100] and gives a [100] tension texture.

The re-orientation associated with twinning on a single system, for example (*c*), will now be discussed. Fig. 2 shows the twinning elements of this system and the macroscopic reference circle of the original crystal which shears on the plane K_1 in the direction η_1 to become an ellipse. The plane K_2, whose trace is the line OB, η_2, is undistorted on twinning by movement to the position OD. It can be shown that the change of orientation due to twinning is crystallographically equivalent to rotation

Fig. 2

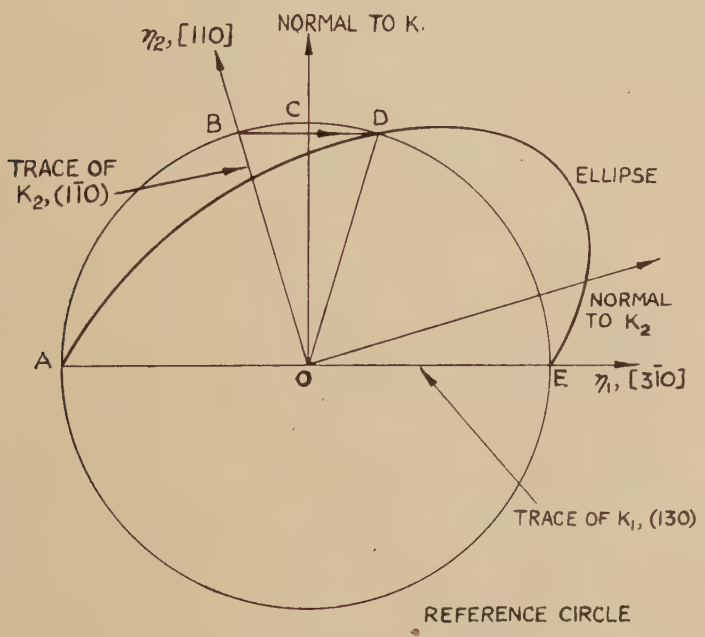

Geometry of twinning. Plane of diagram is plane of shear displacement. K_1 and K_2 are the first and second undistorted planes. η_1 is the shear direction, η_2 is the intersection of the second undistorted plane on the plane of shear displacement. The position of K_2 is that within the untwinned crystal (Schmid and Boas 1950).

through 180° about the twin plane normal although this corresponds to neither the macroscopic nor the atomic movements. For simple tensile stresses only those which give a positive resolved shear stress on the plane K_1 in the direction η_1 will produce twinning, that is to say, those within the quadrant COE. Thus in the stereographic projection, fig. 3, twinning under tension can occur for those grains only which have the stress direction within the quadrant (130)(001)[3$\bar{1}$0], corresponding to the quadrant COE of fig. 2. The sector (100)(001)[3$\bar{1}$0] may be neglected as here the system K_1=(1$\bar{3}$0) is the more favourable. In order

to determine the twinned orientation of a grain or part of a grain whose stress axis is represented by the point P, fig. 3, a great circle is drawn through this point and the shear plane normal, K_1. The angular distance between P and K_1 is measured and the new orientation of P will be at an equal distance along the great circle on the opposite side of K_1, i.e. at the point P'. Thus the twinned orientations corresponding to the area (130)(100)(001) lie within the region $T_{130}T_{100}(001)$.

§ 3. Tension Textures

The re-orientation with twinning on system (*c*), $K_1=(130)$, has just been derived, and that for the system (*d*), $K_1=(172)$, is illustrated in fig. 4. Orientations with the stress axis originally within the area (100)(001)QR twin to the areas $T_{100}T_PT_LT_QT_R$ and $T_{001}T_PT_L$. The re-orientations for the reciprocal system (*e*) are very similar and may be considered as augmenting system (*d*). For conditions where twinning

Fig. 3

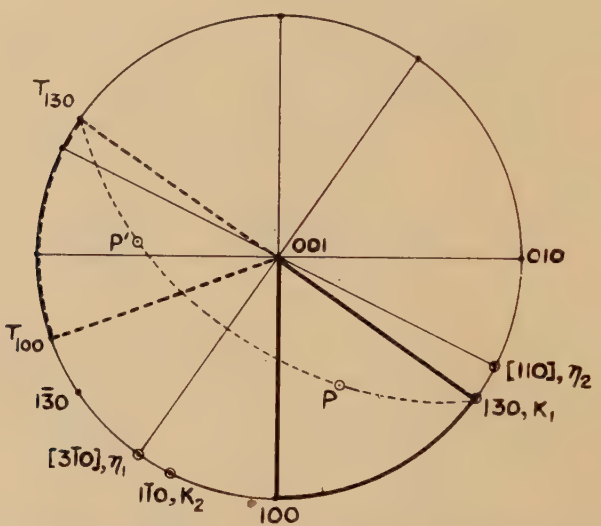

Standard projection showing the twinning elements for the system $K_1=(130)$, the orientations for which twinning occurs under tension (heavy outline), and the orientations after twinning (heavy broken line).

predominates the texture will be determined principally by twinning re-orientations. Superposition of figs. 3 and 4 as in fig. 5 (*a*) shows that for orientations with stress axes within the region (100)(001)C twinning may occur on either system (*c*) or system (*d*) ; in the region (001)BC on the system (*d*) alone, and in the remaining area of the unit quadrant (010)BA no twinning can occur. The twinned orientations may be obtained similarly by superposition within the reference unit quadrant, also shown in fig. 5 (*a*). The operation of both these twinning systems removes orientations from the area (100)(001)EFG to the area (010)(001)EFG which thus becomes a region of preferred orientation.

The density of orientations is not constant throughout this latter area but is highest in the region (010)BH where the superposition of twinned orientations is greatest. Subsequent retwinning leads progressively into the area (010)BA from which no twinning can occur. This last region is therefore the final texture which could be attained by tension twinning alone on the assumption that such severe deformation could be reached without fracture, fig. 5 (*b*).

The rotations for the slip system (*a*) are those associated with single crystal slip in the direction indicated by the arrow along the great circle in fig. 5 (*c*), and the preferred orientation resulting from twinning and some slip is shown by the cross-hatching. As the slip system (*b*) has not been fully established and, moreover, is believed to be of very minor importance it has been neglected in this analysis. Further slip rotation

Fig. 4

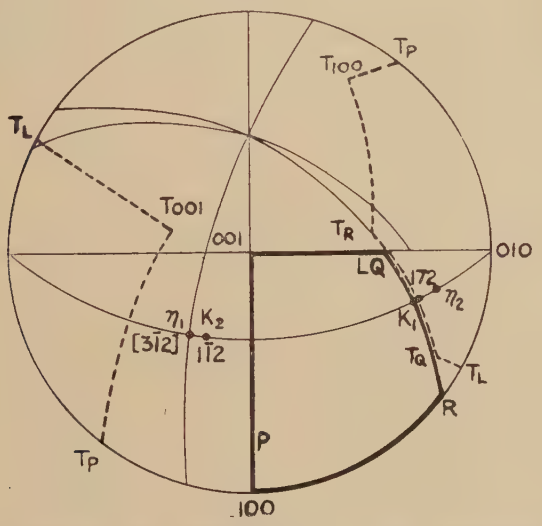

Twinning elements for the system K_1=(172) and re-orientations under tension.

does not, however, lead to a (100) texture since in the neighbourhood of (100) twinning is likely to be the more favourable deformation mode. The position of the boundary between the regions of slip and twinning depends upon the relative critical shear stresses for these modes. In the absence of an quantitative data on the magnitudes of these stresses the boundary (001)Z has been drawn in fig. 5 (*d*) for a ratio of unity. Thus a grain of stress axis orientation near (010) rotates by slip towards (100) but on crossing the (001)Z boundary twins back to the neighbourhood of (010) from whence it may again rotate by slip. This cyclic process moves the highest density of orientations to the vicinity of Z, i.e. near the (110) pole and maintains a spread of orientations from Z to the (010) end of the (010)(001) boundary. In this was the texture corresponding to twinning and a considerable amount of slip is derived as shown by the cross-hatching in fig. 5 (*d*).

§ 4. Compression Textures

The compression textures obtained by twinning and varying amounts of slip are derived in a manner precisely similar to that just described. The orientations of stress axis for which twinning may occur are seen by reference to fig. 2. In order to produce a positive resolved shear stress in the direction η_1 on the plane K_1 the simple compressive stress must lie within the quadrant COA. Thus for the system (*c*), table 1, twinning will occur on the (130) plane in the shear direction [3$\bar{1}$0] for stress axis orientations within the quadrant (130)(001)[310], fig. 6. The sector (130)(001)(010) may be neglected since in this region twinning on the symmetrical system $K_1=(\bar{1}30)$, $\eta_1=[\bar{3}10]$ is more favourable. Twinning

Fig. 5

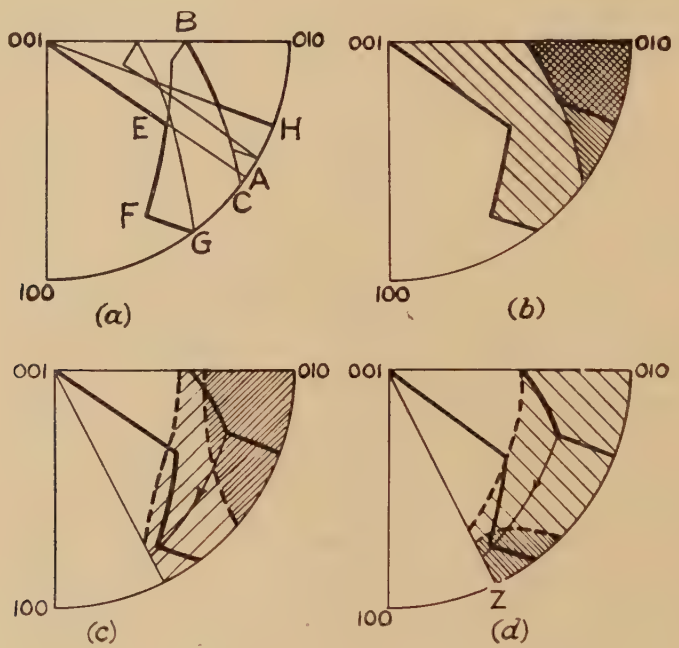

Tension textures, cross-hatching shows density of orientations.

(*a*) Twinning re-orientations in the unit quadrant for both twinning systems derived by superposition of figs. 3 and 4.

(*b*) Texture resulting from twinning alone.

(*c*) Texture resulting from twinning and some slip. Slip rotation indicated by the arrow.

(*d*) Texture resulting from twinning and a large amount of slip.

from the remaining region (010)(001)[310] gives re-orientations such that the corresponding stress axis positions are within the area [310](001)X. In fig. 7 are shown the re-orientations for the system (*d*), $K_1=(\bar{1}72)$. Here twinning takes place from the area (0$\bar{1}$0)YZ to the area $\mathrm{T}_{0\bar{1}0}$YZ. Combination of figs. 6 and 7 shows that the operation of both systems removes orientations from the area (010)Y[310] in fig. 8 (*a*) to the area (100)(001)Y[310]. The overlapping of twinned areas is greatest in the

region ABC and thus the compression texture corresponding to deformation by twinning alone is that shown by the density of cross-hatching in fig. 8 (*b*).

Fig. 6

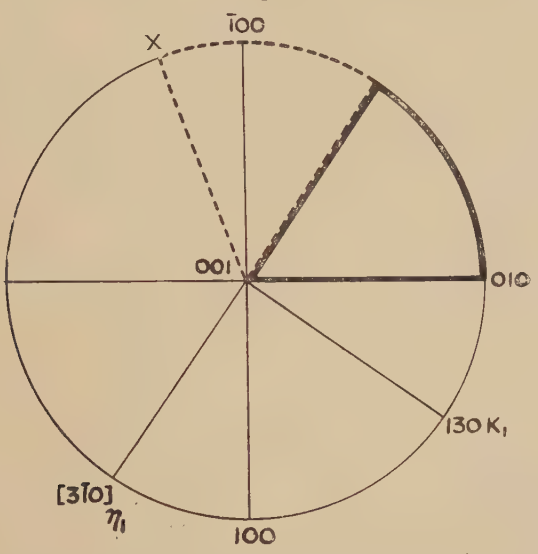

Twinning elements for the system K_1=(130) and re-orientations under compression.

Fig. 7

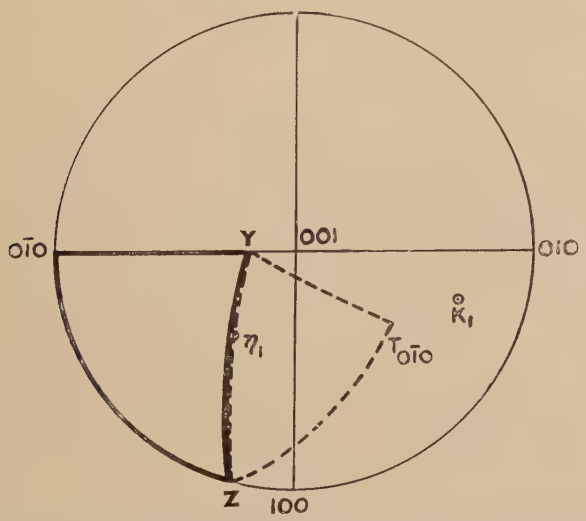

Twinning elements for the system K_1=(172) and re-orientations under compression.

The direction of rotation resulting from slip on the system (*a*) is towards the pole of the operative slip plane (010) indicated by the arrows in fig. 8 (*c*). A small amount of slip in addition to the twinning will produce the

texture shown in this figure. For twinning together with a considerable amount of slip the texture will be as in fig. 8 (*d*), where again the slip-twin boundary (001)X has been drawn for equal critical shear stresses on the slip and twinning systems.

Fig. 8

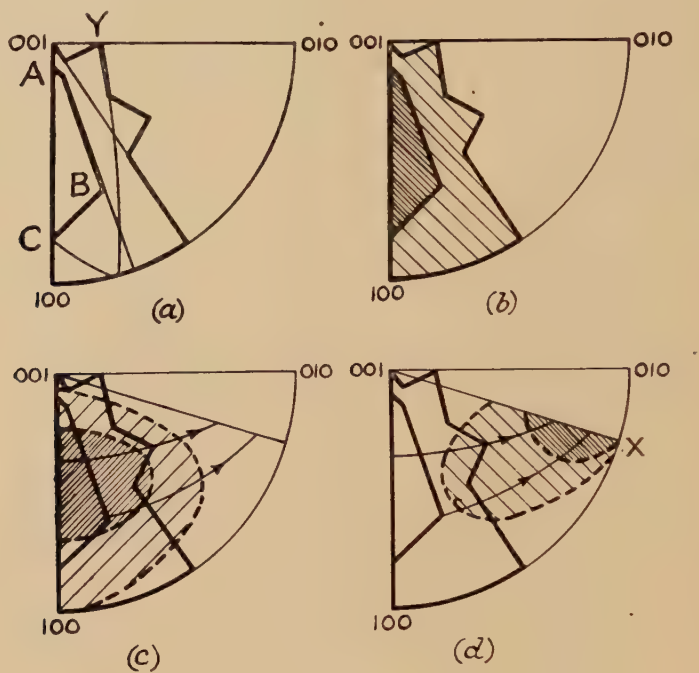

Compression textures.

(*a*) Twinning re-orientations for both systems derived from figs. 6 and 7.
(*b*) Texture for twinning alone.
(*c*) Texture for twinning and some slip.
(*d*) Texture for twinning and a large amount of slip.

Table 2. Tension and Compression Textures

Deformation processes	Plane normals parallel to		Plane normals perpendicular to compression axis (perpendicular texture)
	Tension axis (tension texture)	Compression axis (compression texture)	
Twinning	(010)	Zone (100)–(001)	(010)
Twinning+ Some slip	(010) → (130)	Zone (100)–(001) broadened	(010) spread towards (110)
Twinning+ large amount of slip	(110)	~(170)	Zone (001)–(110)

While none of the tension and compression textures can be fully described in terms of ideal textures, their main features may be tabulated as in the first three columns of table 2.

§ 5. Rolling Textures

Sheet Rolling. The compressive stresses normal to the plane of the sheet lead to textures in which the planes listed in column 3 of table 2 lie in this plane. The texture for any direction perpendicular to the compression axis (perpendicular texture), such as the rolling direction, may be obtained by drawing on the standard stereographic projection narrow bands, bounded by small circles, whose intensity corresponds to that of their poles in the compression texture. Thus to the regions A, B and C in the compression texture of fig. 9 (*a*) there correspond the bands in fig. 9 (*b*). It will be seen that with additional regions intermediate between A, B and C, forming a compression texture similar to fig. 8 (*b*), there is a high density of orientations in the perpendicular texture in the neighbourhood of (010). This and the other perpendicular textures are listed in column 4 of table 2. The minor component of rolling, namely tension in a specific direction perpendicular to the compression axis, may then be introduced by applying the tension re-orientations to these textures. Comparison of columns 2 and 4 of table 2 shows immediately that the tension textures are consistent with the perpendicular textures, and therefore the re-orientations may occur simultaneously producing the compression texture parallel to the sheet normal and the tension texture parallel to the rolling direction.

Rod Rolling. The textures derived for the direction perpendicular to the compression axis, column 4, table 2, do not imply any additional spatial relation between these two directions, and are thus equally valid for an array of similar radial stresses. The rod may be envisaged as an aggregate of sheets in which each sheet normal is aligned parallel to any one of the radial stresses, and each rolling direction parallel to the common rolling direction. The preferred orientation of the rod axis is thus the texture derived for the sheet rolling direction, i.e. the tension texture. On this view the texture in any radial direction should be a random distribution of all plane normals perpendicular to the tension texture. If, as is more likely, the predominating influence is the compressive stress parallel to the particular radial direction under consideration, then some evidence of the simple compression texture may be found in this radial direction. In general, therefore, a longitudinal section may have a complex texture varying from point to point on a given section, and from one section to another.

§ 6. Effect of Temperature and Degree of Deformation

On the basis of Cahn's observations that the slip mechanism is relatively more important above 300° C it might be concluded that the room temperature deformation textures would be primarily those

resulting from twinning alone, figs. 5 (*b*) and 8 (*b*). The amount of deformation attainable by twinning is, however, not unlimited, the limit depending theoretically on the shears associated with the twinning systems and the amount of successive retwinning which occurs before the final texture is reached. It may be estimated from a knowledge of these shears that this limit is likely to be about 30–40% deformation,

Fig. 9

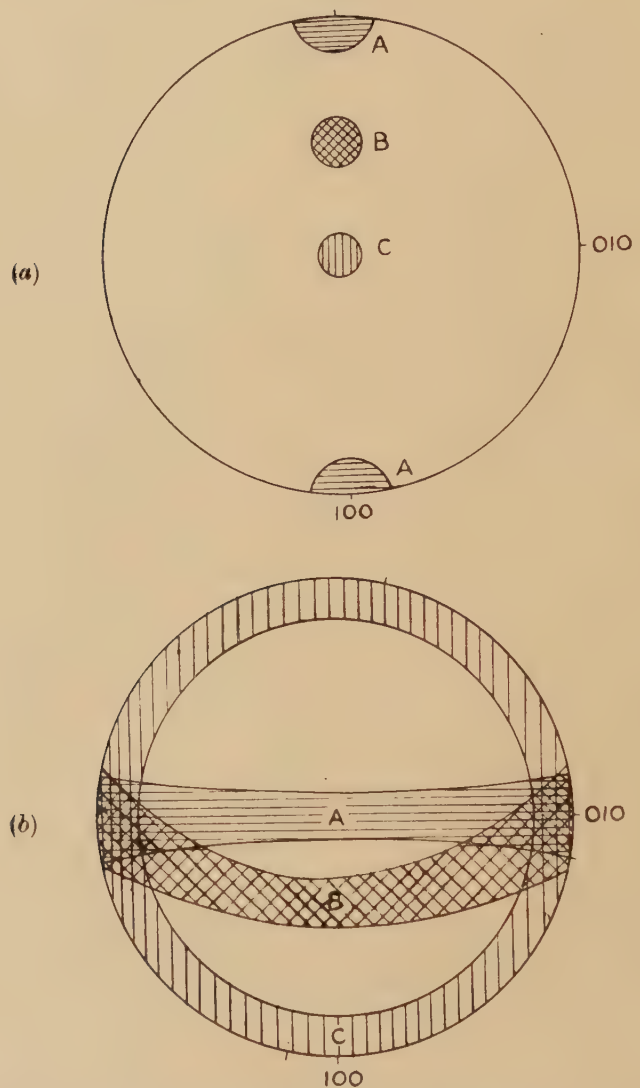

Illustrating the derivation of the texture perpendicular to the compression axis for a given compression texture.

(*a*) Shows the compression texture, and (*b*) the corresponding bands whose superposition gives the perpendicular texture.

and therefore the room temperature textures for deformations appreciably greater than this will show some influence of slip, figs. 5 (*c*) and 8 (*c*), tending in the limit to the textures shown in figs. 5 (*d*) and 8 (*d*).

Above 300° C, as a result of both slip and twinning, textures similar to figs. 5 (*c*) and 8 (*c*) may be expected in the early stages of deformation, while after severe deformation the textures of figs. 5 (*d*) and 8 (*d*) will be produced.

Table 3. Rolling Textures

Deformation	Room temperature		Elevated temperature (> ~300° C)	
	Planes in rolling plane	Plane normals parallel to rolling direction	Planes in rolling plane	Plane normals parallel to rolling direction
Low	Zone (100)–(001)	(010)	Zone (100)–(001) broadened	(010) → (130)
High	Zone (100)–(001) broadened	(010) → (130)	~(170)	(110)

The textures defined are those for sheet rolling. The textures for the axis in rod rolling are given by columns 3 and 5.

These conclusions are summarized in terms of 'ideal' textures in table 3. The only experimental work with which these predicted textures may be compared is that of Harris (1951) who has studied the preferred orientation in rolled bars by Geiger Counter methods. He finds that light reduction by cold rolling gives a texture in which (010) plane normals lie parallel to the rolling direction with some spread of orientation towards (130). Light reduction by hot rolling gives a similar texture with a slightly greater spread of orientation towards (110), while a heavier reduction by hot rolling gives a strong (110) texture with a spread towards (010). These observations are in good agreement with the predictions in columns 3 and 5 of table 3 as is more clearly demonstrated by comparison of figs. 5 (*b*), 5 (*c*) and 5 (*d*) with the figs. 4 (*a*), 2 (*a*) and 3 (*a*) respectively of Harris's paper. Some refinement of the treatment will be possible when the relative magnitudes, at various stages of the deformation, of the critical shear stresses for the slip and twinning systems have been determined. On this ratio depends the position of the slip-twinning boundary discussed above, which in turn defines the limit of the texture when appreciable slip occurs, e.g. fig. 5 (*d*). It has been assumed that this ratio is unity and the agreement between fig. 5 (*d*) and fig. 4 (*a*) (Harris)

suggests that this is indeed approximately so, at least in the later stages of deformation. The spread of orientation beyond (110) towards (100) may, however, indicate that the critical stress for twinning is slightly greater than that for slip.

Acknowledgments

The authors wish to thank Dr. R. W. Cahn, of the Atomic Energy Research Establishment, Harwell, and Mr. G. B. Harris, lately of this Laboratory, for making available the results of their experiments on the deformation of α-uranium prior to publication.

The work described above has been carried out as part of the research programme of the National Physical Laboratory, and this paper is published by permission of the Director of the Laboratory.

References

Cahn, R. W., 1951 a, *Acta Crystallographica*, **4,** 470 ; 1951 b, *Revue de Metallurgie*, in press.

Calnan, E. A., and Clews, C. J. B., 1950, *Phil. Mag.*, [7], **41,** 1085 ; 1951 a, *Ibid.*, **42,** 616 ; 1951 b, *Ibid.*, **42,** 919.

Harris, G. B., 1952, *Phil. Mag.*, **43,** 113.

Jacob, C. W., and Warren, B. E., 1937, *J. Am. Chem. Soc.*, **59,** 2588.

Schmid, E., and Boas, W., 1950, *Plasticity of Crystals* (London : Hughes). Translation of *Kristallplastizität*, 1935 (Berlin : Springer).

IX. *A Calculation of the Elastic Shear Constants of β-brass*

By H. Jones
Department of Mathematics, Imperial College, London*

[Received October 16, 1951]

Abstract

The stability of β-brass, with respect to shears across the (110) plane in the direction [1$\bar{1}$0], is considered and is shown to be due, mainly, to the change of the Fermi energy as a result of the shearing of the Brillouin zone. Calculations are made which show that this effect contributes approximately 10^{11} dynes/cm^2 to the shear constant $\frac{1}{2}(c_{11}-c_{12})$, and a rather larger amount to c_{44}. The constitution of the elastic shear constants, as the sum of three terms, is examined and a satisfactory account of the observed values is obtained. The difficulty experienced in attempting to retain the β-phases by quenching is briefly discussed.

§1. Introduction

It is well known that the interaction between closed ionic shells, in metals or alloys with the body centred cubic structure, leads to a negative contribution to the elastic constant corresponding to a pure shear over the (110) plane in the direction [1$\bar{1}$0]. In the alkali metals, because of the large atomic volumes, the ions are so well separated that this effect is very small and the body centred structure is stabilized mechanically by electrostatic interactions. In the other pure metals which have body centred cubic structures, e.g. W or Cr, the ionic shells are incomplete and these metals are rendered stable, according to Zener (1951), by exchange spin interactions. Alloys which are body centred cubic are the β-phases, occurring at electron-atom ratios of approximately 3/2, of which β-brass is typical. The distance between nearest atoms in β-brass is very nearly the same as that between nearest atoms in pure copper where it is known that the non-Coulomb ionic interactions very largely determine the rigidity. The question arises therefore: what is the stabilizing influence in β-brass which ensures a positive value for the shear constant $\frac{1}{2}(c_{11}-c_{12})$? Isenberg (1951) in a recent paper, having in mind that the disordered β-phases are stable only at high temperatures and cannot, in general, be quenched writes 'the stability of disordered β-brass under a (110) [1$\bar{1}$0] shear is due in some way to thermal vibrations'. It is the purpose of this paper to examine in detail one possible cause, not directly concerned with thermal vibrations, of the observed stability of the β-phases.

* Communicated by the Author.

A calculation of the elastic constants of aluminium, made by Leigh (1951), shows that the change of the Fermi energy of the conduction electrons under a shear can lead to large contributions to the shear constants. In monovalent metals it is known that this effect is, in general, small because in these cases the Fermi surface which contains the occupied electronic states is not in contact with the Brillouin zone (BZ) boundaries. In β-brass of composition CuZn there are 1·5 electrons per atom to be placed inside the $\{110\}$ zone which contains two states per atom. It may be assumed, therefore, that in this metal the Fermi surface will be in contact with the zone boundaries and, indeed, this was made the basis of a theory of the occurrence of this phase at an electron-atom ratio of approximately 3/2 (Jones 1937).

In the following section we calculate the contribution, arising from the Fermi energy, to the two shear constants c_{44} and $\frac{1}{2}(c_{11}-c_{12})$; for the sake of brevity the latter will frequently be denoted by c'. The conclusion is reached that this contribution amounts to at least 10^{11} dynes/cm^2 for the constant c' in β-brass and therefore provides the explanation of the mechanical stability of the phase. In § 3 it is shown that the contribution from the Fermi energy along with the estimated electrostatic effect and the non-Coulomb interactions accounts in a satisfactory manner for the observed values of c_{44} and c' as determined by Lazarus (1949). Finally, a reason is suggested for the difficulty experienced in attempting to retain the disordered β-phase by quenching.

§ 2. The Fermi Energy Effect

In this section we shall calculate how the Fermi energy changes as the crystal is sheared at constant volume. We shall assume throughout that no electronic states outside the $\{110\}$ BZ are occupied. If the energy of a state within the BZ depends upon the momentum in the same way as for a free electron, but the above assumption is maintained, then the contributions to c_{44} and c' can easily be worked out exactly, as shown at the end of this section. The approximation of regarding the electrons as free for states within the BZ is, however, very unsatisfactory for β-brass and we shall take a more general dependence of the energy on the momentum into account. In order to carry out the calculation in this more general case, we have assumed that the effect on the Fermi energy of each pair of planes of the BZ can be calculated separately and the total effect obtained by summing over all pairs of faces. It is proved, at the end of this section, that for nearly free electrons this last assumption introduces negligible errors.

The wave vector $\mathbf{k}$ specifying an electronic state is defined so that $\hbar\,\mathbf{k}$ is equal to the momentum of the electron. The number of states per unit volume of metal associated with a volume element $d\mathbf{k}$ is thus $(1/4\pi^3)d\mathbf{k}$, where account has been taken of the doubling of each state by the spin. If we measure energies in Rydberg units ($Ry = 21{\cdot}79.10^{-12}$ ergs) and lengths in units of the first Bohr hydrogen orbit ($a_H = 0{\cdot}529.10^{-8}$ cm) the energy ϵ of a free electron in terms of $\mathbf{k}$ is given simply by $\epsilon = k^2$.

If a denotes the lattice constant, the planes which form the boundaries of the BZ are given by

$$\mathbf{n} \cdot \mathbf{k} = (\pi/a)|\mathbf{n}|^2, \quad \ldots \ldots \ldots \quad (1)$$

where $\mathbf{n}$ is one of the set of vectors $\{110\}$ each of magnitude $\sqrt{2}$.

We shall now calculate the effect on the Fermi energy of a single pair of these planes ($\pm\mathbf{n}$) on the assumption that the energy at any point $\mathbf{k}$ is given by

$$\epsilon = k^2 - k_z^2 + p_{\mathbf{n}}^2 f(z), \quad \ldots \ldots \ldots \quad (2)$$

where $p_{\mathbf{n}} = \sqrt{2}\pi/a$ is the perpendicular distance from the origin of k-space to either plane, and $f(z)$ is a non-dimensional function of $z = k_z/p_{\mathbf{n}}$. The axes in k-space have been chosen so that k_z coincides with the normal to the two planes $\pm\mathbf{n}$. We need not, at this stage, specify $f(z)$ in further detail except to notice that for small z it behaves like z^2 and that $f'(1) = 0$.

When the energy has the form (2) the density of states function $N(\epsilon)$ can be calculated immediately and we obtain

$$N(\epsilon) = (1/4\pi^3) \int |\text{grad } \epsilon|^{-1} dS = (1/2\pi^2) k_{\max}, \quad \ldots \ldots \quad (3)$$

where $k_{\max}$ is the greatest value of k_z on the energy surface ϵ (Jones 1937). For values of $\epsilon > \epsilon_1$, where ϵ_1 is the energy of the surface which just touches the planes $\pm\mathbf{n}$, $N(\epsilon)$ is constant and equal to $(1/2\pi^2)p_{\mathbf{n}}$.

The number of electrons per unit volume n is given by integrating $N(\epsilon)$ from zero to the energy at the surface of the filled states $\epsilon_{\max}$, and if $\epsilon_{\max} > \epsilon_1$ we obtain from (2) and (3) after an elementary reduction

$$2\pi^2 n / p_{\mathbf{n}}^3 = (\epsilon_{\max}/p_{\mathbf{n}}^2) - \int_0^1 f(z) dz. \quad \ldots \ldots \quad (4)$$

In a similar way we obtain for the Fermi energy per unit volume W

$$4\pi^2 W / p_{\mathbf{n}}^5 = (\epsilon_{\max}/p_{\mathbf{n}}^2)^2 - \int_0^1 f^2(z) dz. \quad \ldots \ldots \quad (5)$$

If we denote the integral in equation (4) by u_1 and that in (5) by u_2, and if we now eliminate $(\epsilon_{\max}/p_{\mathbf{n}}^2)$ between (4) and (5) we obtain

$$4\pi^2 W = (4\pi^4 n^2/p_{\mathbf{n}}) + 4\pi^2 n u_1 p_{\mathbf{n}}^2 - (u_2 - u_1^2) p_{\mathbf{n}}^5. \quad \ldots \quad (6)$$

Thus if we keep n constant, i.e. the atomic volume constant, (6) gives the change in W under a pure shear which alters the value of $p_{\mathbf{n}}$.

Let W_0 denote the energy of free electrons at the same number density n, then $(W - W_0)$ can be regarded as the depression of the Fermi energy brought about by the pair of planes $\pm\mathbf{n}$. Thus for the body centred cubic structure, if we sum $(W - W_0)$ over the six pairs of planes which form the BZ, the changes in this sum due to a shear should give a good approximation to the change in the Fermi energy under this shear. Thus we write for the Fermi energy W^F

$$W^F = \Sigma W(p_{\mathbf{n}}) - 5W_0. \quad \ldots \ldots \quad (7)$$

For a pure shear in which all the strain components are zero except e_{xy} we find

$$c_{44}{}^F = \left(\frac{\partial^2 W^F}{\partial e_{xy}{}^2}\right)_0 = W'' \Sigma \left(\frac{\partial p_{\mathbf{n}}}{\partial e_{xy}}\right)_0^2 + W' \Sigma \left(\frac{\partial^2 p_{\mathbf{n}}}{\partial e_{xy}{}^2}\right)_0, \quad \ldots \quad (8)$$

where $c_{44}{}^F$ denotes the contribution to the elastic constant c_{44} arising from the change in W^F, and the subscript to the derivatives means that these are to be taken at $e_{xy}=0$.

It may easily be shown that to second powers of the strain component

$$(a/\pi)^2 p_{\mathbf{n}}{}^2 = |\mathbf{n}|^2 - 2n_1 n_2 e_{xy} + \tfrac{1}{2}(n_1{}^2+n_2{}^2)e_{xy}{}^2, \quad . \quad . \quad . \quad (9)$$

and thus, the sums in (8) may be evaluated and we obtain

$$c_{44}{}^F = \tfrac{1}{2}p^2 W'' + \tfrac{3}{2}pW'. \quad . \quad . \quad . \quad . \quad . \quad . \quad . \quad (10)$$

In a similar way, for the pure shear $e_{zz}=e$, $e_{xx}=e_{yy}=(1+e)^{-\frac{1}{2}}-1$, we find

$$\tfrac{1}{2}(c_{11}-c_{12})^F = \tfrac{1}{3}\left(\frac{\partial^2 W}{\partial e^2}\right)_0 = \tfrac{1}{3}W''\Sigma\left(\frac{\partial p_{\mathbf{n}}}{\partial e}\right)_0^2 + \tfrac{1}{3}W'\Sigma\left(\frac{\partial^2 p_{\mathbf{n}}}{\partial e^2}\right)_0, \quad . \quad . \quad (11)$$

where

$$(a/\pi)^2 p_{\mathbf{n}}{}^2 = |\mathbf{n}|^2 + (n_1{}^2+n_2{}^2-2n_3{}^2)e + 3n_3{}^2 e^2, \quad . \quad . \quad . \quad . \quad (12)$$

and thus

$$\tfrac{1}{2}(c_{11}-c_{12})^F = \tfrac{1}{4}p^2 W'' + \tfrac{7}{4}pW'. \quad . \quad . \quad . \quad . \quad . \quad (13)$$

In equations (10) and (13) we have written p for the value of $p_{\mathbf{n}}$ in the unstrained state, and W is given by (6).

It will be noticed that (10) and (13) have the same form as the contributions to the shear constants, arising from central forces between nearest ions, in a face centred cubic lattice (Fuchs 1936). The reason for this is evidently that the reciprocal lattice of a body centred cubic space lattice is face centred cubic, and $\partial W/\partial p_{\mathbf{n}}$ behaves like a central force acting along the line joining the points $+\mathbf{n}$ and $-\mathbf{n}$ in the reciprocal lattice. From equations (6), (10) and (13) we now obtain easily

$$(1/\kappa)c_{44}{}^F = -\tfrac{1}{4}\nu^2 + 4\nu u_1 - \tfrac{35}{4}(u_2-u_1{}^2), \quad . \quad . \quad . \quad . \quad . \quad (14)$$

$$(1/\kappa)\tfrac{1}{2}(c_{11}-c_{12})^F = -\tfrac{5}{8}\nu^2 + 4\nu u_1 - \tfrac{55}{8}(u_2-u_1{}^2), \quad . \quad . \quad . \quad . \quad (15)$$

where $\kappa=(p^5/2\pi^2)(Ry/a_{\mathrm{H}}{}^3)$ and $\nu=2\pi^2 n/p^3$. The number of conduction electrons per atom in the alloy is given by $\pi\nu/\sqrt{2}$, so that for CuZn $\nu=3/\pi\sqrt{2}=0{\cdot}6752$. The lattice constant $a=2{\cdot}945$ A.U. and therefore $\kappa=2{\cdot}4159.10^{12}$ dynes/cm^2.

No further progress can be made without a knowledge of the form of the function $f(z)$. We shall assume a form of the type used by Leigh (1951) viz. $f(z)=z^2-\lambda z^{2/\lambda}$ in which $\lambda \ll 1$. This satisfies the conditions $f(z)\to z^2$ as $z\to 0$ and $f'(1)=0$, and since $f(1)=1-\lambda$ we see that λp^2 is the amount by which the energy at a plane of the BZ is less than the corresponding energy of a free electron. Using $a=2{\cdot}945$ A.U. and expressing the energy in electron volts we find that the diminution of energy is equal to $8{\cdot}67\lambda$ ev.

With this form for $f(z)$ the integrals u_1 and u_2 can be evaluated and we find from (14) and (15)

$$(1/\kappa)c_{44}{}^F = -\tfrac{1}{4}\nu^2 + \frac{4(1-\lambda)}{3(2+\lambda)}\left[(2+3\lambda)\nu - \frac{7(1-\lambda)(8+38\lambda+27\lambda^2)}{3(2+\lambda)(2+3\lambda)(4+\lambda)}\right], \quad . \quad (16)$$

$$(1/\kappa)\tfrac{1}{2}(c_{11}-c_{12})^F = -\tfrac{5}{8}\nu^2 + \frac{2(1-\lambda)}{3(2+\lambda)}\left[2(2+3\lambda)\nu - \frac{11(1-\lambda)(8+38\lambda+27\lambda^2)}{3(2+\lambda)(2+3\lambda)(4+\lambda)}\right]. \quad . \quad . \quad . \quad (17)$$

Fig. 1 shows the two shear constants, for values of λ from 0 to 0·2, calculated according to these expressions. When $\lambda=0{\cdot}15$, for example, the lowering of the energy of a state at the zone boundary would be 1·30 ev and the shear constants are then $c_{44}{}^F=1{\cdot}8$ and $c'^F=1{\cdot}2(10^{11}$ dynes/cm^2). It can be seen from the figure that, for values of λ which are at all plausible, the shear constant c'^F will lie somewhere between 1 and 2 (10^{11} dynes/cm^2). The Fermi energy appears therefore to provide the required stabilizing factor against the homogeneous shear (110) [1$\bar{1}$0].

The above calculation of the contribution from the Fermi energy to the shear constants depends on the assumption that the effect of each pair of zone boundary planes can be calculated separately. This

Fig. 1

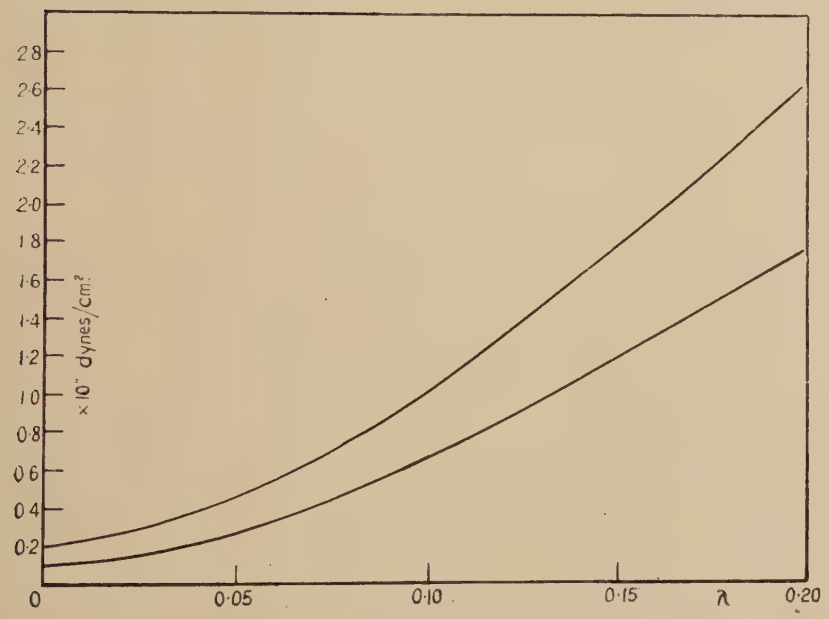

The Fermi energy contributions to the shear constant according to (16) and (17). Upper curve $c_{44}{}^F$, lower curve $\frac{1}{2}(c_{11}-c_{12})^F$.

assumption should not lead to serious inaccuracy when the Fermi surface touches the BZ boundaries over only a small fraction of the whole surface. Clearly if the zone were almost completely filled the assumption would be quite invalid.

In the special case when $\lambda=0$, so that the surface of the Fermi distribution is a sphere cut off by the planes of the BZ, it is possible to calculate the contribution to the shear constants without making the above assumption. An elementary calculation, which need not be reproduced, shows that in this case

$$4\pi^2 W=R^4\Sigma p_{\mathbf{n}}-\tfrac{1}{5}\Sigma p_{\mathbf{n}}{}^5-4R^5, \quad . \quad . \quad . \quad . \quad . \quad (18)$$

$$2\pi^2 n=R^2\Sigma p_{\mathbf{n}}-\tfrac{1}{3}\Sigma p_{\mathbf{n}}{}^3-\tfrac{10}{3}R^3, \quad . \quad . \quad . \quad . \quad . \quad (19)$$

where R denotes the radius of the sphere which forms part of the surface of the electron distribution. The p_n are given by equations (9) and (12) for the two different shears, from which the sums taken over the six pairs of planes forming the BZ can be calculated. In this way we obtain

$$(1/\kappa)c_{44}{}^{(0)}=-\tfrac{3}{4}\xi^4+\tfrac{5}{2}\xi^2-\tfrac{7}{4}, \quad . \quad . \quad . \quad . \quad . \quad . \quad (20)$$

and

$$(1/\kappa)\tfrac{1}{2}(c_{11}-c_{12})^{(0)}=-\tfrac{7}{8}\xi^4+\tfrac{9}{4}\xi^2-\tfrac{11}{8}, \quad . \quad . \quad . \quad . \quad (21)$$

where ξ is given by the equation

$$(10/3)\xi^3-6\xi^2+\nu+2=0. \quad . \quad . \quad . \quad . \quad . \quad . \quad (22)$$

The superscript (0) is used to indicate the special case of free electron energies within the BZ.

If we put $\xi=\sec\theta$ then θ is the angle which the radius of the circle of occupied states on the (110) plane subtends at the centre of the zone. For β-brass, using the previously given value of ν, we find from (22) $\xi=1{\cdot}0042$ so that $\theta=5°15'$.

If we write $\xi=1+\delta$ equations (20) and (21) give, to second powers of δ

$$(1/\kappa)c_{44}{}^{(0)}=2\delta-2\delta^2, \text{ and } (1/\kappa)\tfrac{1}{2}(c_{11}-c_{12})^{(0)}=\delta-3\delta^2, \quad . \quad . \quad (23)$$

and from (22) we find

$$\nu=2/3+2\delta-4\delta^2, \quad . \quad . \quad . \quad . \quad . \quad . \quad . \quad (24)$$

so that on substituting this into (16) and (17), taken when $\lambda=0$, we find

$$(1/\kappa)c_{44}{}^{(0)}=2\delta-5\delta^2, \text{ and } (1/\kappa)\tfrac{1}{2}(c_{11}-c_{12})^{(0)}=\delta-(9/2)\delta^2. \quad . \quad (25)$$

It appears therefore that the approximate values of the shear constants, as given by (16) and (17), differ from the directly calculated values only by second powers of δ. The fractional error is the same in both cases viz. $(3/2)\delta$ which is $0{\cdot}63\%$. Thus the approximation involved by adding the effects of the different pairs of planes acting separately is negligibly small for very small values of λ, and it would appear unlikely that, over the whole range shown in fig. 1, there can be any serious error. Thus, if the energy discontinuities over the BZ boundaries in β-brass are, as is generally believed, about 2 or 3 electron volts, we are forced to the conclusion that the Fermi energy contributes at least 10^{11} dynes/cm^2 to the shear constant c' and thus stabilizes the structure with respect to homogeneous shears over the $\{110\}$ planes.

§3. The Constitution of the Shear Constants and the Stability of the β-phase

Besides the Fermi energy contribution there are two other important terms in the shear constants: an electrostatic term which contributes $171{\cdot}2\ a^{-4}Z_{\text{eff}}{}^2$ and $23{\cdot}0\ a^{-4}Z_{\text{eff}}{}^2$ in units of 10^{11} dynes/cm^2 to the two constants c_{44} and c' respectively (a in A.U.), and the non-Coulomb interaction between the ionic shells. If $a^3w(r)/8$ denotes the potential energy of a pair of ions at a distance r apart, arising from the non-Coulomb forces, the contributions which these forces make to c_{44} and c' are

respectively $(4/9)r^2w''+(8/9)rw'$ and $(4/3)rw'$. It is known that $w(r)$ varies very rapidly with r and it is usual to assume that the variation may be represented by $\exp(-r/\rho)$, where ρ is a length approximately equal to 0·3 A.U. Let $rw'=X$, then $r^2w''=-(r/\rho)X$ and the two contributions to c_{44} and c' become $(4/9)(2-r/\rho)X$ and $(4/3)X$ respectively.

To determine the electrostatic contribution we need to know the value of Z_{eff} which is very difficult to estimate accurately. It must, of course, lie between 1 and 2, and for the sake of obtaining approximate numerical results we shall simply assume $Z_{\text{eff}}{}^2=2{\cdot}0$. For the same reason we shall assume $\lambda=0{\cdot}15$ which would correspond to what is believed to be a likely energy gap over the BZ of about 3·0 ev, so that the Fermi energy contributions according to fig. 1 are $c_{44}=1{\cdot}8$ and $c'=1{\cdot}2$ (10^{11} dynes/cm^2).

The actual values of the shear constants of β-brass have been measured by Lazarus (1949) who gives

$$c_{44}=8{\cdot}24,\ c'=0{\cdot}97\ (10^{11}\ \text{dynes/cm}^2).$$

Adding the three contributions together and equating to the observed values we get the equations

$$1{\cdot}2+0{\cdot}61+(4/3)X=0{\cdot}97,$$

$$1{\cdot}8+4{\cdot}55+(4/9)(2-r/\rho)X=8{\cdot}24.$$

From which, since $r=2{\cdot}549$ A.U., we find $X=-0{\cdot}63.10^{11}$ ergs/cm^3 and $\rho=0{\cdot}29$ A.U. This value of X corresponds to a positive energy of 1·33 kcals per mole arising from the repulsive forces between the ions, which appears to be quite reasonable, as does also the value of ρ. The contribution to the bulk modulus from the non-Coulomb ionic interaction is readily seen to be $-(4/9)(2+r/\rho)X$ which, according to the above values, amounts to $3{\cdot}01.10^{11}$ dynes/cm^2. The observed value is $11{\cdot}62.10^{11}$ dynes/cm^2 whilst the Fermi energy contribution, assuming free electrons, is $6{\cdot}54.10^{11}$ dynes/cm^2 (Jones 1949). Since a change of volume affects the energy of the lowest state of the conduction electrons, and therefore a term occurs in the bulk modulus which is absent in the case of pure shears, the agreement is as good as can be expected.

According to this theory of the constitution of the elastic constants, therefore, the β-phase is rendered stable with respect to homogeneous shears across the (110) planes in the direction $[1\bar{1}0]$ by the effect of the zone boundaries on the Fermi energy. We are forced, therefore, to the conclusion that even the disordered β-phase would be mechanically stable at low temperatures with respect to any homogeneous shear. The reason that this phase does not occur at low temperatures is evidently because it becomes thermodynamically unstable relative to neighbouring phases, e.g. the ordered β′-phase or the ζ and μ types (Hume Rothery, Reynolds and Raynor 1940).

If, as Zener (1947) suggests, the characteristic temperature of the β-phase is less than that of neighbouring phases the free energy of the β-phase decreases, as the temperature rises, relatively more rapidly than

that of the other phases. This would explain the occurrence of the β-phase only at high temperatures and the general V shape of the phase boundaries.

The question now arises why it is so rarely, if ever, possible to quench the disordered β-phase and so obtain this structure in the metastable state. We suggest that the reason for this lies in the peculiar nature of the stabilizing influence of the Fermi energy. This operates only with respect to homogeneous shears over regions containing a good many atoms. It is, therefore, quite different from the stabilizing effect of forces which operate mainly between nearest neighbouring atoms. At any temperature, however low, local distortions should occur very easily in the β-phase and hence make the existence of any metastable state very improbable.

References

Fuchs, K., 1936, *Proc. Roy. Soc.* A, **153,** 622.
Hume Rothery, W., Reynolds, P. W., and Raynor, G. V., 1940, *Jour. Inst. Met.*, **66,** 191.
Isenberg, I., 1951, *Phys. Rev.*, **83,** 637.
Jones, H., 1937, *Proc. Phys. Soc.*, **49,** 250 ; 1949, *Physica*, **15,** 13.
Lazarus, D., 1949, *Phys. Rev.*, **76,** 545.
Leigh, R. S., 1951, *Phil. Mag.* [7], **42,** 139.
Zener, C., 1947, *Phys. Rev.*, **71,** 846 ; 1951, *Ibid.*, **81,** 440.

X. *Quantitative Measurement of Preferred Orientation in Rolled Uranium Bars*

By G. B. Harris*

[Received September 26, 1951]

Synopsis

The preferred orientation of uranium bars hot-rolled and cold-rolled in the α range has been determined quantitatively by x-ray diffraction using a Geiger counter. It is shown that hot rolling with a slight reduction causes the 010 planes to become strongly and the 110 planes weakly oriented perpendicular to the rolling direction. Further hot rolling causes the 110 planes to become strongly and the 010 planes weakly oriented perpendicular to the rolling direction. Cold rolling with light reduction causes the 010 planes to become strongly and the 130 planes weakly oriented in the planes perpendicular to the rolling direction.

§1. Introduction

Though the tendency of the crystals to align themselves in particular preferred orientations in rolled or otherwise mechanically deformed metal bodies has long been recognized, and techniques for qualitatively observing preferred orientations by x-ray diffraction have been extensively developed, Barrett (1943), comparatively little theoretical or experimental work has been done on the quantitative determination of preferred orientation by x-ray methods.

The Geiger counter x-ray spectrometer, in which the intensity of x-rays diffracted from a specimen is measured directly with a Geiger counter, has obvious advantages for this work over the more usual photographic method of recording the diffracted x-rays, and has been successfully applied to it by Decker, Asp and Harker (1948), and by Field and Merchant (1949). In both these investigations the Geiger counter was set to pick up x-rays diffracted from one set of lattice planes, and the specimen, in the form of a flat plate, was rotated about two axes perpendicular to the x-ray beam, so that the variation in the Geiger counter response enabled a pole figure to be drawn, showing the relative amounts of crystalline material with these lattice planes oriented at different ' latitudes and longitudes ' relative to the normal of the plate. The results had to be corrected for the different geometrical diffraction conditions at different settings of the plate ; Decker, Asp and Harker verified their calculated corrections by measurements on the silver grains in an exposed x-ray film, which were assumed to be randomly oriented.

* Communication from the National Physical Laboratory.

With α-uranium, the comparatively low symmetry of the crystal structure (orthorhombic, $a=2{\cdot}852$ A, $b=5{\cdot}865$ A, $c=4{\cdot}945$ A; space group Cmcm) enables an alternative method to be used, which yields a pole figure more directly related to the anisotropy of physical properties associated with preferred orientation. Because of the low symmetry, there are a large number of different sets of planes in the crystal lattice, which have slightly different spacings by which they can be distinguished. If the Geiger counter and specimen are simultaneously rotated in the spectrometer through the Bragg angle settings for these planes, it is possible to measure directly the relative amounts of crystalline material with each set of planes oriented parallel to the face of the specimen. Hence a pole figure can be drawn, showing the relative preponderance or scarcity of crystals with different crystallographic directions oriented along one axis in the specimen. This type of pole figure is convenient for relating the value of any directional physical property (e.g. electrical conductivity) measured in this direction to the values along the principal axes in a single crystal of the metal.

Fig. 1

Types of specimen section examined.

The method outlined above has been applied to the measurement of preferred orientation in cast, hot-rolled and cold-rolled uranium bars of diameters ranging from 0·7–1·5 in. (1·9–3·8 cm).

§2. Preparation of Specimens

Specimens for the study of preferred orientation were cut from uranium bars with a carborundum slitting-wheel. The three types of specimen examined are illustrated in fig. 1.

A *transverse* section was obtained by cutting a bar along two parallel planes perpendicular to its axis and examining a plane face of the slice removed.

A *tangential* section was obtained by cutting a transverse slice of a bar along a plane containing its axis and examining the face of this cut in the semi-cylindrical specimen obtained. The normal to the plane of the section at any point is perpendicular to both the axial direction and the radius passing through the point.

A *radial* section was obtained by cutting a tangential specimen along a plane parallel to the axis of the bar, but at some distance from it, and examining a region of the section half-way between the edges in which it meets the cylindrical surface of the bar. In this region the normal to the plane of section is along a radius of the bar.

In practice the above geometrical conditions were fufilled with an accuracy of $\pm 3°$ in all the sections cut.

All sections were hand-polished, then polished electrolytically and examined under the microscope between crossed polarizers. The detailed procedure was identical with that described by Chipman (1950). Grains of different orientation appeared with different brightness, because of the anisotropic reflectivity of uranium, so that the grain size of the specimens could be estimated, and the presence of preferred orientation inferred when the contrast between grains was weak.

§3. Photographic X-ray Examination

Before quantitative measurements were made on the Geiger counter spectrometer, all the specimens except those from bar 287/10 (see below) were examined by photographic x-ray methods. On a photograph it is possible to estimate, from the 'spottiness' of the diffraction lines, whether enough crystals are covered by the x-ray beam to give a true picture of the statistical distribution; with the Geiger counter spectrometer anomalies caused by covering too few crystals are detected only after measurement of the integrated intensities and calculation of the pole figure.

x-ray diffraction photographs of sections were taken in 11 cm diameter cylindrical cameras with filtered cobalt $K\alpha$ radiation (wavelength 1·790 A). Specimens were placed with the plane of section on the axis of the camera at an angle of 20° or 38° to the incident beam. With an angle of 20° lines from the following lattice planes were focussed on the film: (020), (110), (021), (002), and (111). Lines focussed with an angle of 38° were (131), (040), (023), (200), (041), and (113).

By comparing the relative intensities of the lines in sections of cast bars (assumed to be randomly oriented) and rolled bars, the preponderance or scarcity of crystals with the corresponding lattice planes parallel to the plane of section in the rolled bars could be estimated.

§4. Geiger Counter Spectrometer Measurements

In order to obtain a more detailed picture of their preferred orientation, the specimens were examined on a Geiger counter spectrometer. In this instrument the x-rays diffracted from a specimen fall on a Geiger counter which, through suitable electronic circuits, supplies a voltage proportional to the x-ray intensity to an electronic potentiometric recorder. The specimen face being at an angle θ to the beam, diffracted rays are brought to a focus in front of the Geiger counter on a slit at an

angle 2θ to the incident beam. Over a period of several hours the X-ray tube current slowly fluctuates, sometimes by as much as 10%. To compensate for these changes, which are ascribed to frequency changes of the A.C. supply, the measured area of each peak is divided by the tube current measured as it was recorded. Using filtered copper $K\alpha$ radiation (wavelength 1·542 A) and values of θ up to 45°, lines of lattice spacing greater than 1·11 A could be observed.

It is necessary to observe the orientations of a large number of crystals in order to be sure that any departure from randomness is statistically significant. The main criterion used in this work for deciding when enough crystals had been observed was the absence of spottiness in the Debye–Scherrer rings on a photograph.

Smooth rings could not be obtained from stationary specimens of either cast or rolled uranium. Consequently specimen holders were made in which the specimen face was translated or rotated in its own plane, so that the X-ray beam scanned a fairly large region of the surface. In view of the well known fact that in rolled bars and slabs of many metals, deformation is greater in regions adjacent to the rolls than in the centre of the bar or slab, Orowan (1943), Kasz and Varley (1950), arrangements were made to scan narrow bands on the surface at constant distance from the axis of the bar.

§5. Interpretation of Geiger Counter Spectrometer Results

Preferred orientation in a polycrystalline specimen, being a non-random distribution of orientations of the crystal axes relative to directions in the specimen, can have a definite meaning only if the part of the specimen examined contains a statistically significant volume of crystals in every orientation. Furthermore, any systematic variation of crystal orientation between different regions of the specimen can be expressed only by determining separately the preferred orientation in a number of regions, each containing enough crystals to satisfy this condition.

These considerations inevitably limit the accuracy in practice of the quantitative treatment described below, which appear to be implicit in most published work on preferred orientation. The accuracy of the method increases with the ratio of specimen size to grain size, other things being equal.

In the Geiger counter spectrometer measurements described above, X-ray reflections contributing to a particular line were received from all crystals with the corresponding lattice planes parallel to the specimen face, i.e. from all crystals in which the a, b and c crystallographic axes are at three particular angles, α, β and γ respectively to the normal to the specimen face. By measuring the intensities of a large number of lines, with different values of α, β and γ, it is possible to build up a picture of the relationship between these angles and the volume of crystals with the corresponding orientations, which can be consistently represented by a standard stereographic projection of the crystal axes and related

directions in a crystal of α-uranium, with contours superposed to represent the preponderance or scarcity of orientations in which the various crystallographic directions are perpendicular to the plane of section. Such a diagram will be called an *inverse pole figure* (e.g. figs. 2–4). If obtained from a transverse section, so that it shows which crystallographic directions are oriented along the rolling direction, it will be called a *W inverse pole figure* (German ' Walzrichtung '). If obtained from a tangential section, so that it shows which crystallographic directions are oriented along a tangential direction, it will be called the *Q inverse pole figure* (German ' Querrichtung '). These names are consistent with the nomenclature used in the literature to describe orientations in rolled sheet, Barrett (1943), if it is assumed that the compression direction is radial in bar-rolling.

The fraction of the total volume of material observed, which consists of crystals whose orientations are within a small solid angle $d\Omega$ about a point (α, β, γ) on an inverse pole figure, can be expressed as

$$p(\alpha, \beta, \gamma)\, d\Omega/4\pi,$$

where $p(\alpha, \beta, \gamma)$ is a quantity which, in general, depends only on α, β and γ. Since every crystal must have some orientation, it follows that

$$\frac{1}{4\pi}\int\int p(\alpha, \beta, \gamma)\, d\Omega = 1,$$

the integral being taken over the whole inverse pole figure. For randomly oriented material p is independent of α, β and γ, so that, in this particular case

$$\frac{p}{4\pi}\int\int d\Omega = 1\,;$$

hence

$$p = 1.$$

Values of p greater than 1 at any point show that the corresponding crystallographic direction is preferentially oriented perpendicular to the plane of section ; values less than 1 show that such orientations are ' preferentially avoided '.

If $p^{\mathrm{W}}(\alpha, \beta, \gamma)$ is the p value of a point on the W inverse pole figure and $p^{\mathrm{Q}}(\alpha, \beta, \gamma)$ is the p value of a point on the Q inverse pole figure, and if all directions in the bar perpendicular to the rolling direction are equivalent in respect of orientations, it can be shown that

$$p^{\mathrm{Q}}(\alpha, \beta, \gamma) = \frac{1}{2\pi}\int_0^{2\pi} p^{\mathrm{W}}(\alpha', \beta', \gamma')\, d\phi,$$

where $(\alpha', \beta', \gamma')$ lies on a great circle perpendicular to (α, β, γ) and ϕ is its angular distance from some arbitrary zero on this great circle. A perfect ' fibre ' texture in a rolled bar can thus be recognized by examining two sections.

6. Calculation of p Values from Intensity Measurements

It can be shown, Field and Merchant (1949), that the intensity of the x-ray line diffracted from the surface of a thick specimen, when a beam is incident on it at the Bragg angle θ for the particular line examined, is given by

$$I_0 = AD/2\mu$$

where A is the intensity of the incident beam,

D is the fraction of the incident intensity coherently diffracted by the specimen per unit path-length,

μ is the x-ray absorption coefficient of the specimen.

I_0 is thus independent of the Bragg angle θ, other things being equal.

The quantity D can be expressed as the product of three factors, viz. :—

$$p(\alpha, \beta, \gamma)\frac{(\delta\theta)^2}{4},$$

the fraction of the total volume of material oriented within an angle $\delta\theta$ of the appropriate orientation ($\delta\theta$ being the effective ' line breadth ') :

$F^2(hkl)$, a factor depending on the crystallographic indices of the line, having the same value for a particular line in all specimens of the same material (the 'F^2 value' used in crystal structure analysis by x-ray diffraction) ;

B, a factor depending on the imperfections in the structure of the crystals, constant for all lines from the same specimen.

Thus

$$I_0 = \frac{AB}{2\mu}\, p(\alpha, \beta, \gamma)\frac{(\delta\theta)^2}{4} F^2(hkl),$$

for a given set of reflecting planes of index (hkl). B and μ are constants and experiment showed that for a given specimen $\delta\theta$ is also constant. The quantity $I(hkl)$ measured by the Geiger counter spectrometer is equal to KI_0/A where K is an instrumental constant and hence

$$I(hkl) = C \,.\, p(\alpha, \beta, \gamma)F^2(hkl)$$

where C is a constant which includes B, μ, $\delta\theta$ and K and may vary from specimen to specimen.

For a randomly oriented specimen

$$I'(hkl) = C'F^2(hkl).$$

Hence the ratio of the line intensities from preferentially and randomly oriented specimens is given by

$$\frac{I(hkl)}{I'(hkl)} = \frac{C}{C'} \,.\, p(\alpha, \beta, \gamma).$$

To eliminate the factor C/C', it can be assumed that, as the mean value of $p(\alpha, \beta, \gamma)$ for all orientations is 1, the ratio of the sums of the intensities

of a large number of reflections for preferentially and randomly oriented specimens is equal to C/C'. Hence

$$p(\alpha, \beta, \gamma) = \frac{I(hkl)}{\Sigma I(hkl)} \cdot \frac{\Sigma I'(hkl)}{I'(hkl)}.$$

Values of $I'(hkl)/\Sigma I'(hkl)$ were obtained by measuring the intensities of 20 lines from transverse, tangential and radial sections of 1 in. cast bar GE/9. The value for each line from each section, the mean of the three values, and the corresponding value deduced from Jacob and Warren's calculated line intensities are given in table 1. There are variations up to a factor of 2 between intensities of the same line from different sections, but, as they do not fit into consistent pole figures, these anomalies can be attributed to insufficient scanning. The mean values, which were used in subsequent calculation of p values, do not differ greatly from Jacob and Warren's calculated intensities ; the differences can probably be reconciled by small adjustments in the assumed crystal structure of α-uranium. p values calculated from the experimental figures may be expected to be correct to $\pm 20\%$

Results

The preferred orientations observed are summarized in table 2.

Bar 24692. This bar, $1\frac{1}{2}$ in. (3·8 cm) in diameter, was hot-rolled in the α-range from a cast billet. x-ray photographs of a transverse section, taken with scanning annuli of mean radii 0·15, 0·3 and 0·45 in. (0·4, 0·75 and 1·15 cm), showed enhancement of the (020) line and reduction of the (002) line, both effects increasing with the radius. These changes indicate preferred orientation of the (010) planes perpendicular to the rolling direction ; the degree of preferred orientation increases with distance from the axis of the bar.

Geiger counter intensity measurements were made on transverse and tangential sections at a mean distance of 0·4 in. from the axis. The results are summarized in fig. 2, the W and Q pole figures. The (010) planes are strongly oriented, and the (110) planes very weakly oriented, perpendicular to the rolling direction ; the (113) planes are oriented radially in the region examined. However, since the (010) and (113) planes are not quite perpendicular, the W and Q pole figures are not quite consistent with each other, though each is consistent in itself. The anomaly can be explained if the preferred orientation is different along different tangential directions, but it can only be inferred from the results that there are strongly preferred orientation directions perpendicular to the axis of the bar, i.e. that the texture is far from a perfect ' fibre ' texture.

Bar 067921. This bar, 1 in. (2·5 cm) in diameter, was hot-rolled in the α-range with a heavier reduction than bar 24692. An x-ray photograph taken with a scanning circle of 0·25 in. radius shows great enhancement of the (110) line and slight enhancement of the (020) line,

Table 1. Values of $I(hkl)/\Sigma I(hkl)$ for Sections of Cast Bar GE/9

hkl	$I(hkl)/\Sigma I(hkl)$				
	Transverse Section	Tangential Section	Radial Section	Mean	Jacob and Warren's calculated value
114	0·0203	0·0360	0·0415	0·0326	0·0183
133	0·0271	0·0419	0·0426	0·0372	0·0290
221 004 202	0·0758	0·1439	0·1008	0·1068	0·0761
042	0·0139	0·0157	0·0119	0·0138	0·0171
132	0·0109	0·0083	0·0077	0·0090	0·0077
113	0·0227	0·0225	0·0285	0·0246	0·0239
041	0·0105	0·0134	0·0245	0·0161	0·0068
200	0·0223	0·0177	0·0101	0·0167	0·0162
023	0·0408	0·0264	0·0217	0·0296	0·0325
040	0·0114	0·0141	0·0239	0·0165	0·0136
131	0·0791	0·0616	0·1236	0·0881	0·0735
130	0·0061	0·0063	0·0089	0·0071	0·0077
112	0·1045	0·1056	0·1364	0·1155	0·0853
022	0·0061	0·0124	0·0090	0·0092	0·0051
111	0·0997	0·1345	0·0891	0·1078	0·1247
002	0·1303	0·0649	0·0884	0·0945	0·1041
021	0·1680	0·1144	0·1052	0·1292	0·2140
110	0·1407	0·1534	0·1128	0·1356	0·1485
020	0·0098	0·0069	0·0129	0·0099	0·0111

024
222 was not detected in either section

Table 2

Bar No.	Treatment	Preferred Orientation Planes perpendicular to rolling direction
24692	Hot-rolled with light reduction	(010) strong (110) weak
067921	Hot-rolled with heavier reduction	(110) strong (010) weak
287/10	Cold-rolled with light reduction	(010) strong (130) weak

Fig. 2

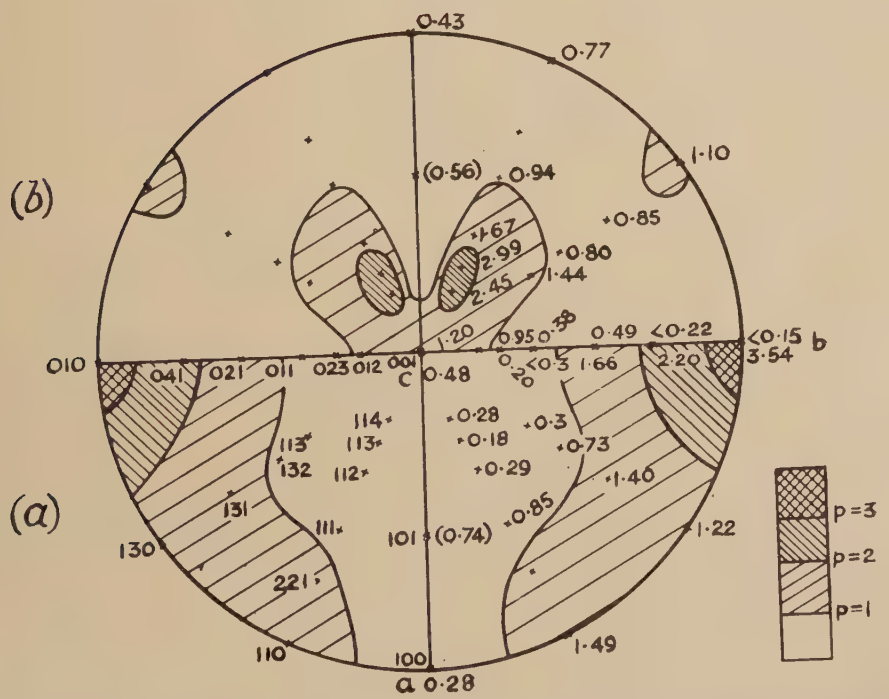

Pole figures showing distribution of crystallographic plane normals in bar 24692 after light reduction by hot-rolling, (*a*) along the rolling direction, (*b*) along a tangential direction.

with weakening of the (021) line and disappearance of the (002) and (112) lines. These changes indicate a strong orientation of the (110) planes, and weak orientation of the (010) planes, perpendicular to the rolling direction.

Geiger counter intensity measurements were made on transverse and tangential sections at mean distances of 0·25 in. and 0·2 in. respectively from the axis of the bar. The results are summarized in fig. 3. The W pole figure confirms the photographic results, and the Q pole figure shows the (023) planes radially oriented. Since the (023) and (110) planes are not quite perpendicular, it can only be stated that there are preferred orientation directions perpendicular to the axis of the bar.

Fig. 3

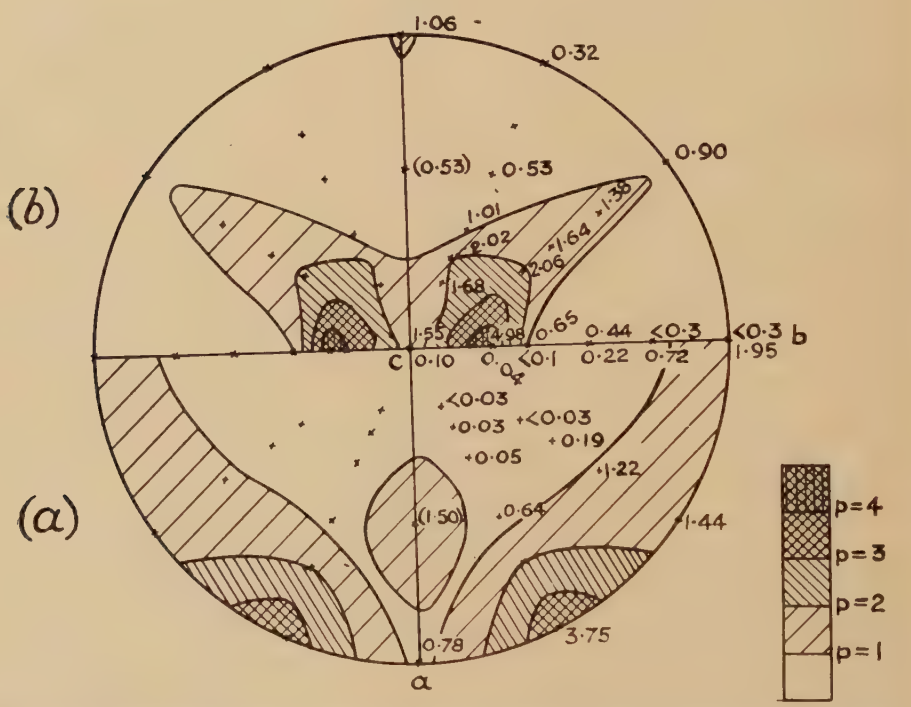

Pole figures showing distribution of crystallographic plane normals in bar 067921 after heavy reduction by hot-rolling, (*a*) along the rolling direction, (*b*) along a tangential direction.

Bar 287/10. This bar was cold-rolled with a light reduction. Micrographic examination showed a large grain size without perceptible elongation of the grains along the rolling direction. Line intensities were measured on the Geiger counter spectrometer with transverse and tangential sections, at a mean distance of 0·1 in. from the axis. The results are summarized in fig. 4. The W pole figure shows that the (010) and (130) planes are oriented perpendicular to the rolling direction

and the Q pole figure shows that the (100) planes, and all planes perpendicular to (130) are preferentially oriented radially in the region examined.

Fig. 4

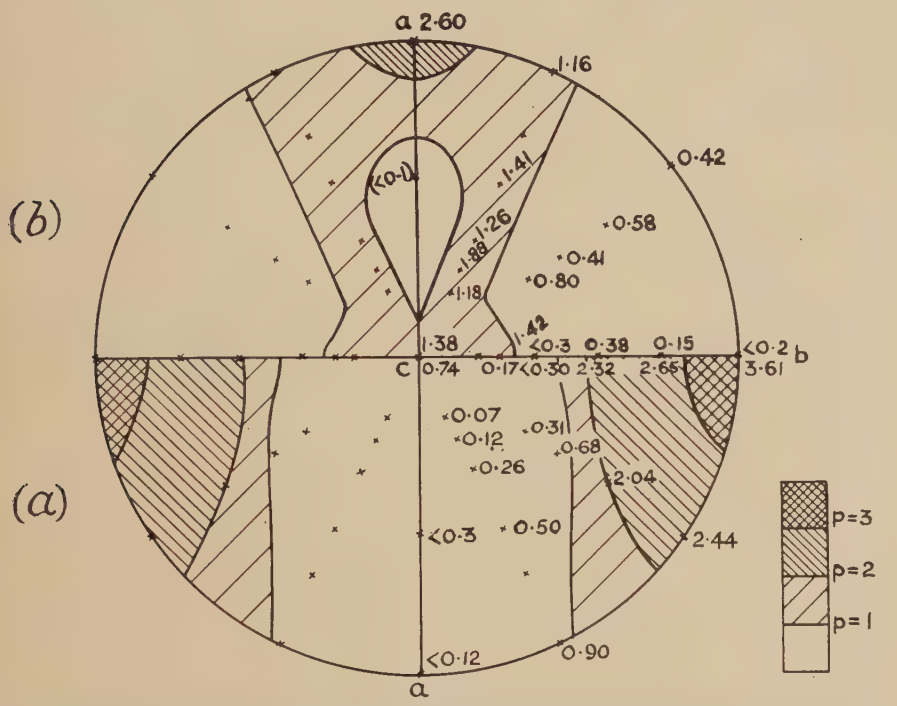

Pole figures showing distribution of crystallographic plane normals in bar 287/10 after light reduction by cold-rolling, (*a*) along the rolling direction, (*b*) along a tangential direction.

Acknowledgments

The work described above was carried out in the Metallurgy Division of the National Physical Laboratory as part of the programme of the Division of Atomic Energy, Ministry of Supply, and this paper, which has the approval of the Ministry of Supply, is published by permission of the Director of the National Physical Laboratory.

The author acknowledges the help of Miss H. M. Murphy and Miss E. D. Whittle, who took the x-ray photographs.

References

Barrett, C. S., 1943, *Structure of Metals*, (New York: McGraw Hill), Chapters ix, xviii–xxi.

Chipman, J., 1950, *J. Inst. Met. Abs.*, **17**, 345. U.S. Atomic Energy Commission Publication 1946, MDDC-539.

Decker, Asp, and Harker, 1948, *J. App. Phys.*, **19**, 388.

Field and Merchant, 1949, *J. App. Phys.*, **20**, 741.

Jacob and Warren, 1937, *J. Amer. Chem. Soc.*, **59**, 2588.

Kasz and Varley, 1950, *J. Inst. Met.*, **76**, 407.

Orowan, 1943, *Proc. Inst. Mech. Eng.*, **150**, 140.

XI. CORRESPONDENCE

Metallic Conduction—The Internal Size Effect. An Addendum

By D. K. C. MacDonald*
Clarendon Laboratory, Oxford†

[Received July 26, 1951]

In a recent paper under this title (MacDonald 1951), the writer has pointed out that internal ' barriers ' or scattering boundaries in a metal may, in particular, result in anomalous behaviour under an external magnetic field. Thus, specifically, an initial *decrease* of resistance can take place when a magnetic field is applied ; the Hall field characteristics may also deviate significantly from those appropriate to an ideal, homogeneous, bulk metal. We wish here to make one or two observations in the latter connection.

First, let us mention a recent note on ' The Hall Potential across an Inhomogeneous Conductor ' by J. Volger (1950). Volger is not concerned, as we were, with the situation arising in a region of metal when the electron mean free path becomes comparable with the *size* of the region ; in general, however, whenever the *length* of an element is comparable with the *breadth* (across which the Hall field is generated) deviations from the simple theory may arise and Volger also suggests that this may be of significance when interpreting experiments on inhomogeneous conductors —particularly granular semi-conductors.

Secondly, we wish to amend somewhat our qualitative discussion of the generation of the Hall field in a ' striated ' conductor, where the striation-separation is comparable with the electron free path. An internal boundary or ' striation ' might be regarded as having various limits of behaviour, as follows. Firstly, if all electrons penetrated the barrier *without significant scattering*, elastic or otherwise, then there will of course be no effect either on the conductivity or on the Hall field. If, however, electrons were *reflected elastically* then the conductivity in the absence of a magnetic field would be unaffected but the Hall field arising when a magnetic field is applied would take the form sketched in our fig. 1 (*b*). (*loc. cit.*)‡. *Diffuse, inelastic, reflection* will again cause the Hall field to take the same qualitative form, but now also the resistivity (in the absence of a magnetic field) will be increased over that of the homogeneous

* Communicated by the Author.

† Now at the Physics Division, National Research Council, Ottawa, Canada.

‡ We may remark that, in recent personal discussion, Professor C. J. Gorter has questioned our assumption (MacDonald and Sarginson 1950) that the Hall field must fall to zero as the external boundary of a metal is approached, suggesting the possibility of additional ' locally bound ' electrons forming a true surface charge-layer.

metal; application of a magnetic field can then in general produce a decrease. Finally, *diffuse scattering* will again increase the resistivity over the homogeneous bulk metal but the Hall field will no longer fall to zero at the internal boundaries, but may be expected to follow qualitatively the variation of our fig. 1 (*c*) ; again we may expect that a magnetic field can produce some initial decrease of resistance although this will be less pronounced than in the corresponding case of *diffuse reflection*.

In general, experimental studies of the Hall effect in metals at low temperatures, especially those exhibiting the anomalous minimum of electrical resistance, should be of considerable interest.

References*

MacDonald, D. K. C., 1951, *Phil. Mag.*, **42**, 756.
MacDonald, D. K. C., and Sarginson, K., 1950, *Proc. Roy. Soc.* A, **203**, 223.
Volger, J., 1950, *Phys. Rev.*, **79**, 1023.

The Moving Griffiths Crack

By C. J. Tranter
Military College of Science, Shrivenham†

[Received November 1, 1951]

In her recent paper ' The Moving Griffiths Crack ', Dr. E. H. Yoffe (1951) reduces the problem of the calculation of the stress field about a straight crack moving through an elastic medium to that of finding a function $A(s)$ which satisfies the dual integral equations

$$\left.\begin{aligned} \int_0^\infty sA(s)\cos xs\,ds &= \text{constant} \qquad (-a<x<a), \\ \int_0^\infty A(s)\cos xs\,ds &= 0 \qquad (|x|>a). \end{aligned}\right\}$$

These equations are included in the more general pair considered by L. V. King (1935–36) and I have recently given solutions (1950, 1951) to still more general pairs. It is the purpose of this note to point out that the solution of the above dual equations can be obtained immediately and more simply from King's result.

References

King, L. V., 1935–6, *Proc. Roy. Soc.* A, **153**, 24.
Tranter, C. J., 1950, *Quart. Journ. Mech. Appl. Math.*, **3**, 411 ; 1951, *Quart. Journ. Math. Oxford* [2], **2**, 60.
Yoffe, E. H., 1951, *Phil. Mag.* [7], **42**, 739.

---

* The following reference was omitted in error from the earlier paper :—
Sondheimer, E. H., 1950, *Phys. Rev.*, **80**, 401.

† Communicated by the Author.

High-energy Components of the β-particle Spectrum of $MsTh_2$

By C. G. Campbell, W. J. Henderson* and J. Kyles
Department of Natural Philosophy, University of Edinburgh†

[Received October 17, 1951]

A new investigation of the β-particle spectrum of $MsTh_2$ has been made using one half of the double semi-circular focusing spectrometer of Feather, Kyles and Pringle (1948).

The method of source preparation followed closely that outlined by MacLane and Peterson (M.D.D.C. 1742) and Peterson (M.D.D.C. 1709). In order to obtain activities of the order of 1 mc the cerium carrier was not removed from the $MsTh_2$, since this process proved to be one of low yield, but the amount of carrier added was kept down to about 0·015 mg. The nitrates of cerium and $MsTh_2$ were evaporated on 0·2 mg/cm² aluminium foil of area 1 cm by 0·2 cm. These sources were used in the spectrometer at an emission angle of 45° so that the effective breadth was reduced and sharpness of focusing was improved.

Scintillation counters were employed as detectors (E.M.I. Type 5045 photomultipliers with anthracene as the phosphor). Tested with monoenergetic β-particles these counters gave a plateau in the counting rate/multiplier voltage curve, starting at a voltage which increased as the energy of the incident β-particles decreased.

The magnetic field was determined from a Fermi plot of the ThC spectrum obtained with a source of thorium active deposit, the end-point for ThC being taken as 2·256 mev. That the $MsTh_2$ sources were free from the decay products of thoron, was shown by the fact that there was no evidence of the F-line of the ThB spectrum. Moreover, for β-particles of 1·80 mev energy the half-life of the sources used agreed with the accepted value for $MsTh_2$ to within 1%.

For the investigation of the high-energy region of the $MsTh_2$ spectrum the multiplier voltage was set so that unnecessary sensitivity to low energy (scattered) particles was avoided. This adjustment at the same time reduced the effective γ-ray background registered by the counter. Only as low energy regions were explored was the multiplier voltage appropriately increased.

A Fermi plot of the spectrum was constructed and was found to be non-linear except near the end-point. Extrapolation of the final linear portion gave a maximum energy of $2{\cdot}16 \pm 0{\cdot}03$ mev. This value is considerably greater than the values of Lecoin (1938) and Lee and Libby (1939), but is in reasonably good agreement with the absorption measurements of Feather (1930, 1938). An attempt was then made to deduce the end-points of possible partial spectra by resolving the Fermi

* On leave from the National Research Council of Canada.
† Communicated by Professor N. Feather.

plot into straight lines, and this showed evidence of partial spectra with end-points at $1{\cdot}6 \pm 0{\cdot}1$ MEV and $1{\cdot}85 \pm 0{\cdot}1$ MEV. At lower energies the shape of the continuous spectrum is masked to a large extent by conversion lines, but there seems to be evidence for the existence of at least one other partial spectrum with an end-point at about 1 MEV energy. Coincidence experiments are now being undertaken in an attempt to establish these values more exactly.

REFERENCES

FEATHER, 1930, *Phys. Rev.*, **35,** 1559–1567 ; 1938, *Proc. Camb. Phil. Soc.*, **34,** 115–119.
FEATHER, KYLES and PRINGLE, 1948, *Proc. Phys. Soc.*, **61,** 466–478.
LECOIN, 1938, *J. Phys.*, **9,** 81–93.
LIBBY and LEE, 1939, *Phys. Rev.*, **55,** 245–258.

A Note on the Statistics of the Weiss Field

By G. M. BELL
The Clarendon Laboratory, Oxford*

[Received October 17, 1951]

CONSIDER an assembly of N magnetic dipoles of magnitude p, with two orientations relative to an applied field, H. If N_1 are oriented along the field and N_2 against it, the relative magnetization is given by $m=(N_1-N_2)/N$. Suppose that the N dipoles occupy all sites of a lattice of co-ordination number q, that each parallel pair of nearest neighbours has an interaction energy, $-w/2$, and each parallel pair, $w/2$, where $w>0$.

Let N_{12} be the number of anti-parallel nearest neighbour pairs. Then, leaving out certain constant terms, the nearest neighbour interaction energy can be written as $N_{12}w$ (Rushbrooke 1949).

In a random arrangement $N_{12}=qN_1N_2/N=qN(1-m^2)/4$ and in a zero-th order approximation this is taken as the actual value of N_{12}. The nearest neighbours thus contribute $-qNwm^2/4$ to the energy (omitting the constant $qwN/4$). A similar term, with different values of q and w, is given by each type of neighbour pair. (It should be noted that, in the limiting case where a system's interaction with any other system does not depend on the distance, the zero-th order method becomes accurate.) The interaction energy for the assembly is thus $-Nk\lambda m^2/2$ where k is Boltzmann's constant and a constant depending on the lattice structure and exchange forces.

Now it is well-known that, using classical (localized) statistics, m now has the same value as in an effective field H^1, where $H^1=H+k\lambda m/p$. However, correct values of m and E_m cannot simultaneously be derived

---

* Communicated by Professor M. H. L. Pryce, F.R.S.

from a magnetic partition function which depends on H^1 as if the latter was an external field in the theory of paramagnetism. This can be seen from writing

$$(P.F.)_m = \left\{\exp\frac{pH^1}{kT} + \exp\frac{-pH^1}{kT}\right\}^N$$
$$= \sum_{N_1+N_2=N} \frac{N!}{N_1!\,N_2!} \exp\left\{(N_1-N_2)\frac{pH+k\lambda m}{kT}\right\}. \quad . \; . \; (1)$$

All values of N_1 and N_2 satisfying the relation $N=N_1+N_2$ are summed over, but all except one pair of such values are incompatible with the given value of m or $(N_1-N_2)/N$.

There is the same inconsistency when the Weiss Field is used with Fermi-Dirac Statistics (Stoner 1938, 1939). However, a partition function from which correct expressions for the energy and magnetization are derivable can be constructed by summing, for each value of m, over only those sets of occupation numbers which are consistent with that value of m. Thus, in the case $H=0$, put

$$(P.F.)_m = \Sigma_m \left[\exp\frac{-\lambda m^2 N}{2T}\left\{\sum_{\Sigma d_s=\frac{1}{2}(1+m)N} \exp\frac{-\Sigma_s d_s\epsilon_s}{kT}\right\}\right.$$
$$\left. \times \left\{\sum_{\Sigma d_s=\frac{1}{2}(1-m)N} \exp\frac{-\Sigma_s d_s\epsilon_s}{kT}\right\}\right]. \quad . \; . \; . \; . \; . \; . \; (2)$$

The d_s are the occupation energies of the microscopic energy states denoted by 's' and can take only the values 0 or 1. The method of steepest descents is used to evaluate the sums inside the square brackets which are taken over the states with positive and negative spin component, respectively. It is then found that

$$\ln\left\{\sum_{\Sigma_s d_s=\frac{1}{2}(1+m)N} \exp\frac{-\Sigma_s d_s\epsilon_s}{kT}\right\} = \int_0^\infty n(\epsilon)\ln\left[\exp\left\{\eta_1 - \frac{\epsilon}{kT}\right\}+1\right]d\epsilon - N\eta_1$$
$$. \; . \; . \quad (3)$$

where $n(\epsilon)d\epsilon$ is the number of levels in the energy interval $d\epsilon$ and η_1 is given by

$$\int_0^\infty n(\epsilon)\left[\exp\left\{\frac{\epsilon}{kT}-\eta_1\right\}+1\right]^{-1} d\epsilon = N_1 = \tfrac{1}{2}N(1+m). \quad . \; . \; . \quad (4)$$

Similarly

$$\ln\left\{\sum_{\Sigma_s d_s=\frac{1}{2}(1-m)N} \exp\frac{-\Sigma_s d_s\epsilon_s}{kT}\right\} = \int_0^\infty n(\epsilon)\ln\left[\exp\left\{\eta_2 - \frac{\epsilon}{kT}\right\}+1\right]d\epsilon - N_2\eta_2$$
$$. \; . \; . \quad (5)$$

where, $$\int_0^\infty n(\epsilon)\left[\exp\left\{\frac{\epsilon}{kT}-\eta_2\right\}+1\right]^{-1} d\epsilon = N_2 = \tfrac{1}{2}N(1-m). \quad . \; . \; . \quad (6)$$

Eqns. (3) and (5) are now substituted into (2). Then, using (4), (6), $(P.F.)_m$ is differentiated logarithmically to obtain its largest

term, which by the usual property of thermodynamic functions yields its effective value. From the differentiation we have

$$(\eta_1-\eta_2)/2-\lambda m/T=0. \quad . \quad . \quad . \quad . \quad . \quad . \quad . \quad . \quad (7)$$

Defining a new parameter η by $\eta=\frac{1}{2}(\eta_1+\eta_2)$, (4) and (6) become

$$\int_0^\infty n(\epsilon)\left[\exp\left\{\frac{\epsilon}{kT}-\eta-\lambda m/T\right\}+1\right]^{-1}d\epsilon=\tfrac{1}{2}N(1+m) \quad . \quad . \quad . \quad (8)$$

$$\int_0^\infty n(\epsilon)\left[\exp\left\{\frac{\epsilon}{kT}-\eta+\lambda m/T\right\}+1\right]^{-1}d\epsilon=\tfrac{1}{2}N(1-m) \quad . \quad . \quad . \quad (9)$$

and the free energy is given by

$$\frac{F}{kT}=N\eta+\tfrac{1}{2}N\lambda m^2/T-\int_0^\infty n(\epsilon)\ln\left[\exp\left\{\eta+\lambda m/T-\frac{\epsilon}{kT}\right\}+1\right]d\epsilon$$

$$-\int_0^\infty n(\epsilon)\ln\left[\exp\left\{\eta-\lambda m/T-\frac{\epsilon}{kT}\right\}+1\right]d\epsilon. \quad . \quad (10)$$

It can be seen that a partition function constructed so as to sum over only consistent values of the sets of occupation numbers gives correct expressions for the magnetization and free energy by differentiation, without any necessity for the addition of extra terms.

References

Rushbrooke, G. S., 1949, *Statistical Mechanics* (Oxford: University Press), p. 291.
Stoner, E. C., 1938, *Proc. Roy. Soc.* A, **165**, 372; 1939, *Ibid.*, **169**, 339.

The Angular Distribution of Protons in the Photo-Disintegration of the Deuteron

By K. Phillips
High Voltage Research Laboratory, Metropolitan-Vickers Electrical Company*

[Received November 1, 1951]

Summary

Using a thin heavy wax target the angular distribution of photo-protons has been observed in photographic plates, for the energy range 6 to 15 MeV.

In the past few years many publications have appeared on the experimental investigation of the angular distribution of photo-protons in the photo-disintegration of the deuteron. Most of the investigations have been

* Communicated by the Author.

carried out using monochromatic γ-ray sources of 6·1 and 7 MEV, e.g. Goldhaber (1948), Phillips, Lawson and Kruger (1950), Hough (1950), Gibson, Grotdal, Orlin and Trumpy (1951) and at 17·6 MEV by Hough, Waffler and Younis (1949). Another recent paper by Fuller (1950) describes an experiment using a 20 MEV betatron as X-ray source. These experiments especially at the higher energies are likely to yield important evidence concerning the nature of nuclear forces.

This short report describes some preliminary results on a similar experiment using a 20 MEV betatron for the X-ray energy range of 5–15 MEV. A collimated beam of X-rays was incident on a 200-micron thick Ilford C.2 nuclear emulsion over which was placed a 10-micron thick deuterium wax target. The plates were inclined at 15 degrees to the horizontal. The exposure to the betatron lasted only for a few minutes so as to prevent undue X-ray blackening. The plates were processed in Azol developer and 1% potassium bromide in the usual manner.

With the aid of a Vickers projection microscope several thousand tracks were examined and only protons with angles of dip in the emulsion within the interval 5–45 degrees were used in the distributions. The upper limit was adopted to reduce the error due to inaccuracies in range measurements for tracks with large angles of dip. The lower limit was introduced in order to eliminate large errors due to the passage of the protons through the wax target. A study of the neutron flux in the betatron enclosure was carried out by examining emulsions exposed with ordinary paraffin wax targets. The effect of these neutrons was found to be almost negligible except at the very low energies, i.e. less than 5 MEV. From the geometry of the experiment it can be shown that the angle of the emitted proton with respect to the direction of the X-ray beam is given by the expression

$$\cos\theta = \sin\beta \sin 15^\circ + \cos 15^\circ \cos\beta \cos\delta,$$

where β is the angle of dip in the emulsion, corrected for shrinkage and δ is the angle of ejection of the photo-proton measured in the plane of the plate.

The protons were divided into four convenient energy groups 5–8, 8–10, 10–13, 13–15 MEV, and the histograms of the number of tracks emitted for unit solid angle and corrected for loss due to the angle of dip criteria, are shown in figs. 1, 2, 3 and 4. The smooth curves are the $\sin^2\theta(1+B_{\mathrm{LAB}}\cos\theta)$ distributions, predicted by the theory of Marshall and Guth (1950).

Assuming a distribution of the form

$$N(\theta) = A_{\mathrm{LAB}} + \sin^2\theta(1+B_{\mathrm{LAB}}\cos\theta)$$

the values of the constant A_{LAB} and B_{LAB} have been determined by statistical analysis of the data and are given in the table for the different X-ray energies. The values of A_{LAB} indicate an increase of the isotropic term with X-ray energy as is characteristic of the parameter due to non-central interaction of the nucleons ; whilst the values of B_{LAB} agree with the theory of Marshall and Guth within the experimental error.

Fig. 1

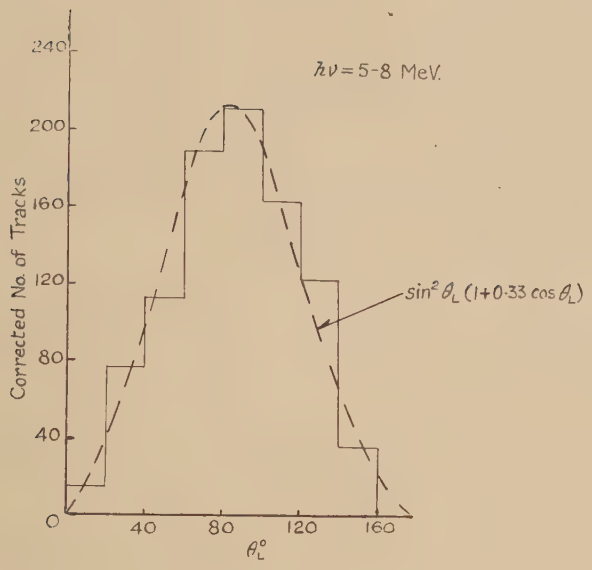

Fig. 2

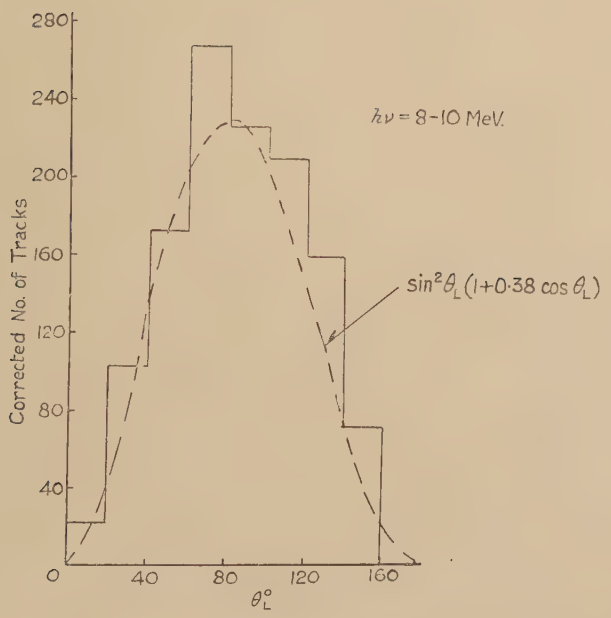

The histograms show the angular distribution of the photo-protons between 0° and 160°, with respect to the direction of the x-ray beam, for four different x-ray energies. The dotted curves indicate the expected distribution predicted by the theory of Marshall and Guth.

Energy $h\nu$ MeV	5–8	8–10	10–13	13–15
A_{LAB}	0·063±0·015	0·083±0·013	0·119±0·010	0·135±0·017
B_{LAB}	0·22 ±0·2	0·24 ±0·16	0·44 ±0·23	0·49 ±0·25

The limits in the above table have been taken as plus and minus twice the standard error.

Fig. 3

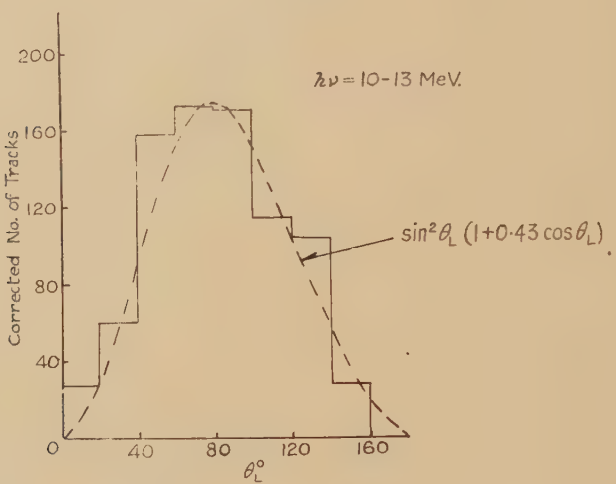

Fig. 4

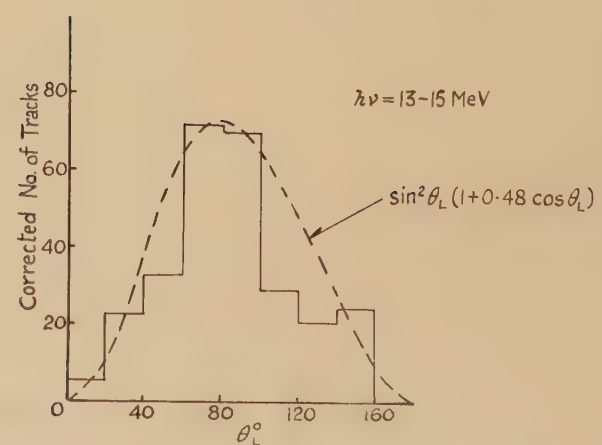

The histograms show the angular distribution of the photo-protons between 0° and 160°, with respect to the direction of the x-ray beam, for four different x-ray energies. The dotted curves indicate the expected distribution predicted by the theory of Marshall and Guth.

The author wishes to acknowledge the assistance given by all the members of the Betatron Team at the Metropolitan-Vickers Research Department and to thank Drs. E. H. S. Burhop and C. T. Griffiths of University College, London, for their help and advice in the early stages of the experiment. He also wishes to thank Dr. C. Dannatt, M.C., O.B.E., Director of Research and Education, and Mr. B. G. Churcher, Manager of the Research Department, Metropolitan-Vickers Electrical Co. Ltd., for permission to publish this paper.

References

Fuller, 1950, *Phys. Rev.*, **79**, 303.
Gibson, Grotdal, Orlin and Trumpy, 1951, *Phil. Mag.*, **42**, 555.
Goldhaber, 1948, *Phys. Rev.*, **74**, 1725.
Hough, 1950, *Phys. Rev.*, **80**, 1069.
Marshall and Guth, 1949, *Phys. Rev.*, **76**, 1879 ; *Ibid.*, **78**, 738.
Phillips, Lawson and Kruger, 1950, *Phys. Rev.*, **80**, 326.
Waffler and Younis, 1949, *Helv. Phys. Acta*, **22**, 414.

A Theorem involving Binding Energies in Relation to β-disintegration

By N. Feather, F.R.S.
The University, Edinburgh*

[Received November 12, 1951]

From time to time many expressions, equivalent so far as they are essentially correct, have been put forward to relate the energy released in β-disintegration to the masses of the nuclei involved, the total energy of binding of the neutrons and protons in such nuclei, or the masses of parent and daughter atoms in the neutral state. Sometimes the difference between the disintegration energies of successive β-active bodies (as of the successive members of a ' chain ' of fission products), or the difference between the disintegration energies of succeeding members of a series of bodies of constant isotopic number, is of interest. In such cases the ' theoretical ' expression for the energy difference may be neater than the corresponding expression for the energy of a single disintegration. In this note a form of expression is deduced for the difference between $T_\beta^- \binom{A}{Z}$ and $T_\beta^- \binom{A'}{Z'}$, the total energies of negative β-disintegration of two species $\binom{A}{Z}$ and $\binom{A'}{Z'}$, which exhibits this neatness in a marked degree. So far as the writer is aware this expression has not previously appeared in the literature.

---

* Communicated by the Author.

If the exact mass of the nucleus $\binom{A}{Z}$ is represented by $N\binom{A}{Z}$ and if m is the mass of the electron, we have

$$T_{\beta}^{-}\binom{A}{Z} = \left[N\binom{A}{Z} - N\binom{A}{Z+1} - m\right]c^2 + \epsilon\binom{Z+1}{Z}, \quad . \quad (1)$$

the term $\epsilon\binom{Z+1}{Z}$ representing the energy derived from the adiabatic reorganization of the extranuclear electrons in the process of disintegration. If the energy of binding of the last-added proton in the nucleus $\binom{A}{Z}$ is written as $B_p\binom{A}{Z}$ and that of the last-added neutron in the same nucleus as $B_n\binom{A}{Z}$, a little consideration will show that (1) becomes

$$T_{\beta}^{-}\binom{A}{Z} = B_p\binom{A}{Z+1} - B_n\binom{A}{Z} + T_{\beta}^{-}\binom{1}{0} + \epsilon\binom{Z+1}{Z}. \quad . \quad (2)$$

Again, consideration of the process of formation of the nucleus $\binom{A+1}{Z+1}$ from the nucleus $\binom{A-1}{Z}$, first by the addition of a neutron followed by a proton, then by the addition of a proton followed by a neutron, leads to the result

$$B_n\binom{A}{Z} + B_p\binom{A+1}{Z+1} = B_p\binom{A}{Z+1} + B_n\binom{A+1}{Z+1}. \quad . \quad . \quad (3)$$

From (2) and (3) we obtain

$$T_{\beta}^{-}\binom{A}{Z} = B_p\binom{A+1}{Z+1} - B_n\binom{A+1}{Z+1} + T_{\beta}^{-}\binom{1}{0} + \epsilon\binom{Z+1}{Z}, \quad . \quad (4)$$

and from (4), neglecting the very small difference $\epsilon\binom{Z+1}{Z} - \epsilon\binom{Z'+1}{Z'}$,

$$T_{\beta}^{-}\binom{A}{Z} - T_{\beta}^{-}\binom{A'}{Z'} = B_p\binom{A+1}{Z+1} - B_n\binom{A+1}{Z+1} - B_p\binom{A'+1}{Z'+1} + B_n\binom{A'+1}{Z'+1}. \quad . \quad . \quad . \quad . \quad . \quad . \quad . \quad . \quad . \quad (5)$$

Eqn. (5) is the expression referred to above. For positron disintegration (or capture transformation) the corresponding expression will be found to be

$$T_{\beta}^{+}\binom{A}{Z} - T_{\beta}^{+}\binom{A'}{Z'} - B_n\binom{A+1}{Z} - B_p\binom{A+1}{Z} - B_n\binom{A'+1}{Z'} + B_p\binom{A'+1}{Z'}. \quad . \quad . \quad . \quad . \quad . \quad . \quad . \quad . \quad (6)$$

When (5) and (6) refer to active species $\binom{A}{Z}$, $\binom{A'}{Z'}$ having the same isotopic number D, it will be observed that in one case (5) the binding energies are those of neutrons and protons in nuclei both of isotopic number $D-1$, and in the other case (6) the binding energies are those of neutrons and protons in two nuclei each of isotopic number $D+1$. It is this simplicity which makes the expressions particularly useful in discussing the variation of disintegration energy with mass or charge number for a series of bodies having the same value of $D(=A-2Z)$.

Recently the writer has given a survey of the total energies of β-disintegration of species of isotopic number ranging from 40 to 53 (Feather 1951). For each value of $A-2Z$ a curve is given showing the variation of T_β^- with neutron number $A-Z$. Certain of these curves show discontinuities in the region $A-Z=126$, but the curve for $A-2Z=45$ does not. In applying (5) to this smooth curve we are concerned with the differences between the binding energies of the last-added protons and the last-added neutrons in a series of nuclei for which $A-2Z=44$. This isotopic number has unique significance in the range $39\leqslant A-2Z\leqslant 52$ as the difference between the 'magic' numbers 126 and 82. The terms entering into (5) in this connection are the differences between the binding energies of 'equivalent' protons and neutrons, in respect of shell closure at $Z=82$, $A-Z=126$, respectively. The fact that the curve for T_β^- against $A-Z$ for $A-2Z=45$ is perfectly smooth then implies that the contribution of specifically nuclear forces to the variation of proton binding energy with proton number around $Z=82$ is paralleled precisely by the contribution of specifically nuclear forces to the variation of neutron binding energy with neutron number around $A-Z=126$—at least within the series of nuclei for which $A-2Z=44$. This is a significant result to deduce from what is, in a sense, purely qualitative information.

It is hoped to give a more complete discussion of the experimental material from this point of view in a later publication.

Reference

Feather, N., *Proc. Roy. Soc., Edin.*, in course of publication.

XII. *Notices of New Books and Periodicals received*

Ferromagnetism. By R. M. Bozorth. [Pp. 968.] (London : Macmillan & Co. Ltd.) Price £6 10*s*. (New York : D. Van Nostrand Company Inc.) Price $17.50.

This is an excellent reference book on ferromagnetism. It should be available to everyone working in a field related to ferromagnetism. The book is divided into four parts : a short introduction, one dealing with the properties of magnetic materials, another on magnetic phenomena and theories and a short one on the technique of measurements. This makes it of great use to engineers and physicists alike. The enormous amount of information is presented in a very pleasant way. The number of graphs is about equal to the number of pages and there are many tables and an up-to-date list of references covering 70 pages.

It is obvious that this work is not meant to be a textbook on ferromagnetism. Fundamental theories are only briefly reviewed but great attention is paid to the description of basic physical phenomena and to the theory necessary to understand the physical concepts. The results of recent research are amply used in the presentation of the general picture of ferromagnetism. The author has wisely made no attempt to include theories of a more speculative nature which could be advanced for the explanation of many experimental observations. D. P.

The Interpretation of X-Ray Diffraction Photographs. By N. F. M. Henry, H. Lipson and W. A. Wooster. [Pp. 258.] (London : Macmillan.) Price 42*s*.

Few books have hitherto been written about x-ray diffraction techniques which deal adequately with the indexing and interpretation of diffraction photographs, so that this new, authoritative and detailed practical textbook will be widely appreciated. In writing it, the authors have drawn jointly upon considerable experience gained not only in the practice but also in the teaching of their subject, and they have exercised sound judgment in the choice of subject matter. This is presented largely in a geometrical way but an elegant treatment is also given of the corresponding analytical approach, the style throughout being lucid though concise.

The first two chapters deal in an elementary way with crystal lattices, their symmetry and representations, and with the fundamental physical properties of x-rays. In the third chapter, this leads naturally to the theory of x-ray diffraction, into which the concept of the reciprocal lattice is introduced at an early stage. The methods of indexing and interpreting single crystal photographs are then discussed, and are illustrated by a number of examples in which the more complex problems are approached in a systematic and simple way. Other chapters are devoted to the powder method and the accurate determination of cell dimensions, the study of orientation in single crystals and twins, preferred orientations in polycrystalline aggregates, the calculation and measurement of the intensities of x-ray reflections and the measurement of grain size. The reproduction of photographs and charts to scale, together with the inclusion of worked examples and tables of the physical constants and mathematical functions most frequently required by the experimenter contribute greatly to the practical value of the book. It can confidently be recommended to all who are in any way concerned in the practice of x-ray diffraction. H. D. K.

[The Editors do not hold themselves responsible for the views expressed by their correspondents.]

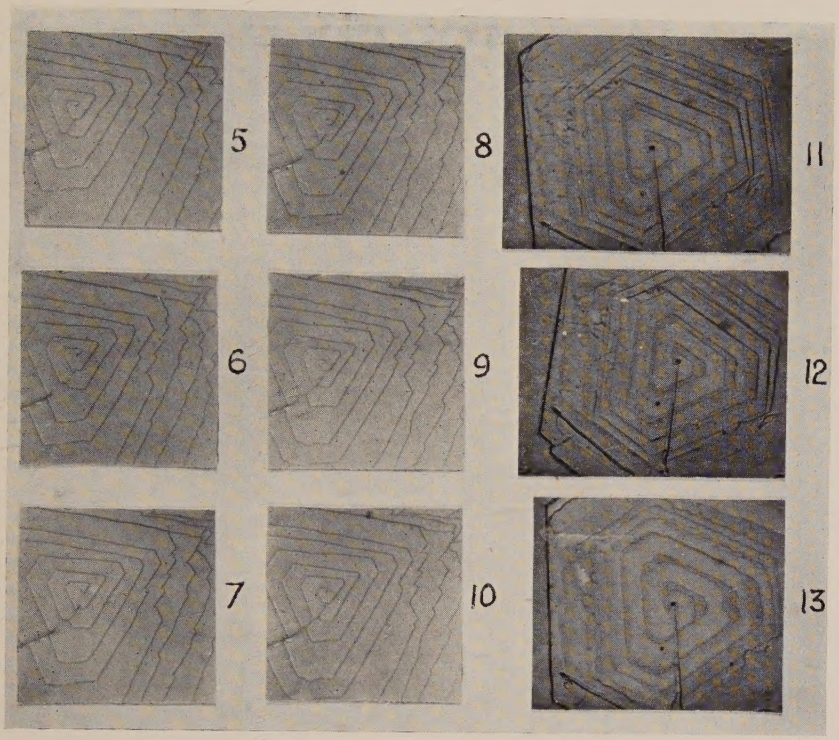

Figs. 5–10

Showing sequence of growth about a single screw dislocation group. Photographs at 10-minute intervals. ×250

Figs. 11–13

Growth from two screw dislocation groups of the same hand. Photographs at 10-minute intervals. ×250

DESCRIPTIONS TO PLATE II

Figs. 14–18

Growth from two co-operating screw dislocation groups of opposite hand. Photographs at 15-minute intervals. ×300

Figs. 19–23

Growth from two co-operating screw dislocation groups of opposite hand. Photographs at 60-minute intervals. (Same crystal five days later.) ×300

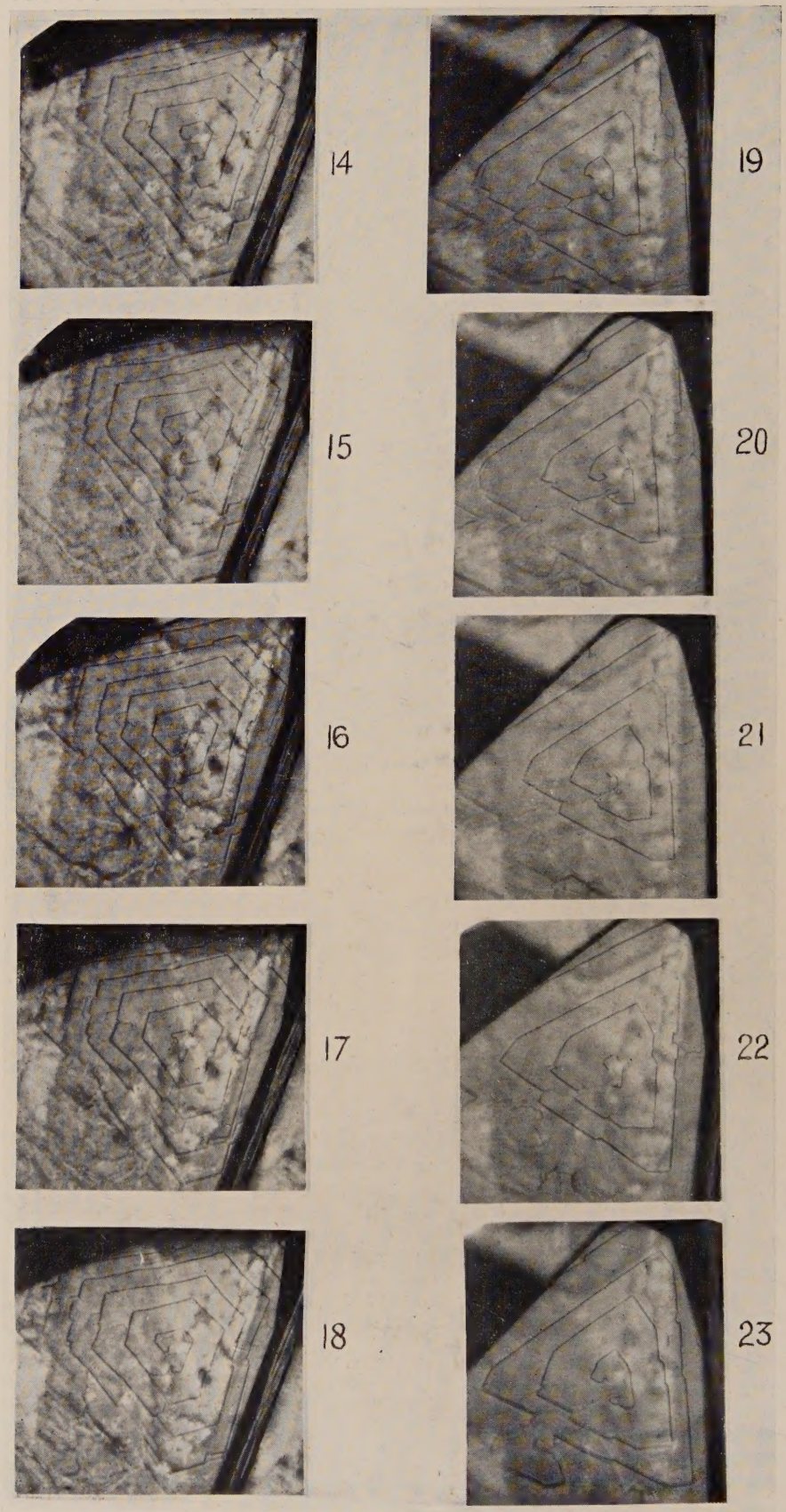
14
19
15
20
16
21
17
22
18
23

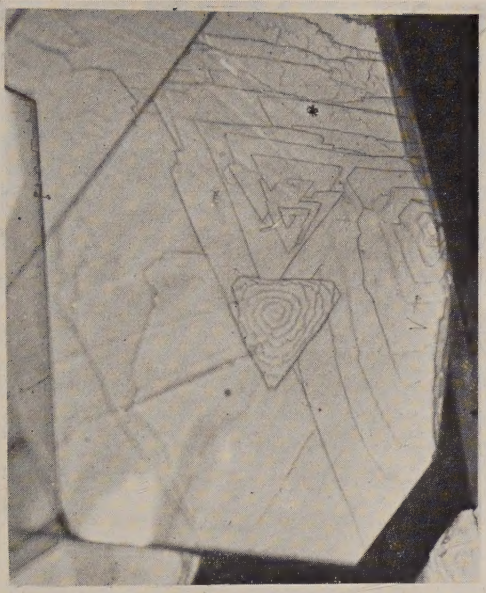

24

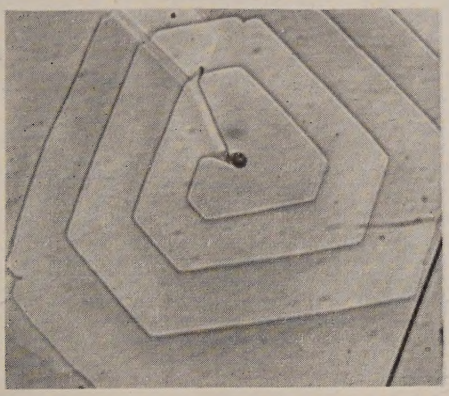

25

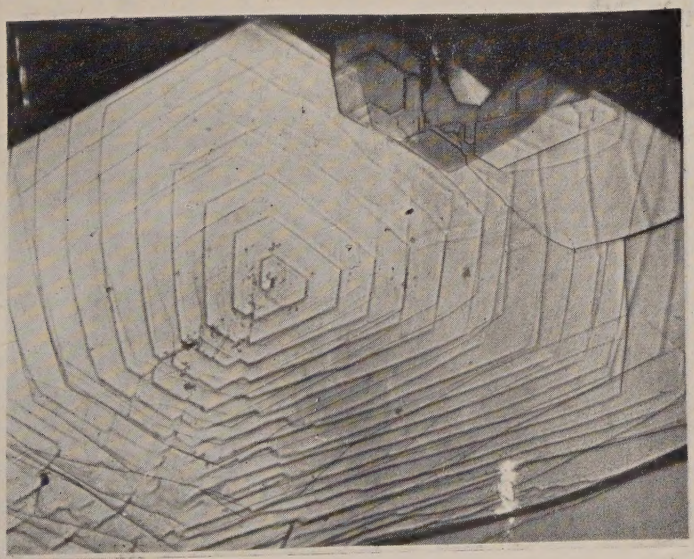

26

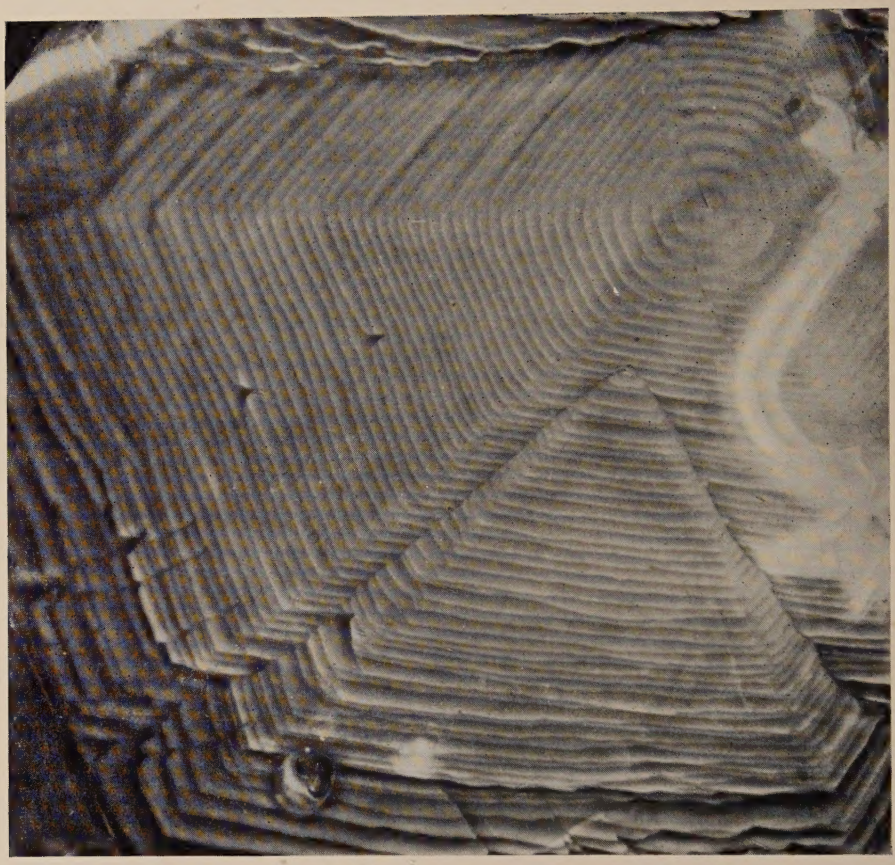

Fig. 27

Illustrating cross-lacing phenomenon and domination of a pair of screw dislocation groups of opposite hand.
(Reflection phase contrast illumination.) (Step-height 294 Å ± 1·5 Å.)
×650

DESCRIPTIONS TO PLATE III

Fig. 24

Showing step-lines on the surface of a crystal containing many screw dislocation groups. ×250

Fig. 25

Crystal plate with spiral step-line on one surface and radial step-line on the other, both centred on same screw dislocation group. ×500

Fig. 26

Crystal plate with spiral step-line on both surfaces. ×250